MICROCOPY RESOLUTION TEST CHART

NATIONAL BUREAU OF STANDARDS-1963-A

AD-A159 532

Final Report

Contract No. N00014-83-K0242

THE EFFECT OF MICROSTRUCTURE
ON THE
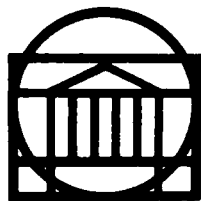CREEP BEHAVIOR OF Ti-6A1-2Nb-1Ta-0.8Mo

Submitted to:

Office of Naval Research
800 N. Quincy Street
Arlington, Virginia 22217

Attention: Dr. Bruce MacDonald
Program Manager

Submitted by:

W. H. Miller, Jr.
Research Assistant

R. T. Chen
Post Doctoral Fellow

E. A. Starke, Jr.
Earnest Oglesby Professor
and Dean

DTIC
ELECTE
SEP 2 5 1985
S D
B

DTIC FILE COPY

SCHOOL OF ENGINEERING AND

APPLIED SCIENCE

DEPARTMENT OF MATERIALS SCIENCE

UNIVERSITY OF VIRGINIA

CHARLOTTESVILLE, VIRGINIA 22901

Final Report

Contract No. N00014-83-K-0242

THE EFFECT OF MICROSTRUCTURE
ON THE
CREEP BEHAVIOR OF Ti-6Al-2Nb-1Ta-0.8Mo

Submitted by:

W. H. Miller, Jr.
Research Assistant

R. T. Chen
Post Doctoral Fellow

E. A. Starke, Jr.
Earnest Oglesby Professor
and Dean

Department of Materials Science
SCHOOL OF ENGINEERING AND APPLIED SCIENCE
UNIVERSITY OF VIRGINIA
CHARLOTTESVILLE, VIRGINIA 22901

AD-A159 532

REPORT DOCUMENTATION PAGE		READ INSTRUCTIONS BEFORE COMPLETING FORM
1. REPORT NUMBER	2. GOVT ACCESSION NO.	3. RECIPIENT'S CATALOG NUMBER
4. TITLE *(and Subtitle)* The Effect of Microstructure on the Creep Behavior of Ti-6Al-2Nb-1Ta-0.8Mo		5. TYPE OF REPORT & PERIOD COVERED Final Report 02/01/83-05/31/85
		6. PERFORMING ORG. REPORT NUMBER UVA/525382/MS86/101
7. AUTHOR(s) W. H. Miller, Jr. E. A. Starke, Jr.		8. CONTRACT OR GRANT NUMBER(s) N00014-83-K-0242 (P00001)
9. PERFORMING ORGANIZATION NAME AND ADDRESS Department of Materials Science University of Virginia, Thornton Hall Charlottesville, VA 22901		10. PROGRAM ELEMENT, PROJECT, TASK AREA & WORK UNIT NUMBERS Proj. No. 431
11. CONTROLLING OFFICE NAME AND ADDRESS Office of Naval Research/Dept. of the Navy 800 N. Quincy Street Arlington, VA 22217		12. REPORT DATE September 1985
		13. NUMBER OF PAGES 127
14. MONITORING AGENCY NAME & ADDRESS *(if different from Controlling Office)* ONR Resident Representitive Joseph Henry Building, Room 623 2100 Pennsylvania Avenue, NW Washington, DC 20037		15. SECURITY CLASS. *(of this report)* Unclassified
		15a. DECLASSIFICATION/ DOWNGRADING SCHEDULE

16. DISTRIBUTION STATEMENT *(of this Report)*

Unlimited

DISTRIBUTION STATEMENT A

Approved for public release
Distribution Unlimited

17. DISTRIBUTION STATEMENT *(of the abstract entered in Block 20, if different from Report)*

18. SUPPLEMENTARY NOTES

19. KEY WORDS *(Continue on reverse side if necessary and identify by block number)*

Ti Alloys, Creep, Microstructure-Properties

20. ABSTRACT *(Continue on reverse side if necessary and identify by block number)*

The effects of microstructure, temperature, stress level and crystallographic orientation on the creep response of Ti-6211 have been investigated. A variety of microstructures simulating the heat affected zone of a weld (HAZ) as well as the as-received structure were tested in a temperature range of 298K to 873K. At stress levels below the tensile yield strength, creep curves level off and saturate in the ambient temperature regime.

(continued on back)

DD FORM 1473 EDITION OF 1 NOV 65 IS OBSOLETE

20. ABSTRACT

The colony type Widmanstätten alpha + beta as-received structure exhibited the highest creep strains at ambient temperatures (T<0.2Tm), Long slip lengths associated with large colony size and a $(0002)_\alpha$ // $\{110\}_\beta$, $(1120)_\alpha$ // $(111)_\beta$ Burgers orientation relationship in addition to sliding along colony boundaries and alpha/beta interfaces account for relatively high creep strains to saturation. Planar arrays of straight dislocations and the predominance of a single operative slip system were observed for samples crept at 298K while thermally activated cross slip was observed for samples crept at 453K. Beta-annealed martensitic microstructures displayed enhanced creep resistance, out-performing other recrystallized equiaxed HAZ microstructures.

Steady state creep was attained at elevated temperatures (T>0.4Tm) where wavy dislocation lines and dislocation loops were more homogeneously distributed than at ambient temperatures. Activation energy determinations indicate that creep mechanisms are dependent on a creep rate/temperature relationship. Above 778K the activation energy of creep is close to that of self-diffusion in titanium, suggesting that diffusion-controlled dislocation mechanisms are the rate-controlling processes at elevated temperatures.

Creep rupture at elevated temperatures occurred by microvoid nucleation and growth. Fracture occurred along colony boundaries in the as-received structure while appearing to be intergranular with the crack propagating along G.B.α/matrix interfaces in the equiaxed microstructures. Sliding along alpha/beta interfaces, colony boundaries, prior beta grain boundaries and slip traces contributed to the creep strain and rupture process.

Cyclic creep with a loading-unloading sequence was performed at room temperature and cyclic creep acceleration was observed. The reduction of internal stress in the unloading period enhanced the creep rate in subsequent loading.

TABLE OF CONTENTS

CHAPTER I

INTRODUCTION

Development of the Kroll and Hunter processes in the 1950's thrust titanium to the forefront of advanced technology materials[1,2]. Applications were restricted to gas turbines[1], structural air frame members and other components requiring superior performance in order to justify the relatively expensive costs of fabrication. Ti-6Al-2Nb-1Ta-0.8Mo is the product of a recent generation of alpha + beta titanium alloys exhibiting high specific strength, elastic modulus and fracture toughness typical of the general class of alloys[1,3,4,5,6]. The alloy's resistance to general corrosion and stress corrosion cracking in salt water coupled with good weldability make Ti-6211 an attractive candidate for modern marine applications[3].

Since Ti-6211 is a weldable $\alpha + \beta$ titanium alloy and its microstructure is strongly dependent on the processing history and thermal treatments[1,3,4,5,7], various microstructures can be generated in the heat-affected zone of the weld[8]. Imam and Gilmore[9] point out that microstructure is an important variable influencing creep strain in titanium alloys. It is, therefore, of practical importance to study the creep behavior of Ti-6211 weld zone microstructures if the alloy is to be used for large welded structures.

Many titanium alloys have been shown to exhibit appreciable amounts of creep at ambient temperatures and at stress levels far below the tensile yield strength of the material[3,6,10,11]. Room temperature creep in Ti-5Al-2.5Sn and Ti-6Al-4V has been studied extensively by several authors[9,12,13,14]. Chu[15-18] previously measured various creep properties and stress relaxation values at room temperature for Ti-6Al-2Nb-1Ta-0.8Mo. Mechanistic studies related to microstructure and deformation behavior, however, have not been made.

Creep of Ti-6211 tested at ambient temperature is of the transient type[6,15-18]. Steady-state creep with a minimum creep rate is generally achieved at elevated temperatures following primary creep. The contribution of diffusion to creep strains and the amount of sliding at grain boundaries, colony boundaries, alpha/beta interfaces and slip traces becomes more significant at high temperature[3,6]. Investigating creep behavior of Ti-6211 at elevated temperatures serves as a comparison for ambient temperature effects and aids in the determination of basic creep deformation mechanisms.

Cyclic loading may enhance or reduce the creep rate depending on material properties and testing conditions[15]. Odegard and Thompson[12,14] have shown that prestrains can accelerate or diminish subsequent creep in the Ti-6Al-4V system depending upon the amount of prestrain and the associated change in internal stress. Imam and Gilmore[9] have reported that stress reversals can

accelerate creep in Ti-6Al-4V. Since, in practical applications, a structural component may be frequently subjected to fluctuating load conditions, the effects of cyclic loading on creep behavior were included in this study.

The effects of modifying microstructure, creep stress levels, creep temperature and cyclic loading conditions on creep deformation were considered in this study. Based on the analysis of creep curves as well as the examination of surface deformation and deformation substructures, the overall material behavior characteristics of creep in Ti-6211 will be discussed.

CHAPTER II

LITERATURE REVIEW

Ti-6211 Phase Relations

The objective of this research is to investigate the effect of microstructural parameters and test conditions on the creep behavior of Ti-6A1-2Nb-1Ta-0.8Mo. In order for a high strength low temperature titanium alloy to be properly utilized on large marine structures it must be weldable and exhibit acceptable properties in the fusion and heat-affected zones of the weld[7]. Due to rapid thermal cycling between ambient temperatures and temperatures approaching the melting point, the FZ and HAZ regions of the weld undergo allotropic phase transformation[6].

Pure titanium consists of a high temperature body-centered cubic beta phase which transforms by diffusionless shear[7] during cooling at 1155K to a low temperature hexagonal close-packed alpha phase. Titanium alloying additions can be divided into groups of either alpha stabilizers, beta stabilizers[1], or neutral additions. Alpha stabilizers consist of "pure" alpha stabilizing

elements which raise the beta transus temperature (Al and interstitials O_2, N_2 and C) and "alpha strengthening" elements which have high alpha soluability (Sn, Si and Zr) but do not raise the beta transus[19]. The amount of alpha stabilizer which can be added is restricted by the formation of α_2, a coherent ordered phase based on Ti_3Al. α_2 precipitation has been found to increase the colony or packet size in Ti-6211, thus increasing the effective slip length[4]. Ti_3Al may also precipitate in the alpha phase and cause embrittlement in some alloy systems during ageing at 773K[1,4]. The effect of Ti_3Al depends upon the alloy system in question. Embrittlement may be avoided if a 9 wt % limit is placed on the "Aluminum Equivalent" as given by equation 1[19].

Aluminum Equivalent = Al + 1/3Sn + Zr + 10(O + C + 2N)   (1)

The beta phase is stable at room temperature only in alloy systems where the solute element is a transition metal[7]. Beta stabilizers fall into two distinct categories[1]: beta isomorphous additions (V, Nb, Ta and Mo), which form solid solutions at all concentrations of the solute element lowering the beta-transus, and beta eutectoid formers (Fe, Cu, Mn and H) which lower the beta-transus and form intermetallic compounds. The beta-eutectoid formers are rarely used commercially since they result in sluggish eutectoid reactions[1]. Certain beta stabilizers, when added to alloys such as Ti-6Al-4V, simultaneously raise resistance to deformation at room tem-

perature while drastically lowering resistance to deforma-
tion at elevated temperatures. Superplasticity[20,21] is
desirable in many cases because of the ease of formability
at high temperature and resulting high strength upon
cooling.

Commercial titanium alloys are generally classified as
alpha, alpha + beta, or beta alloys according to the
dominant phase present[19]. Due to the complexity of
multi-component phase diagrams, alpha + beta titanium
alloys are often represented by psuedo-binary diagrams
containing a fixed amount of alpha-stabilizer as shown in
Figure 1[1]. The most practical creep-resistant titanium
alloys are the near-alpha alloys[19].

Mechanical properties of titanium alloys depend not
only on the phases present but also on the morphology of
each phase. By altering processing techniques[1,4] and
annealing temperatures along with subsequent cooling rates,
microstructures can be developed displaying equiaxed,
platelet, or grain boundary alpha in a retained beta or
martensite matrix. Either phase may be coarse or fine,
continuous or discontinuous, blocky or elongated[5].
Crystallographic texture of Ti-6211 can be varied greatly
by an appropriate ITMT below the beta transus[1,4]. Common
textures include basal texture where the basal planes are
parallel to the rolling plane and transverse texture where
basal planes are perpendicular to the rolling plane and
parallel to the rolling direction. Such texture variations
have been found to significantly alter mechanical

properties.

Widmanstätten Alpha + Beta

Processing involving excursions above the β-transus followed by slow cooling results in a Widmanstätten alpha + beta colony structure[4,5,19]. The β-transus temperature, near 1283K in Ti-6211, is dependent upon relative percentages of alloying elements. A colony structure (array of parallel platelets) or primary alpha platelet structure denotes a specified crystallographic orientation with respect to the prior beta phase. The slow cooling rates which generate the colony structure result in a Burgers orientation relationship between α and β phases of the type $\{0002\}_\alpha$ // $\{110\}_\beta$ and $(11\bar{2}0)_\alpha$ // $(111)_\beta$[1,5]. This Burgers orientation relationship is crucial in deformation studies due to slip length considerations. The Widmanstätten $\alpha + \beta$ microstructure can be annealed high in the $\alpha + \beta$ phase field to increase the volume fraction of the beta phase. Likewise, the equilibrium v/o of the beta phase decreases with decreasing temperature below the beta transus[5].

Primary alpha forms by nucleation and growth in alloys where the final hot working operation is completely below the β-transus temperature. The resulting morphology may range from elongated platelets to equiaxed grains[19]. The prior beta phase, conversely, refers to those regions of microstructure which were beta phase at the annealing temperature or at the finishing temperature of the hot working operation[19,22].

depends only on the instantaneous values of stress and not on previous strain history this is not true for higher temperature creep. The determination of a proportional limit for creep (the stress level below which no creep strain may be recorded is very useful. This limit may be experimentally determined by incrementally loading individual specimens and is represented as a fraction of the yield stress of the particular microstructure.

Creep at High Temperature

Temperature considerations during creep testing often refer to the homologeous temperature (T/Tm)[30]. High temperature creep mechanisms differ significantly from those active at temperatures below $Tm/2$. Significant mechanistic changes in Ti-6211 creep occur between $0.3Tm$ and $0.5Tm$ making this region a particularly attractive candidate for further study. Steady state creep conditions generally occur when the rate of creep recovery is fast enough to offset strain hardening effects, allowing a balance to occur between competing factors. Steady state creep rates display both temperature and stress dependencies as given by the following equations[30,34].

Temperature Dependence:

$$\dot{\varepsilon}_s \propto \exp(-Q/RT) \qquad (4)$$

Stress Dependence:

prehensive than, and includes, Andrade creep[30,34,35]. Andrade initially proposed the equation:

$$\varepsilon = \varepsilon_o (1 + \beta t^{1/3}) e^{(kt)} \qquad (3)$$

which represented the components of transient creep + viscous creep and was based on a compilation of curves to obtain Figure 2. A similar equation to Andrade's but obtaining a better fit was proposed by Garofalo[30,35]. With Cottrell's equation several distinct types of creep may be satisfactorally represented[30,34]:

$$n' = 0 \qquad \dot{\varepsilon} = \text{constant}\ldots\ldots\ldots\text{Steady state creep}$$

$$n' = 1 \qquad \varepsilon = \alpha \ln t \ldots\ldots\ldots\text{Logarithmic creep}$$

$$n' = 2/3 \qquad \varepsilon = \beta t^{1/3}\ldots\text{Andrade's transient creep}$$

$$n' \ (n \sim 1/3) \qquad \varepsilon = At^n \ldots\ldots\ldots\text{General low temperature}$$
$$\text{creep } (n = 1-n')$$

Dislocations with the lowest activation energy move first upon the initial applications of a stress. As low energy dislocations are exhausted creep may continue by moving dislocations of higher activation energies. As this activation energy the creep rate decreases until saturation eventually occurs. It is interesting to note that low temperature logarithmic creep obeys a mechanical equation of state[15,30]. In such a case the strain at a given time

avoid tertiary creep. Stress rupture testing[30,31] intentionally enters the tertiary creep regime where higher loads are necessitated and the test is carried out to the failure of the material. The information obtained from this type of test is the time to cause failure at a given nominal stress and constant temperature. The general procedures for creep testing may be found in several ASTM specifications:

ASTM Des. E8-69, ASTM E-139, ASTM E-150

Creep at Ambient Temperatures

Tertiary creep is rarely experienced at ambient temperatures since creep saturation generally occurs due to lack of recovery. The driving force for creep and the overcoming of deformation obstacles (Peierls Stress) is a result of the combined actions of thermal fluctuations and stress[31]. At low temperatures processes such as dynamic recovery and cross slip may play important roles in the creep scenario since they are not dependent upon temperature enhanced diffusion.

Cottrell proposed a significant equation for a general time law for creep[30,34]:

$$\dot{\varepsilon} = \beta t^{-n'} \qquad (2)$$

where β and n' are experimentally determined constants. Differing creep behaviors are represented by varying values of n'. Cottrell's equation is more com-

at high stress levels, high temperatures or a combination
of the two under constant load conditions where a reduction
in cross-sectional area (A_o) occurs due to necking or void
formation. This region may be associated with the coarsen-
ing of precipitates, recrystallization or diffusional
changes in the present phases and must be avoided totally
in structural applications[30]. Constant stress tests
avoid this type of curve since the load is reduced in order
to keep the stress constant prior to necking. In addition
to elastic and plastic deformation experienced after a load
is applied there exists an anelastic component[12,14] to
creep which is recoverable with time. This anelastic com-
ponent is not generally significant in titanium alloy
testing. The minimum creep rate is the most important
single design parameter. This information is facilitated
in most applications to yield a "creep strength" (15,30),
which is traditionally defined as the stress at a given
temperature required to give either a creep rate of 0.0001
% per hour (1 % /10,000 hr) or 0.00001 % per hour (1 %
/100,000 hr).

It is permissible to assign a creep strength to a
particular material for an arbitrary strain percentage/hour
as long as all testing remains self-consistent. Since very
long time frames are unrealistic for actual testing, $\dot{\epsilon}_s$ may
be based on creep curves of shorter duration. The value of
minimum creep rate is then larger than the true value,
thus, the error is on the conservative side[30]. Ordinary
creep tests are carried out at relatively low stresses to

positive aspect of creep, as McVetty points out, might involve highly localized stresses which may be redistributed by creep deformation, thus preventing failure. In some cases the load-carrying capacity of a structural member may be increased by virtue of deformations resulting from creep. Creep in the majority of cases, however, must be viewed as detrimental.

A basic creep curve may be plotted as strain versus time and includes the three distinct regions labelled in Figure 2 as[30,31]:

I   Transient Creep (Primary Creep)

II   Steady State Creep (Secondary Creep)

III Tertiary Creep

ε_o represents the elastic component of strain observed upon loading. The transient region of the curve, also known as primary creep, exhibits a continuously increasing creep resistance due to strain hardening in the material as a result of deformation. The steady state or secondary creep regime exhibits a nearly constant creep rate given by $d\varepsilon/dt$ or $\dot{\varepsilon}$ and is essentially due to a balance between the competing processes of strain hardening and recovery[30,31,33]. The average slope in this regime is called the minimum creep rate and is important to design parameters. The tertiary region of the curve occurs mainly

partially martensitic heat-affected and near-fusion zones[25]. Several authors suggest post-weld annealing to increase ductility and toughness in the weld zone when possible[14,25].

Creep Overview

Creep is defined as a time-dependent plastic strain experienced under either monotonic constant load or constant stress conditions[30,31]. Many materials undergo limited creep in the ambient temperature range as has been shown to be the case with titanium[3,6,10,11]. Creep rates, creep resistance and rupture times have been found to be dependent on microstructure, stress level and texture to varying degrees[9,13-18]. In general, the strength of a metal decreases with increasing temperature due to an increase in the mobility of individual atoms and the enhanced role of diffusion at elevated temperatures. Increased deformation along grain boundaries as well as the interaction of additional slip systems at higher temperatures enhance creep rates and overall creep deformation leading to a more rapid failure.

McVetty clearly states that creep may be viewed as beneficial or detrimental depending on individual applications and material tolerances[32]. Extended deformation, exceeding permissible tolerances, might well render a machine inoperative. Likewise, some machine parts tend to become unstable with excessive deformation. A

side of the boundary which does not have the Burgers orientation with the adjacent beta phase[29]. The degree of ductility depends on the rate of void growth. If the rate is large, the void reaches a critical size for fracture at a lower applied stress and strain and hence, the ductility is less. The authors proposed that void growth occurs in the alloy tested by local plastic flow at the tip of the void rather than by the linking up of smaller voids well ahead of the main void. Coarse dimpled fractographic structures arise from flow occurring within the plastic zone of the unstably propagating crack[29].

Weld Zones

Whittenberger and Moore stated that weld interfaces have no measureable affect on the overall creep deformation of Ti-6211 which has been diffusion welded[20]. The authors produced diffusion welds without external constraints and with little overall deformation through the use of a soft interlayer between faying surfaces of the harder material. These results, however, do not correllate well with the rapid temperature fluctuations and recrystallization associated with phase transformations in typical Ti weld regions. Bowden found severe ductility losses to occur due to cracking in simulated weldments in Ti-6211 and similar alloys[7]. Odegard and Thompson found that welds do significantly reduce creep rates in Ti-6Al-4V[14]. Baeslack and Mahajan found weldments in highly-alloyed α + β titanium alloys such as Ti-4.5Al-5Mo-1.5Cr to contain

30 % to 50 % of the CRSS. Starke and Lin[5] found tensile dislocation structures in Ti-6211 to be predominantly straight and primarily screw type with only a few edges seen. Screw dilocations in hexagonal networks are commonly observed in hcp metals[27,28].

Deformation twins were observed, both on the surface and by TEM, in Ti-6211 tensile tested in the TD direction[5]. No twins were observed for any other simple tension or simple compression tests for the other materials. Paris, LeFevre and Starke also found occurrences of course deformation twins in beta Ti-V alloys where twinning was associated with moderate volume fractions of the ω phase as a result of high beta stabilizer content[79].

Several authors have shown that thick G.B.α formation during post-weld heat treatments can promote intergranular, low-ductility failure[23,29]. Baeslack and Mahajan[23] found that fracture occurred due to slip incompatibility where voids initiated at G.B.α/transformed-β interfaces and grew into G.B.α and transformed-β regions in the alloys tested (Ti-6Al-2Sn-4Zr-6Mo and Ti-5Al-5Sn-2Zr-4Mo). Greenfield and Margolin[29] note that void nucleation increases with strain and is shown to depend upon both the alpha morphology and its size in Ti-5.25Al-5.5V-0.9Fe-0.5Cu. Void nucleation does not occur in this alloy along the edge of broad Widmanstätten alpha platelets because slip in alpha is readily accommodated by slip in beta. Void nucleation can and does occur at G.B.α but only on that

including stress axis, slip plane and slip direction as well as orientation of the α/β interface in Ti-8Al-1Mo-1V. Their results indicate that the macroscopic flow behavior of colonies comprised of ductile lamellae depends on the ability of a slip system, once activated in the softer α phase, to shear through the harder β phase. The authors observed a variation of more than 2X in CRSS for yielding of individual colonies and the σ_{ys} of a similar colony was found to increase as the slip direction of the dominant macroscopic slip plane approached normality to the α/β interface[24]. Neither the alignment of the slip system in the alpha phase with a potential slip system in the beta phase lamellae nor the orientation of the lamellae to the stress axis appear to significantly influence the yield stress. Planar non-uniform slip has been found to dominate in colonies which yield at low stresses while fine, uniform slip occurs in most high strength colonies[24]. Most individual colonies did not obey Schmid's Law (i.e. yielding did not occur in a single colony at a critical value of the shear stress on a given slip system). Slip compatibility within a colony has been witnessed by many authors and slip bands occaisionally pass through colony boundaries[1,5,6,26].

Ankem and Margolin[26] considered interaction stresses along α/β interfaces where the maximum interactions are found when the stress axis lies in or close to the interface and a 40° incline to the $[0001]_\alpha$ direction. The authors found elastic interaction stresses to be as low as

structures[1]. Despite the small slip distance associated with individual platelets, the large number of platelets accounts for reasonable ductility in the overall structure[1,4].

Bowden[7] spent considerable time studying the subject of ductility loss in Ti-6211 in the temperature range of the hot ductility dip (approx. 750-850°C). Strain localization within the grain boundary regions results in intergranular fracture along prior beta grain boundaries. Ductile rupture occurs by void formation and coalescence along beta grain boundaries. This phenomenon has been found to be microstructure controlled. Beta grain shape along with alpha phase morphology are the critical factors involved in producing low hot ductility, rather than rapid thermal cycling experienced during the welding process[7].

Alpha + Beta Colony Structures

Several authors have conducted studies on the deformation behavior of colony structures in beta-processed $\alpha + \beta$ titanium alloys[5,6,24]. Baeslack and Mahajan[25] stated that if a grain boundary is oriented properly with respect to the stress distribution, intense slip will occur in the alpha and also often in the prior beta grain with which it shares a semi-coherent boundary. A slightly different orientation, however, can prevent macroscopic slip and promote grain boundary sliding and corresponding interphase separation. Chan and co-workers[24] correllated experimental behavior to colony orientation parameters

ments. Borradaile and Jeal[19] state that for a comparable duplex microstructure, smaller mean free slip paths improve the tensile properties as predicted by a Hall-Petch relationship. Lin and Starke stated that increases in strength are associated with a decrease in deformation barrier spacing in the Ti-6211 alloy[4,5]. It has been found that excursions above the β-transus for strengthening purposes are always accompanied by a loss in ductility[5]. Similarly, the incidence of facets appears to be inversely proportional to the ductility. These two conditions are obviously related due to the equiaxed nature of the beta grains that form above the β-transus. During subsequent cooling, soft alpha forms at the beta grain boundaries and because of the equiaxed nature of the beta grains, the α phase is always favorably oriented for slip, resulting in strain localization. In studies involving Ti-6246 and Ti-5524, Baeslack and Mahajan[23] have shown that intergranular cracking and an associated lack of ductility were promoted by the inability of the transformed beta to accomodate slip in the Widmanstatten-α and grain boundary alpha (G.B.α).

Lin, Starke, et al have successfully shown that by quenching Ti-6211 high in the α + β phase field some of the β may be transformed to martensite, resulting in an increase in yield strength of approximately 25 % with no accompanying loss in ductility[5]. Shih verified that the slip length is equivalent to phase size. The accicular alpha acts as the slip length in these duplex

cyclic creep and crack
propagation.

The choice of material for a particular application is
dependent on an optimum combination of several competing
characteristics[19]. Material performance during
mechanical testing is dependent upon alloy composition,
processing history and heat treatment schedule. There are
several microstructural parameters which may affect the
mechanical properties of α + β titanium alloys; some of the
more dominant are[5]:

1.) Thickness of alpha in prior beta grain boundaries.

2.) Size of accicular alpha.

3.) Size and shape of prior beta grains.

4.) Widmanstätten colony size.

5.) Shape of the alpha phase.

Shih, Lin, Spooner and Starke have previously
correlated microstructure and texture to the mechanical
properties of the α + β titanium alloy Ti-6211[4]. They
found that high strength, high ductility and high strain
life combinations are achieved by developing equiaxed-α
microstructures completely surrounded by a strong alpha +
martensite deformation barrier. This is achieved through
appropriate ITMT processing and recrystallization treat-

ing upon critical alloy composition and both are super-saturated in β-stabilizing elements[7]. Tempering hcp martensite leads to heterogeneous β-phase precipitation along martensite plate boundaries with little resultant age-hardening in Ti-6211[7]. This is similar to a heterogeneous alpha phase nucleation along beta grain boundaries in the primary alpha structure. Such boundary nucleation and growth significantly alters mechanical properties of α + β titanium alloys.

Shih, Bowden, and Starke and co-workers have previously discussed alternative Ti-6211 microstructures[1,3,4,5,7].

Deformation Characteristics

Before discussing in detail the concept of creep it is important to understand the deformation of titanium in relation to microstructure.

Titanium has been used in structural alloy form in the aerospace industry for over 30 years[1,2]. The properties of prime concern in mechanical testing can be broken down into three major categories[19]:

1.) Zero time mechanical properties: tensile strength, ductility, fracture toughness.

2.) Real time static properties: creep strength and stabiltiy.

3.) Real time dynamic properties: High and low cycle fatigue,

Recrystallized_Equiaxed_α_+_β

Recrystallized equiaxed α + β, a variation of the hot worked and slow cooled Widmanstätten colony structure, is obtained by cooling from above the β-transus at increased rates. The "Basket-weave" [22] microstructure favors the nucleation of additional variants. This in turn decreases the number of platelets in the Widmanstätten-α packets until a point is reached where the transformed region consists of a totally random mixture of alpha platelets exhibiting no orientation relationship[22]. When this type of microstructure is formed only very small colonies remain interspersed among larger α-platelets thus reducing deformation barrier spacings. Large blocky alpha plates form as a result of even slower controlled cooling rates or step-cooling[22].

Titanium_Martensite

A martensitic structure is formed by suppression of nucleation and growth mechanisms when rapidly quenched from above the β-transus. An increase in v/o of beta during annealing coupled with the subsequent martensitic transformation during quenching results in the prevention of a phase orientation relationship. The resultant decrease in deformation barrier spacing yields a viable strengthening mechanism. The volume fraction and size of martensitic regions can be varied by quenching from different temperatures below the β-transus but above 973K[5]. Either α' (hcp) or α'' (orthorhombic) martensite[7] will form depend-

$$\dot{\varepsilon}_s \propto [\sinh(\alpha\sigma)^n \ldots \text{at high stress.} \quad (5)$$

$$\dot{\varepsilon}_s \propto \alpha\sigma^n \ldots\ldots\ldots\ldots\ldots \text{at low stress.} \quad (6)$$

These equations generally reduce to a combination of effects given by an Arrhenius-type of equation[30]:

$$\dot{\varepsilon}_s = k\sigma^m \exp(-Q/RT) \quad (7)$$

At high temperature metals take on a "viscoelastic" [14,30,35] effect and the strength of the metal decreases as diffusive effects increase. Dislocation climb becomes an important mechanism due to the greater dislocation mobilities. At elevated temperature creep strength becomes dependent on $\dot{\varepsilon}_s$ and time of exposure. The Monkman-Grant[30,34] relationship becomes valid for high temperature low stress tests where intergranular fracture takes place.

$$\dot{\varepsilon}_s \times t_f = \text{const.} \qquad t_f = \text{time to fracture} \quad (8)$$

Another important temperature in the high temperature creep regime is the Equicohesive Temperature. The ECT[34] is the temperature at which the fracture mode shifts from transgranular to intergranular fracture.

Several mechanistic models[35-38] exist for high temperature creep. The dislocation-climb model is given by:

$$\dot{\varepsilon}_s \propto D_s \sigma^{4.5}/kT \quad (9)$$

where the rate-controlling process is the climb of dislocations having an edge component. The Jog-Dragging Screw Dislocation model considers the movement of jogged screw dislocations and is represented by:

$$\dot{\varepsilon}_s \propto D_s \rho \sinh \sigma b^2 l/kT \quad (10)$$

The Recovery-Creep model previously discussed is given by:

$$\dot{\varepsilon}_s = (-\partial\sigma_i/\partial t)/(\partial\sigma_i/\partial\varepsilon) = r/h \quad (11)$$

where: σ_i = internal stress due to strain-hardening, r = rate of recovery and h = rate of strain hardening.

Nabarro-Herring Creep is another diffusion controlled creep process given by:

$$\dot{\varepsilon}_s \propto D_l \sigma/kTL^2 \quad (12)$$

and dependent upon a fine grain size and high temperature. Coble Creep is similar to Nabarro-Herring but depends on grain boundary diffusion as opposed to lattice diffusion:

$$\dot{\varepsilon}_s \propto D_b \sigma/kTL^3 \quad (13)$$

Cross slip generally occurs at intermediate temperatures. It is important to note that quite often more than one creep mechanism may act at any one time yielding complicated mechanisms operating in either series or parallel[31].

Impression Creep

Stress relaxation tests have frequently been used to describe time dependent strain phenomena[33,34]. More recently, however, a new creep test known as impression creep has been gaining popularity[39-44]. Several authors have described the advantages of the new test. Chu and Li[39] have recently explained the concept which uses a circular cylinder with a flat end as an indenter. The indenter reaches a steady state velocity after a short transient period in which the circular end makes a shallow impression in the specimen surface. This test is useful since the same dependencies exist (σ and T) as in conventional unidirectional creep. The three basic mechanisms: bulk diffusion, surface diffusion and dislocation creep have three different stress and indenter size (radius) dependencies[39,40]. Only a small amount of testing material is necessary for impression creep. Stress and temperature tests may be performed on the same crystal and no tertiary creep is experienced. A punch radius vs. impressing velocity curve yields immediate evidence of dislocation creep if it exists; this due to the separation of mechanisms by punch size effects.

Titanium Creep Overview

Titanium in general has a relatively high melting point (approx. 2085K) but creep resistance at even moderate temperatures (around 800K) is poor in comparison

to other elements[45]. The notion of room temperature creep in titanium goes back to Adenstedt in 1949[10] (for pure α titanium). Titanium and its alloys have been shown to be subject to creep at ambient temperatures and at stress levels far below the tensile yield strength[3,6,10,11].

Of the common titanium alloys Reimann found[10] Ti-6Al-4V to show the least amount of room temperature creep. Creep in Ti-6Al-4V is sensitive to microstructural variables such as grain size, microchemistry, phase morphology and preferred orientation. Some authors have shown creep to exist at around 25 % σ_{ys} at room temperature during initial forward loading[9]. The determination of a proportional limit and is highly subjective. This value is based at least partially on the precision[12] of the strain measuring instrument. Imam and Gilmore found the proportional limit to be a strict function of microstructure in Ti-6Al-4V[9]. Reimann found that no creep was experienced in Ti-6Al-4V if the applied stress was less than 85 % σ_{ys}[10]. Proportional limits have consistently dropped in recent years since measurement sophistication has improved and Reimann's findings have since been disputed.

Odegard and Thompson[12] have suggested that proof testing or prestraining Ti-5Al-2.5Sn exhausts the most easily operated dislocation sources and work-hardens the material to a considerably more creep-resistant state. These pre-strains are beneficial for design criterion especially if the operating range of the material will fall

below 80 % σ_{ys}[14]. Reimann[10] also states that stress
relief after forming a component may be beneficial.
Reimann as well as Imam and Gilmore[9] found that
"the creep strain observed during reverse loading was smaller than that observed during initial forward loading", for
creep stresses well below the yield stress. This has been
attributed to the Bausinger Effect. Chu[18] reported that
creep in the amounts investigated, from 0.2 % to 2.7 %, is
beneficial to low-cycle fatigue life, in essence postponing
the onset of fatigue damage in Ti-6211[18]. Creep tests
with long durations, on the order of 10,000 hours, are
generally preferred. Chakrabarti and Nichols[13], however,
successfully creep tested Ti-6Al-4V for 1000 hour periods
at low temperature and 500 hours at higher temperatures.
Ambient temperature saturation at stress levels below the
tensile yield strength generally occurs within the first
few hundred hours from loading. Creep rupture tests
require longer periods of time since they are dependent
upon the onset of tertiary creep and fracture.

Strengthening Additions

The two primary approaches to increasing creep
resistance in titanium involve either the reduction of slip
lengths in the microstructure[4] or the addition of Si and
Zr to the alloy. Winstone et al [46] found Zr to be the
most effective strengthener in terms of creep resistance in
several titanium alloys investigated. Similarly, Paton and
Mahoney[45] found some of the highest creep strengths to be

associated with silicon in solution in alloys subject to their investigation[46]. Creep resistance of Si alloys is improved by Si precipitation on mobile dislocations resulting in a pinning of these dislocations and an inhibition of their further movement[45]. Essentially a strong dynamic strain ageing (DSA)[46] arises from a silicon-interstitial atom interaction. These considerations along with the ability of silicon to make O_2 play a more significant role in creep resistance make Si a viable strengthener[46]. Precipitation of Si into Ti_5Si_3, on the other hand, has been found to substantially reduce creep resistance due to the depletion of Si from the matrix[46]. Despite these facts there is still some inability in the field to completely identify with certainty the mechanisms by which creep resistance is imparted by alloying[45].

Impurity Effects

Chu[17] stated that the strength of Ti-6211 $\alpha + \beta$ rolled or beta rolled material is increased by approximately 10 ksi when O_2 content rises from 0.05 % to 0.13 %. The effect of oxygen on the creep strength is similar to the effect on σ_{ys} of the alloy[17]. Rosen and Rottem[47] have produced similar findings for the Ti-6Al-4V alloy where the reduction of ductility is only slight with controlled O_2 penetration. These authors have attributed mechanical property changes to oxygen penetration into the matrix during high temperature exposure. Oxygen has a dual effect on titanium[47,48].

Oxygen may act as a very powerful α-stabilizer thus reducing the beta phase, as well as entering the material as an interstitial in solid solution. Hall[48] found that Ti-6Al-4V creep resistance increases by a factor of four when exposed to air at 900°C for 30 minutes prior to testing. There is danger, however, in overexposure, where O_2 causes the formation of a brittle surface layer known as alpha case[47]. Rosen[47] found that exposure at 900°C for 3 hours resulted in heavy penetration of O_2 leading to extreme brittleness and hardness while decreasing the toughness and strength of the alloy. The removal of α-case from exposed specimens changes neither the properties nor the mechanism of plastic deformation[47]. Hall found increased creep resistances at short exposure times (30 minutes or less) to be due to the rise of coplanar slip which promotes well-defined slip bands. Many dislocations of the same sign are closely spaced in these slip bands leading to an increase in the internal stress and opposition to dislocation motion[48]. Rosen and Rottem speculate that exposure at 900°C for 30 min causes a slight increase of oxygen in solid solution in the bulk and creation of very fine, perhaps coherent oxides which can be very effective in pinning dislocations[47]. Further exposure results in more homogeneous dislocation distributions and large amounts of dislocation debris yielding a reduced creep resistance. Above approx. 758°C O_2, N_2 and H diffuse rapidly into titanium alloys[47,48]. Hydrogen is always detrimental and has been experimentally shown to increase

creep rates in Ti-5Al-2.5Sn through the formation of hydrides[14,49].

Titanium Creep at Ambient Temperatures

Studies concerning room temperature creep in tough materials such as titanium are important since design stresses for ambient temperature applications are often large fractions of the yield stress[3]. The creep saturation values obtained are largely dependent on applied stresses and microstructure at low temperatures. The presence of a weld, which is an integral element of large scale titanium fabrication, necessitates high stress level creep testing of equiaxed weld zone microstructures.

In a study involving Ti-5Al-2.5Sn[12], Thompson and Odegard found the ambient temperature proportional limit for creep to be approximately 80 % σ_{ys} with some indication of small creep strains below this value in certain microstructures. Creep was of the transient variety fitting the empirical equation: $\varepsilon = At^n$[12,15-18]. No steady state creep was observed and the magnitude of creep strain was attributed to the case of dislocation source exhaustion[12]. Thompson and Odegard proposed that the creep process in both Ti-6Al-4V and in Ti-5Al-2.5Sn is based on thermally activated overcoming of interstitial solute atoms and that the exhaustion of the easiest dislocation sources[12,14] at each stress level could be the reason for creep saturation. Dislocation studies and related studies give strong evidence to support this

theory[3,12,14,50].

In the 40 % to 90 % σ_{ys} test range for Ti-5Al-2.5Sn at room temperature, activation energies (Q) were found to be in the range of 37 KJ/mole which is approximately 1/4 of the 150 KJ/mole value for self-diffusion in titanium[12]. This finding correllates well with the theory based on the overcoming of interstitial solute atoms. Odegard and Thompson[14] studied Ti-6Al-4V below 80 % σ_{ys} at room temperature and found that dislocation loops were common near triple points where local accomodation stresses are greatest. This agrees with the Ti-6Al-4V study conducted by Chakrabarti and Nichols[13] who found that creep strains in the first 50 hours of testing were 2.5X greater in fine grained microstructures than in coarse grained microstructures[13]. Imam and Gilmore further found that β-annealed equiaxed microstructures exhibit the smallest $\dot{\epsilon}_c$ for Ti-6Al-4V[9]. Chu[15], who has previously studied creep in Ti-6211, shows that creep strains follow the relationship: $\epsilon = At^{0.152}$. Chu[20] discusses a more general case where:

$$\epsilon = aS^m t^n \qquad (14)$$

where S = stress (ksi) and a, m, and n are determined experimentally from the material tested. Chu also suggested that weldments had a higher resistance to creep than rolled plate (by an approximate factor of 18)[16]. Unlike studies on Ti-5Al-2.5Sn where no phase relationship was found[12], a Burgers orientation relationship does exist

between α and β in Ti-6211. Chu finally states that approx. $3/4\sigma_{ys}$ may be used in applications of the material if some creep is tolerable[16].

Titanium Creep at High Temperature

Sastry, Pao and Sankaran[36] have found that two phase Ti alloys have significantly higher creep rates than single phase alpha alloys at high temperatures. Decreasing the Al content results in a reduction in creep rate. In general α or β alloys have higher flow and lower ε sensitivity values than the dual phase alloy Ti-6Al-4V. Indeed, the authors state[36]:

"to obtain a suitable constituative equation for high temperature flow of titanium alloys, the effects of alloy composition, grain size, volume fractions of phases and texture, on temperature and strain and strain rate dependencies of the flow stress must be known". The rule of mixtures was found to be inadequate for describing the high temperature flow of the two phase Ti-6Al-4V alloy. Fine grained microstructures exhibit greater creep due to sliding at high temperature[36]. Dislocation substructures in Ti-6Al-4V show networks formed by cross slip and climb. Rosen and Rottem[47] state that creep in Ti-6Al-4V above 400°C is controlled by dislocation climb while other authors have have stated that deformation mechanisms in Ti-6Al-4V change from dislocation climb at 850-900°C to dislocation glide at 700°C[36]. Sastry and Sankaran do, however, find dislocation climb at 450-600°C and at low

stress levels with the apparent activation energy for creep at Q = 188 KJ/mole[36]. This is significant since the value for self-diffusion in titanium is close to 150 KJ/mole. Winstone, Rawlings and West found activation energies in the range of 280 KJ/mole[46] due to increased silicon in solution. These values are much greater than those for diffusion of substitutional elements in titanium. Paton and Mahoney state that the rate controlling creep mechanism is not simply the diffusion of Si but a more complicated mechanism[45]. While Ti-6211 was not developed for high temperature applications, contributions of diffusion to creep deformation and sliding at α/β interfaces, colony boundaries and prior beta grain boundaries are more significant in the high temperature, steady state creep regime[3,6].

Grain Boundary Sliding

It is a well established fact that grain boundary sliding may contribute substantially to the overall deformation processes in certain alloy systems. Indeed several authors have shown that interface sliding in general may be responsible for large percentages of the total strain experienced in tensile and creep testing[25,45,51,52]. Edward and Ashby have shown that grain boundary sliding concentrates stress on boundaries which lie normal to the tensile stress axis[53]. This sliding may be accomodated elastically, by diffusion,

plasticity or creep. The alternative to boundary sliding is the appearance and growth of cavities and cracks. Several authors have extensively reviewed cavitation in creep and the formation of void sites[54-57]. Grain boundary sliding has been noted as a principle source of creep deformation at elevated temperatures[30]. Baik and Raj[58] state that low temperature transgranular fracture yields to higher temperature cavitation failure which is brought on by grain boundary sliding in Al-5Mg. A specimen will fail intergranularly by cavitation if the cavities grow faster than the neck. Grain boundary migration theory states that a grain boundary moves normal to itself under the influence of a shear stress and relieves strain concentrations[30]. The total strain is the sum of strain due to slip within individual grains plus the strain due to grain boundary sliding.

There is a close relationship between crystallographic slip and grain boundary sliding. Slip is not uniform along all boundaries. At higher temperatures, a shear process is activated in the direction of the grain boundary brought on by the elevated temperature state or by a low strain rate[30]. Many authors have attempted to place high resolution grid networks on specimen surfaces prior to deformation testing[13,25,45,51,52,59,60]. Such "markers" are used to yield quantitative data on interface sliding. Paton and Mahoney used electron beam lithography to place 1μm wide gold grid lines onto titanium-silicon specimen surfaces prior to creep[45]. The authors

concluded that grain boundary sliding was probably not of great importance as a deformation mechanism in the Ti-Si series of alloys tested. Most sliding occurred along prior-β grain boundaries in Ti-5Zr-0.5Si and contributions in all three microstructures tested were less than 10 %, not a major creep mechanism for the test conditions[45]. Anken and Margolin discuss α/β interface sliding in several microstructures of a Ti-Mn alloy[52]. Deformed grid networks after compression testing showed sliding to occur on one side of an α/β interface but not on the other due to phase incompatibilities.

Baeslack and Mahajan tensile tested the titanium alloy CORONA 5 in an investigation concerned with room temperature α/β interface sliding[25]. Substantial grid marker offsets were seen at G.B.α/ transformed beta interfaces. Sliding, however, was not observed at Widmanstätten alpha/transformed beta interfaces. Long time tensile loading did not result in observable creep deformation, which illustrates the fact that the mechanism of sliding is fundamentally different than that of diffusion-controlled sliding at high temperatures.

A multiplicity of equations have been put forth which would calculate relative strain percentages due to grain boundary sliding[59,61-67]. Stevens reviewed many of the flaws contained in early attempts at calculating boundary offsets[64]. The method of calculating such values from observable marker offsets on specimen surfaces has been a matter of much dispute in recent times. Parameters for

calculating ε_{gbs} values generally include specimen surface vs. specimen interior[61] sliding compatibility and whether a specimen is "cut" (specimen surface polished prior to creep testing) or "annealed" (where a specimen is given a heat treatment anneal but not polished prior to testing). Langdon[61,62] summarized that bulk material sliding is roughly equivalent to surface sliding for low total strains in specimens having cut surfaces. Figure 3 illustrates the parameters considered in grain boundary sliding calculations[61,62]. Langdon concluded that:

$$\varepsilon_{gbs} = 2n_1(\overline{w}/\tan\theta)_1 \quad (15)$$

where:

n_1 = number of grains or deformation barriers per unit length measured parallel to the stress axis.

$\overline{w}$ = average value of measured grid offsets in direction perpendicular to the stress axis.

θ = angle between surface trace of the boundary and the stress axis.

This may be simplified to:

$$\varepsilon_{gbs} = k'n_1\overline{w}_1 \quad (16)$$

where: k' = constant of approximately 1.5 determined experimentally from dependencies of $\overline{w}$ on θ.

The value of ε_{gbs} divided by ε_T gives a rough approximation of the percentage of total deformation that is due to boundary sliding.

Figure 4 shows relative grid offsets associated with grain

ROUND TENSILE CREEP SPECIMENS

2.5"

Threaded Ends: 3/8--24
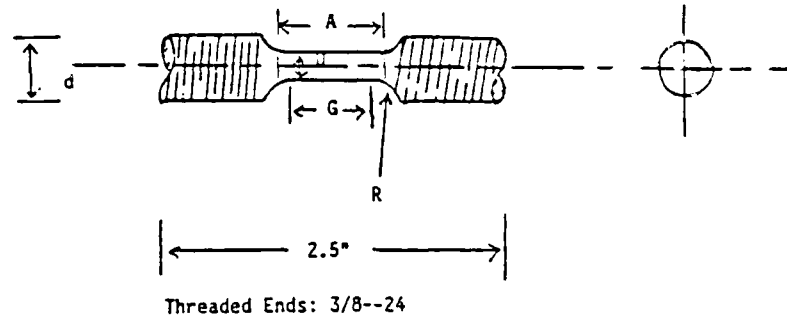
G: Gage Length..........................G = 0.787"

D: Diameter (Gage Section)..............D = 0.197"

R: Radius of Fillet.....................R = 11/64"

A: Length of Reduced Section...........A = 0.945"

d: Diameter of Grip Section.............d = 3/8"
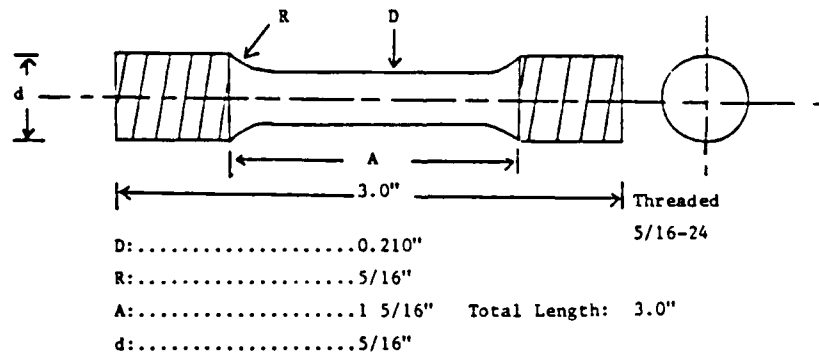
Total Length: 2.5"

LOW CYCLE FATIGUE SPECIMEN

2.0"
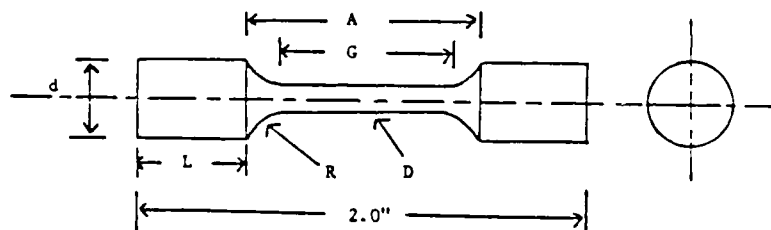
G:.............................0.4"

D:.............................0.18" Not Threaded

R:.............................1/4" Total Length: 2.0"

A:.............................0.5"

d:.............................0.25"

L:.............................3/4"

Figure 6.   Specifications of room temperature creep
and LCF specimens used during the investi-
gation.   High temperature creep specimens
were similar to R. T. creep specimens but
grooved in radius of curvature for extenso-
meter jaws.

STANDARD TENSILE SPECIMEN
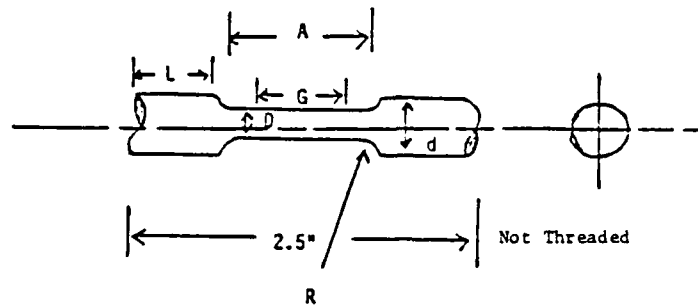
G: Gage Length.........................G = 0.630"
D: Diameter (Gage Section)...........D = 0.156"
R: Radius of Fillet..................R = 0.156"
A: Length of Reduced Section.........A = 0.787"
d: Grip Section Diameter.............d = 0.276"
L: Grip Section Lengths..............L = 0.7"

Total Length....2.5"

HIGH TEMPERATURE TENSILE SPECIMEN

D:.....................0.210"
R:.....................5/16"
A:.....................1 5/16"   Total Length: 3.0"
d:.....................5/16"

Figure 5. Dimensions of tensile specimens used in
Ti-6Al-2Nb-1Ta-0.8Mo study.

TABLE 2. HEAT TREATMENTS AND RESULTANT MICROSTRUCTURES

DESIGNATION	HEAT TREATMENT	MICROSTRUCTURE	PRIOR BETA* GRAIN SIZE	AVERAGE** COLONY SIZE
W1	As-Received	Widmanstätten alpha + beta (Colony Type)	0.19 mm (TD) / 0.79 mm (RD)	45 m / -
W11***	" " "	" " " "	0.22 mm (TD) / 0.83 mm (RD)	55 m / -
W2	1050°C/40min/AC	Widmanstätten alpha + beta (Basket-Weave Type)	0.45 mm	-
W8	1050°C/40min/AC +950°C/4hr/AC	Widmanstätten alpha + beta (Basket-Weave Type) + thick grain boundary alpha	0.45 mm	-
W12***	" " "	" " " "	0.8 mm	-
W3	1050°C/40min/WQ	Martensite	0.45 mm	-
W9	1050°C/40min/WQ +950°C/4hr/AC	Tempered Martensite	0.45 mm	-
W15***	" " "	" " " "	0.6 mm	-

* Prior beta grain size approx. 8 mm below plate surface.

** Average linear intercept length.
  TD: Transverse direction
  RD: Rolling direction

*** Heat II Microstructures.

TABLE 1. Chemical Composition in Weight Percent

	Al	Nb	Ta	Mo	O	N	H	C	Y	Mn	Si	Fe	Cu	Ti
Heat I	5.6	2.16	0.95	0.79	0.066	0.007	0.0046	0.02	<0.002	<0.01	<0.01	-	-	Bal
Heat II	5.9	2.0	0.93	0.60	0.056	0.011	<0.01	0.02	-	<0.01	<0.01	0.06	<0.01	Bal

After a final bake-out for hardening, gold was pulse-plated onto exposed specimen surfaces (cathodes) from a proprietary plating bath known as Autronics-N. Only the gold grid network remained on the surface of the polished and etched microstructure following the removal of the remaining resist squares with the aid of a hot basic solution. This approach yielded clean microstructural features coupled with highly delineated markers (Figure 9c).

Various techniques have been employed to conduct sur-
face deformation studies. Surface scratches were inscribed
on well polished and etched specimen surfaces using sharp
diamond-tip pencils. Gold grid patterns were deposited on
the specimen surface by sputtering gold through a 300 mesh
nickel grid. The inscribed and/or grid-deposited surfaces
were examined using SEM techniques after creep deformation.
Two stage replicas with Au-Pd shadowing were prepared and
examined with TEM to detect offsets at interfaces such as:
grain boundaries, colony boundaries and α/β phase boun-
daries.

Grid Deposition

The most successful attempts at quantitatively
determining surface offsets involved a grid depostion tech-
nique facilitating photolithography. Grid networks of 5μm
wide and 1μm wide gold lines with 30μm and 11μm
separations, respectively, were electroplated onto polished
and etched titanium surfaces prior to deformation. The
process involved spinning a thin layer of Shipley AZ-1450B
positive photoresist onto meticulously clean flat deforma-
tion specimens at 3000 RPM's. The resist was pre-baked and
the specimens were brought into intimite contact with the
glass-backed chrome grid network by a mechanical mounting
press and air pressure. The surface was exposed to intense
ultraviolet light with the grid network in place. Only the
photoresist squares remained after the chrome grid was
removed and the photoresist was developed (Figure 9b).

applied hydraulically by the weight and pan method. Creep strains during ambient temperature testing were monitored and recorded with Micro-Measurements Series EA precision foil strain gages[68], Fisher strip chart recorders and V/E-20A Digital strain Indicators. High temperature creep was accomplished in an argon atmosphere purified with a Centorr 2B-20-Q Gettering Furnace. Creep strains were measured using an LVDT in unison with a high temperature extensometer enclosed in an inconel retort assembly. A three-zone resistance-type furnace and temperature control-ler enabled temperatures to remain uniform to within 2K along specimen gage lengths (Figure 8)[68].

Microscopy

Tensile fracture surfaces and creep rupture specimens were coated with a layer of gold and examined using a JEOL JSM 35 SEM operating at 25KV. TEM thin foils cut from various tensile and creep specimen orientations were prepared using a Tenupol twin jet polishing apparatus and an electrolyte consisting of 6% Perchloric acid, 35% N-Butanol and 59% Methanol operating at $-30^{\circ}C$ and 19 volts. Hydride formation was kept to a minimum by operting at tem-peratures below $-25^{\circ}C$ (thus eliminating preferential alpha phase attack)[49]. Thin foils were examined using a Philips 400 transmission electron microscope operating at an accelerating voltage of 120 KV.

Surface Deformation

specimens were machined and tested in the LS and LT orientations for surface deformation studies. Specimen dimensions and shapes are listed and illustrated in Figures 5 through 7. LCF samples were employed in cyclic creep testing.

Tensile Deformation

Tensile, cyclic creep and LCF tests were conducted on a closed-loop servohydraulic MTS machine equiped with an 8mm clip-on extensometer at room temperature and a 12mm water-cooled extensometer at elevated temperatures. Tensile tests were performed at a constant strain rate of $10^{-3}s^{-1}$. Precision deformation tests were carried out at both ambient and high temperatures at a strain rate of 5 x 10^{-3} sec^{-1}. High temperature tensile deformation testing was performed in laboratory air with induction heating. Cyclic creep tests were performed at room temperature under conditions of constant load amplitude, square wave form and stress ratios of R=0.1 or 0.9 through a two minute period. Test specimens were mechanically polished prior to testing through either the 0.25μm diamond stage or with 0.05μm alumina dependent upon application. High resolution specimens were subsequently cooled cryogenically and elec-tropolished.

Creep Testing

Static creep tests were performed on Tinius-Olsen lever-arm-loading type creep machines. Creep loads were

annealed structures. Heat treatments and resulting microstructures are listed in Table 2. Laboratory heat treatments were conducted in a high purity flowing argon atmosphere with a Lindberg furnace capable of a sustained temperature of 1200°C.

Microstructures of the five different heat treatments were observed and characterized by optical metallography carried out on a Zeiss metallograph with Namarski polarizing filter capability. The modified Kroll's reagent consisting of:

$$85 \text{ ml } H_2O + 10 \text{ ml } HNO_3 + 5 \text{ ml } HF$$

was used as the etchant on all of the microstructures of interest.

Texture

Crystallographic texture determinations were carried out on a Siemens goniommeter using the reflection method. Pole figures (0002) and (10$\bar{1}$1) were plotted with the aid of a computer program to determine preferred orientations.

Specimen Geometry

Cylindrical tensile and creep specimens as well as low cycle fatigue (LCF) specimens were machined such that the axis of loading corresponded to the rolling direction of the as-received plates. In specified cases, as-received specimens were machined parallel to the short transverse plane. This provided better delineation of grain boundaries in the W11 structure. Flat tensile and creep

CHAPTER III

EXPERIMENTAL PROCEDURE

Material

Two heats of the Ti-6Al-2Nb-1Ta-0.8Mo alloy were cast and rolled in the form of one-inch-thick plates. The first plate was received from the David Taylor Naval Ship Research and Development Center (DTNSRDC), Annapolis, Maryland and was designated as Heat I. Heat II was received from the RMI Company, Niles, Ohio. The chemical compositions of both heats are listed in Table 1.

Heat Treatments

Several heat treatments were selected in order to simulate the heat affected zone (HAZ) of a Ti-6211 weld region. Each of four distinct simulated HAZ microstructures were obtained by heating above the 1010°C beta transus and cooling at different rates. The as-received condition (W11) displayed a Widmanstätten alpha + beta colony structure which is common among beta-processed $\alpha + \beta$ titanium alloys. The four HAZ microstructures exhibited large equiaxed grains typical of recrystallized beta-
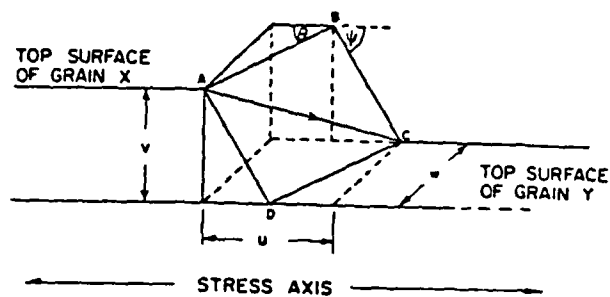
Figure 3.   Illustration of the parameters considered
in grain boundary sliding calculations.
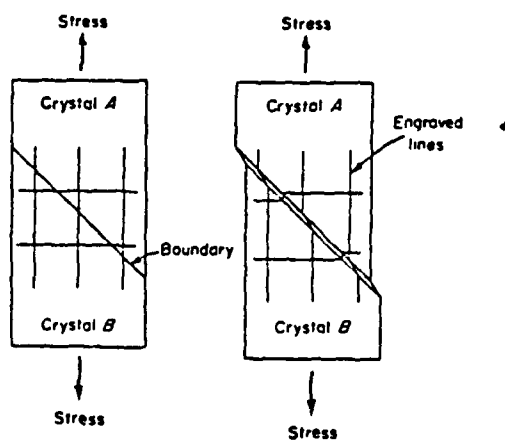
Figure 4.   Relative grid offsets associated with
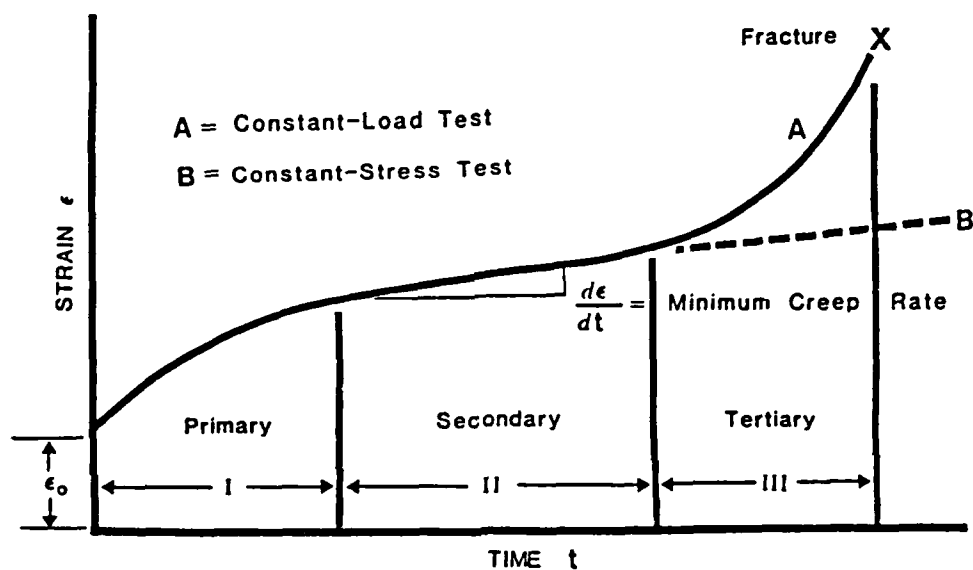grain boundary sliding and shear.

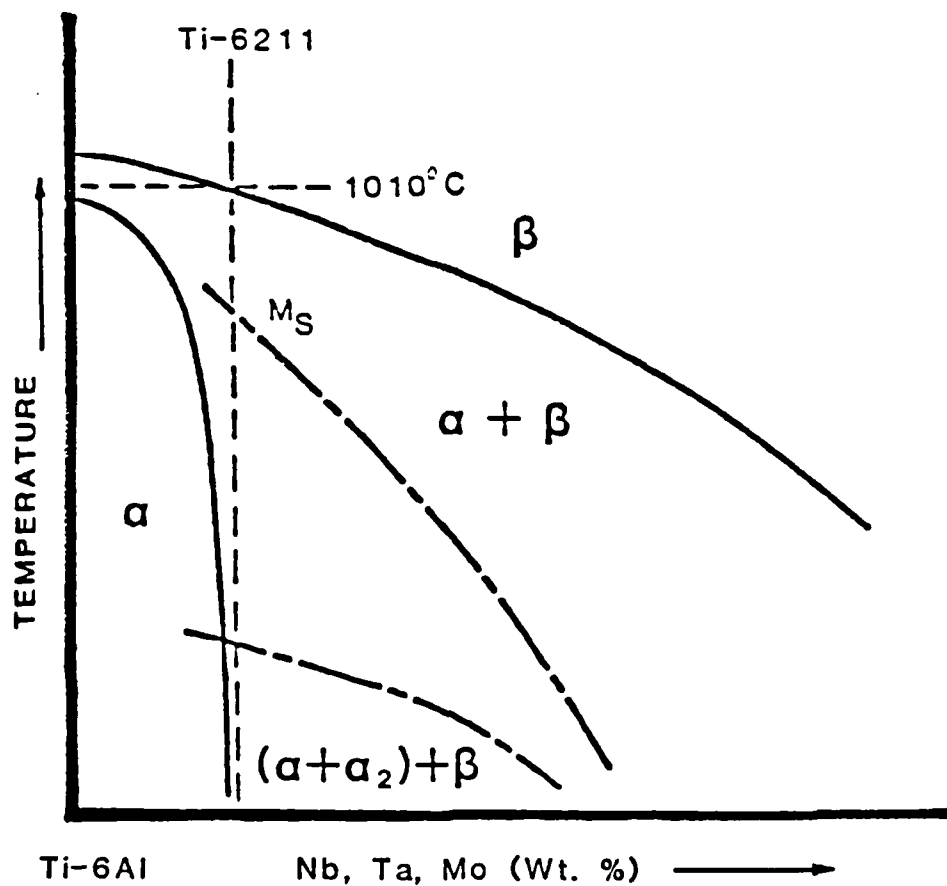Figure 2. Regions of a general creep curve plotted
as strain versus time.

Figure 1. Pseudo-binary phase diagram for Ti-6Al-1Ta-0.8Mo
alloy system showing fixed amount of Al and
varying percentages of beta-stabilizing
alloying elements.

boundary sliding and shear[31]. It should be noted that boundary sliding determinations are only approximations and that standards in the field have not yet been developed due to the complexity of the problem.

SURFACE DEFORMATION SPECIMEN

G: Gage Length.........................0.550"

D: Diameter (Gage Section)............0.175" Total Length: 2.20"

K: Specimen Pin Length................1.630"

h: Hole Diameter (Pin)................1/4" Specimen Thru-
                                              Thickness: 1/16"

1: Specimen Grip Width................0.60"
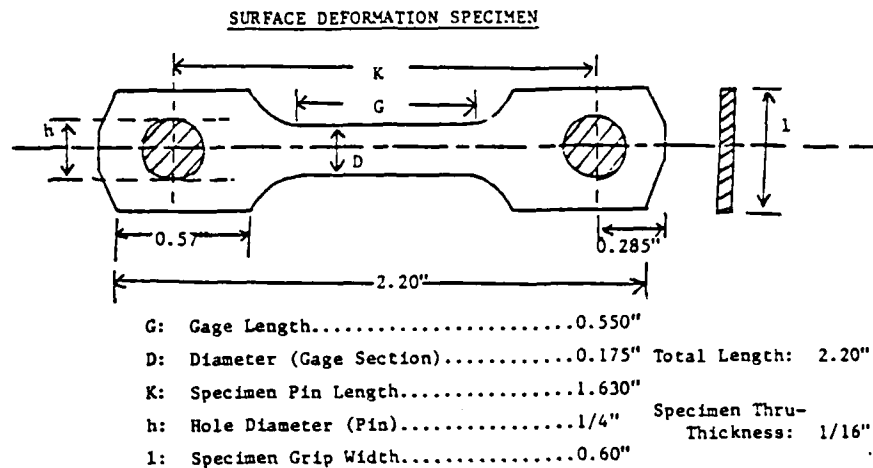
Figure 7.   Flat surface deformation specimen. This
             type of specimen geometry was employed in
             the grid-deposition process.
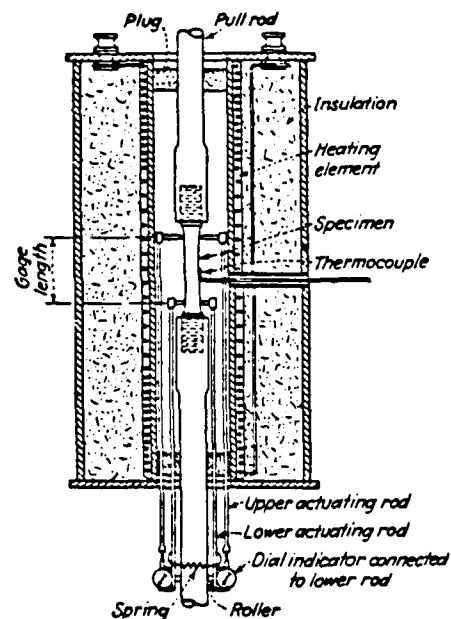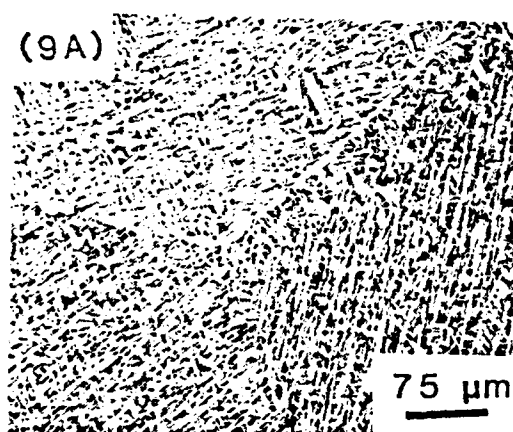

Figure 8.   Diagram of general high temperature
             retort assembly. A similar device was
             used for creep testing in a controlled
             environment for extended periods of time.
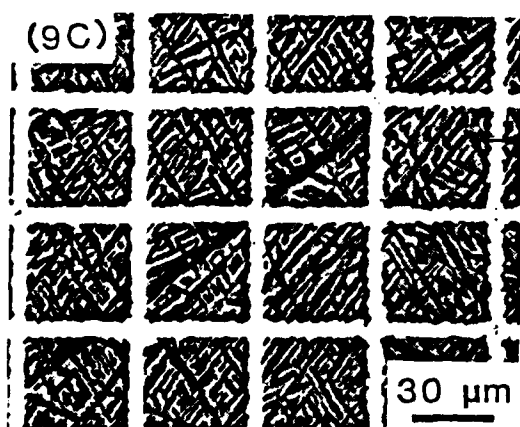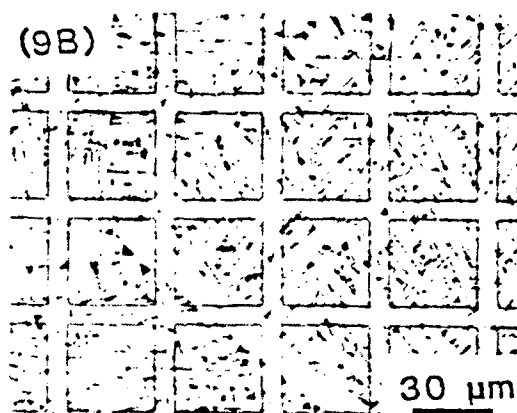
9A) Polished and etched specimen
surface prior to grid deposition
(W15 Structure).

9B) Photoresist squares on specimen
surface after pattern exposure
(W15 Structure).

9C) 5μm gold grid network in place
after electroplating and removal
of remaining photoresist
(W12 Structure).

Figure 9. Grid deposition sequence for surface
deformation studies.

CHAPTER IV

RESULTS AND DISCUSSION

4.1 Microstructure

4.1.1 Microstructural Characteristics

The heat treatment schedule and resulting microstructures of interest were previously summarized in Table 2. Representative features of each microstructure can be seen in the optical micrographs shown in Figures 10 and 11. TEM micrographs in Figures 12 and 13 illustrate the differing phase morphologies of the microstructures of interest. The as-received structure displayed substantially different characteristics from the HAZ structures due to the rolling process. The microstructure of the as-received condition, W1 from Heat I as shown in Fig. 10a, has a large colony type Widmanstätten alpha + beta structure due to hot working in the beta-field followed by slow cooling. Figure 11a indicates the presence of large pancake shaped grains and wavy grain boundaries common to the as-received structure

as a result of the rolling process. Figures 12a and 13a show the presence of light hcp alpha platelets interspersed among a matrix composed of thin dark bcc beta platelets. The parallel platelet array gives rise to a Burgers orientation relationship between alpha and beta plates located in the same colony. The $(0001)\{11\bar{2}0\}$ slip system in the alpha phase is coplanar with the $(110)\{111\}$ slip system in the beta phase. This relationship enables planar slip to pass through the harder β-platelets and traverse and entire colony[1,3,4,5,7].

Thru-specimen integrity for the one-inch-thick plate was verified for both colony and grain sizes in the as-received structure. The general microstructure of Ti-6211 in as-received plate form is shown in Fig. 14. Dislocation networks were frequently observed in the alpha phase of the as-received structure near the ends of discontinuous beta plates where stress concentrations arise. These residual dislocations, as shown in Fig. 15, are the result of the decrease in beta phase during transformation that occurs with decreasing temperature.

All four of the simulated weld zone microstructures exhibited equiaxed grain structures due to recrystallization occurring during heat treatment above the β-transus. The β-transus temperature was found to be approximately 1278K for both heats. The β-annealed W2, W8 and W12 microstructures consist of a basket-weave type Widmanstät-ten alpha in a beta matrix. Figures 10c and 11b show the presence of thick grain boundary alpha in W8 and W12

attributed to tempering in the alpha + beta phase field. Small colonies are present in the basket-weave structures as indicated by Figure 13b. The W2, W8 and W12 structures are similar except for the fact that G.B.α and α-platelets are thicker in the W8 and W12 structures. α platelets in these three microstructures are much thicker than in the as-received structures.

Long straight prior beta grain boundaries are evident in the equiaxed martensitic microstructures (Figures 10d, 10e and 11c). The W3 structure consists of martensitic plates due to quenching from above the β-transus. Small martensitic platelets are randomly distributed without an orientation relationship between neighboring platelets in the W3 structure. The W9 and W15 structures consist of primary alpha in a matrix of tempered martensite (Figures 12e and 13c). The W9 and W15 alpha phase is a result of tempering martensite in the alpha + beta field and α platelets are much thicker than in either the W1 or W11 structures. No Burgers orientation relationship exists between alpha, beta or martensite in the beta-annealed structures. G.B.α, however, is generally oriented with one of the neighboring grains. Thickness of G.B.α is non-uniform in W9 and W15 (Figures 10e and 11c).
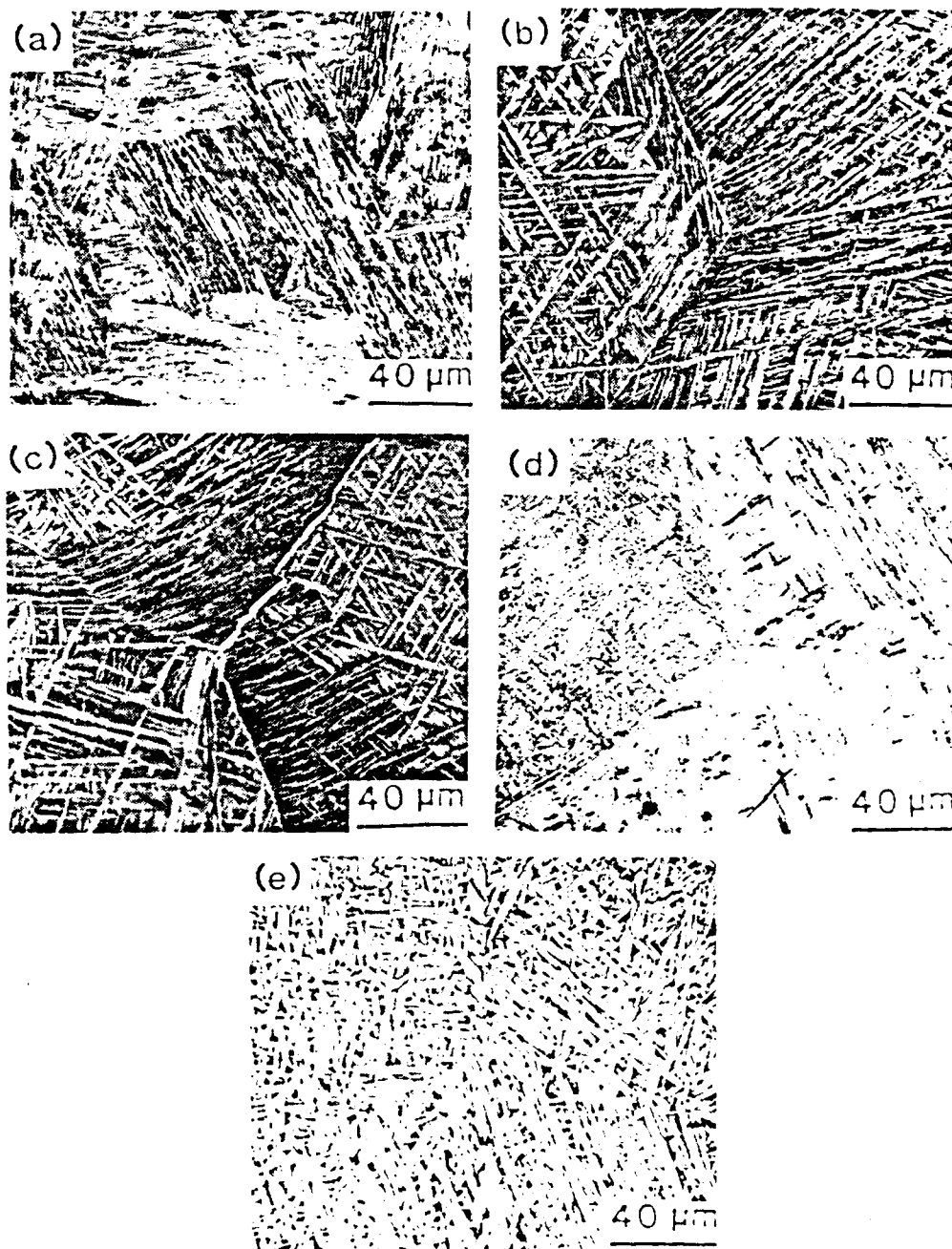
TYPICAL MICROSTRUCTURAL FEATURES OF Ti-6211

Fig. 10. Optical micrographs showing typical features of
(a) W1, (b) W2, (c) W8, (d) W3, (e) W9.

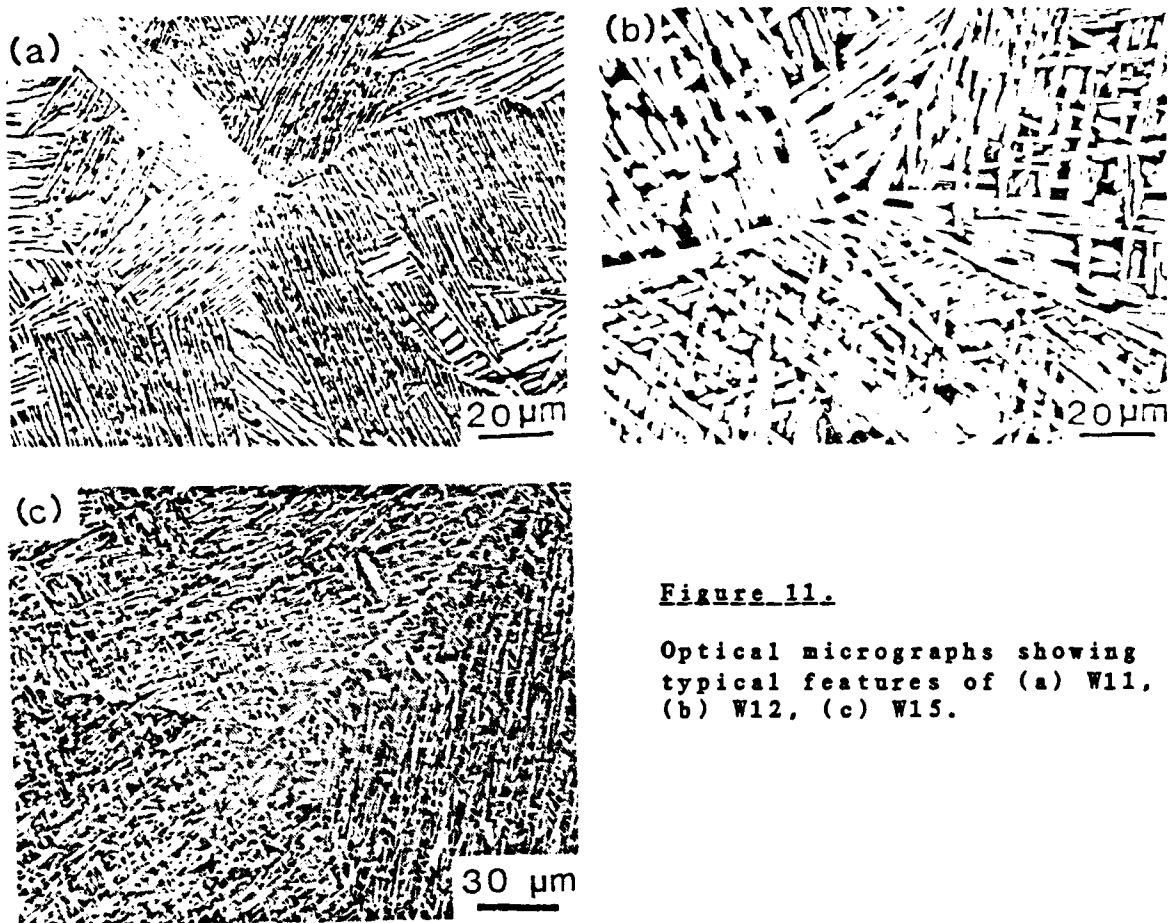# TYPICAL MICROSTRUCTURAL FEATURES

Figure 11.

Optical micrographs showing typical features of (a) W11, (b) W12, (c) W15.
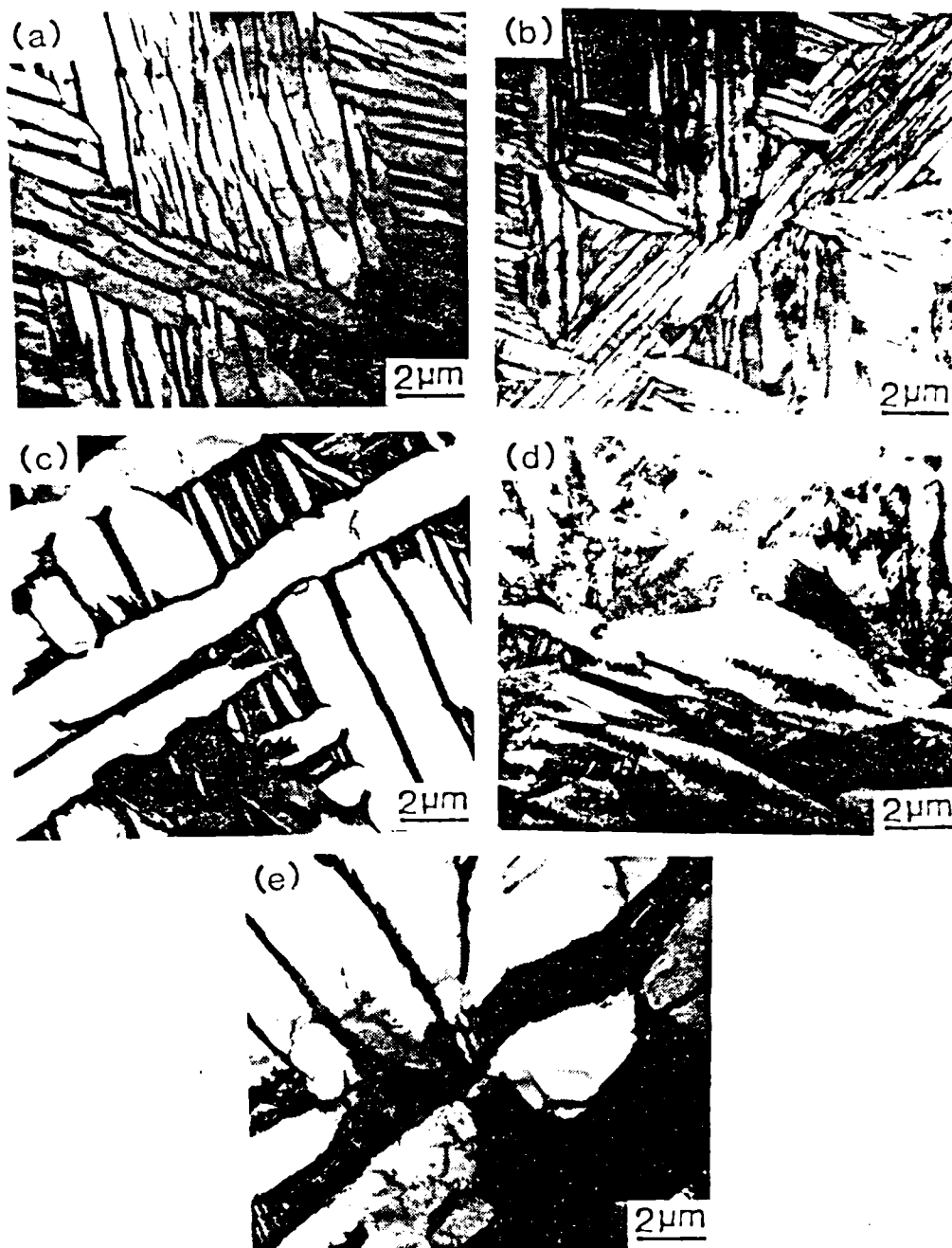
TEM MICROGRAPHS OF FEATURES IN Ti-6211

Fig. 12. TEM micrographs showing typical features in
(a) W1, (b) W2, (c) W8, (d) W3, (e) W9.

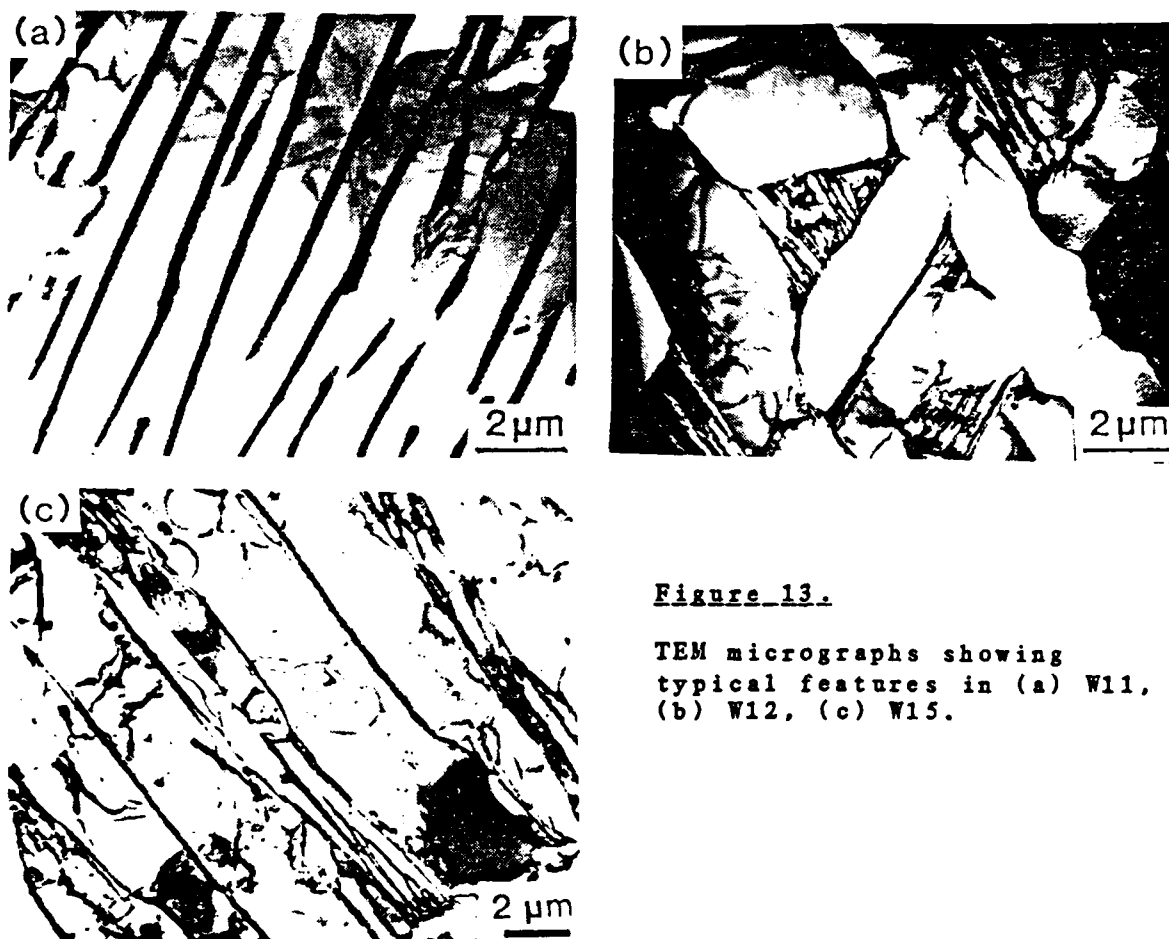TEM MICROGRAPHS OF FEATURES IN Ti-6211

Figure 13.

TEM micrographs showing
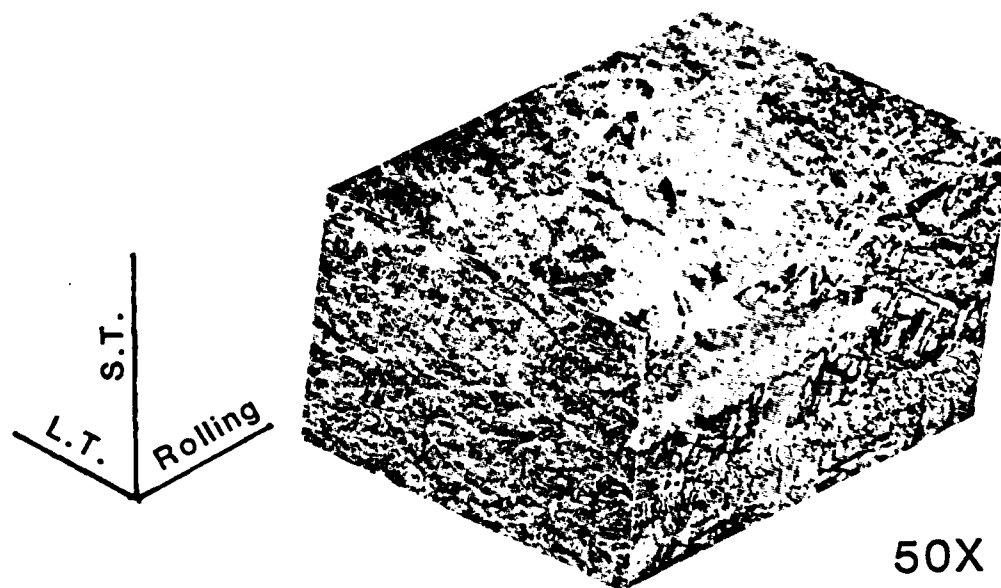typical features in (a) W11,
(b) W12, (c) W15.

S.T.

L.T. / **Rolling**

50X

Figure 14. Microstructure of the Ti-6Al-2Nb-1Ta-0.8Mo as-received plate after etching.

0.2 μm

Figure 15. TEM micrograph exhibiting a dislocation network formed as a result of stress concentrations at the end of a β-plate.

Ambient temperature creep characterization includes all of the microstructures previously described. Many aspects of the study, however, include only the W11, W12 and W15 structures or some combination of these. These three microstructures, all from Heat II, adequately represent the primary characteristics of interest, therefore, the W2 and W3 microstructural variants were not included in certain segments of the investigation.

4.1.2 Texture

A weak texture was found to be present in the as-received structure due to rolling, while the beta-annealed structures exhibited a random texture due to recrystallization. Heat II pole figures $(10\bar{1}1)$ and (0002) from W11 and W12 specimen plates indicate texture does not play a significant role in this study. Certain tests were carried out on the short transverse plane as well as the rolling plane of the W11 structure. This was done primarily for the purpose of testing grain size variation and not to account for texture differences. Texture of the W11 as-received structure taken from a region 8mm below the plate surface is illustrated by the $(10\bar{1}1)$ pole figure shown in Fig. 16a. A random texture is illustrated by the (0002) pole figure for the W12 structure as shown in Fig. 16b. Textures for the Heat I alloy have been characterized previously by Lin, Starke, and co-workers[5]. W11 texture was found to be similar to the W1 structure where a weak

$(11\overline{2}0)[10\overline{1}0]$ texture was seen[5].

TEXTURE OF THE HEAT II ALLOY
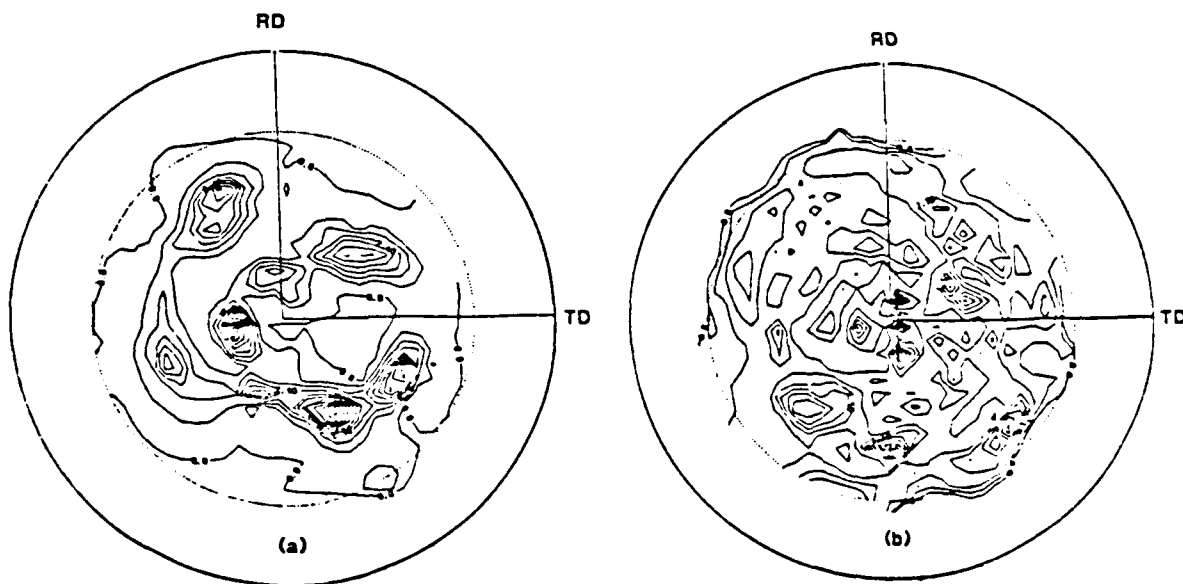
RD

TD

(a)

RD

TD

(b)

Fig. 16.   Computer-assisted plots of a $(10\overline{1}1)$ pole figure
for the W11 microstructure (a) and a (0002) pole
figure for the W12 microstructure (b).

4.2   Tensile Properties

The room temperature tensile properties of the selec-
ted microstructures are listed in Table 3.   The variation
in yield strength for microstructures produced by thermal
modifications is small, the difference being less than 15
%.   Heat II yield strength and ultimate tensile strength

values are consistently lower than Heat I. The difference is most likely due to variation in the oxygen contents (Table I) and its subsequent affect on flow stress. The ductilities of the W1 and W11 structures are greater than those in the equiaxed structures. The beta-annealed structures and the alpha phase along the grain boundaries are much more likely to be favorably oriented for slip. The strain localization that occurs in the G.B.α leads to early crack formation[5]. Grain boundaries in the rolled material tend to be either aligned with or perpendicular to the stress axis due to the nature of the pancake grain shape. Deformation, therefore, tends to occur within individual colonies or along colony boundaries and not along grain boundaries, resulting in greater overall deformation prior to fracture. Curves plotting yield stress and ultimate tensile strength versus temperature in the range of 298K to 873K for the W11, W12 and W15 structures are included in Appendix I. Figure 17a shows dislocation substructures of the W11 microstructure after tensile fracture at room temperature. Figures 17b and 17c show representative dislocation networks from alpha platelets in the W12 and W15 structures, respectively. Dislocations in all three microstructures show some degree of planarity within individual platelets.

TABLE 3. TENSILE PROPERTIES AT ROOM TEMPERATURE

SPECIMEN DESIGNATION	YIELD STRESS (MPA)	UTS (MPA)	PROPORTIONAL LIMIT (MPA)	DUCTILITY (%)
W1	760	864	592	13.4
W11*	702	805	516	13.1
W2	796	895	616	12.5
W3	757	915	553	10.5
W8	751	885	629	12.2
W12*	742	855	549	7.9
W9	784	884	619	7.5
W15*	737	850	533	8.1

* HEAT II MICROSTRUCTURES

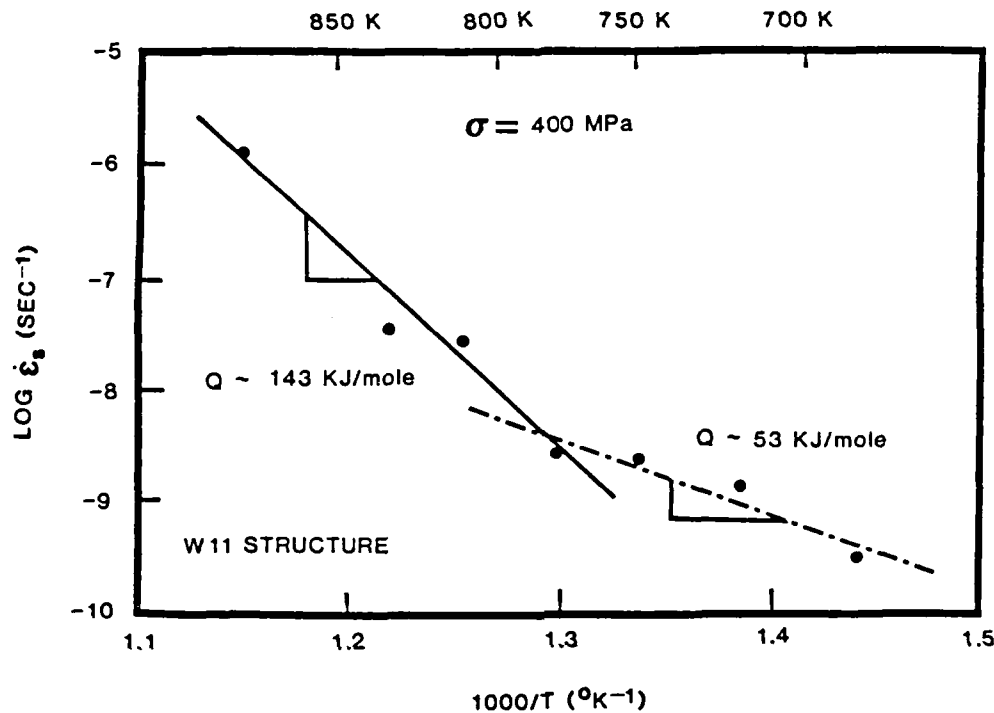**Determination of Activation Energy Q.**

Fig. 25.   Arrhenius plot of steady state creep rate showing apparent activation energy determinations (Q) for the W11 structure.

4.4.2   Deformation_Substructures_ During_ High_ Temperature_ Creep

Dislocations produced during high temperature creep are typically arranged in complex three-dimensional networks[38]. These high temperature dislocation networks are generally tangled and more homogeneously distributed than the parallel arrays of straight dislocations found at low temperature which are indicative of planar slip.

to be relatively close to the findings of several other
authors for oxygen diffusion in alpha titanium (16.2[71],
26[72] and 33.5[8] kcal/mole). The Ti-6211 value of 53
KJ/mole (13 kcal/mole) is also roughly equivalent to the
lower range of values mentioned above and may relate to
oxygen diffusion in alpha due to moderate temperature range
exposure for relatively long periods of time. At higher
temperatures and higher activation energies self-diffusion
overcomes the effects of oxygen diffusion. The Ti-6211
transition temperature is around 778K, close to that of Ti-
6242-Si at 755K. This scenario has not, however, been
rigorously established.

state creep rate, $\dot{\varepsilon}_s$, is found to vary with stress σ and temperature T, according to the Arrhenius type equation:

$$\dot{\varepsilon}_s = k\sigma^m \exp(-Q/RT) \qquad (18)$$

where k is a constant, m is the stress exponent and Q is the apparent activation energy for creep. The stress exponent m was calculated for the W11 structure at 823K. A value of m = 11 was calculated from the slope of Log σ vs Log $\dot{\varepsilon}_s$ data. The apparent activation energy Q for creep can be estimated from a Log $\dot{\varepsilon}_s$ vs 1/T Arrhenius plot. One such plot for the W11 structure at σ=400 MPa can be found in Fig. 25. Two distinct regions were found to exist at σ=400 MPa between approximately 673K and 873K. The region of the curve above approximately 778K yields an activation energy of 143 KJ/mole while the lower temperature regions yields Q values of approximately 53 KJ/mole. The activation energy estimated for the higher temperature regime was very close to that of self-diffusion in titanium (150 KJ/mole)[69]. This finding suggests that the rate-controlling process in high temperature creep of Ti-6211 is diffusion-controlled. The specific dislocation mechanisms, however, cannot be deduced from the limited information.

The creep mechanisms associated with the 53 KJ/mole region of the Arrhenius plot of steady state creep are somewhat harder to discern. Bania and Hall[70] found a similar dual slope Arrhenius type curve to exist in creep studies of Ti-6242-Si alloy. The authors found activation energies for creep below a transition temperature of 755K
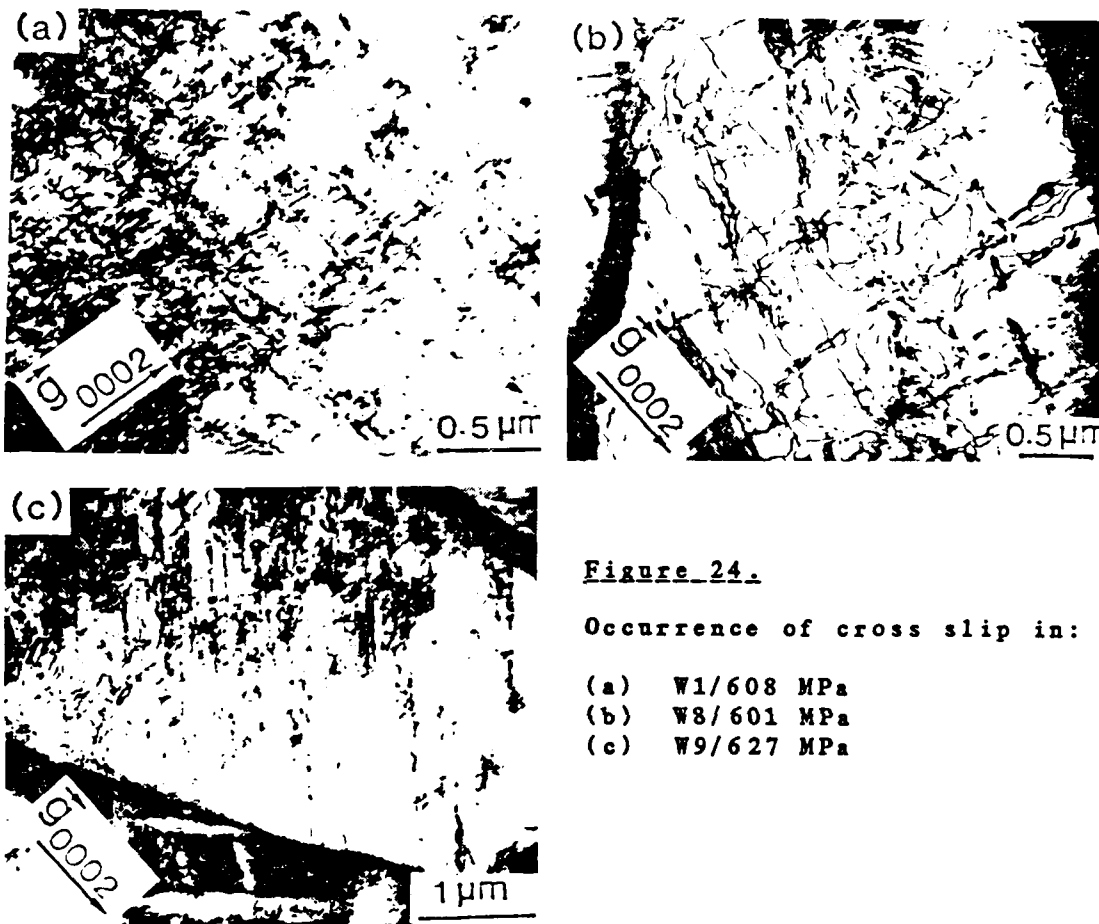
DISLOCATION SUBSTRUCTURES OF CREEP AT 453 K

Figure 24.

Occurrence of cross slip in:

(a) W1/608 MPa
(b) W8/601 MPa
(c) W9/627 MPa

4.4 Creep at Elevated Temperatures

4.4.1 Characterization

Creep tests of specimens with W11, W12 and W15 microstructures were conducted at various stress levels in a temperature range around 0.4 Tm. A summary of the testing conditions and results may be found in Appendix IV. For high temperature low strain rate creep tests, a steady

Lin, Starke and co-workers[5] showed that no cross slip was observed for tensile tested specimens which had experienced stresses much higher than the yield strength. Therefore, it is suggested that the occurrence of cross slip is most likely due to a thermally activated process. In comparison to creep at 298K, increased creep strains to saturation must be attributed to the occurrences of thermally activated cross slip and dynamic recovery.
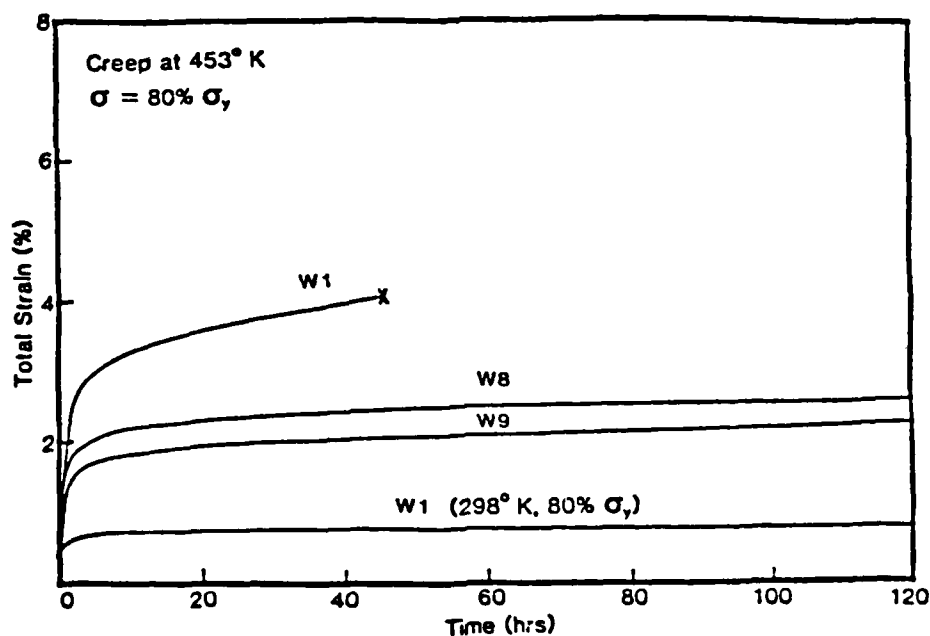
CREEP AT 453 K

Fig. 23. Creep curves for the W1, W8 and W9 micro-structures tested at T = 453K and σ = 80 %. (σ_{ys} is the yield strength at 298K).

Creep data was interrupted due to limit of strain gage at point X.

that of a tensile test. The likelihood of a slip band
breaking a deformation barrier is small and, consequently,
slip length is the limiting factor in creep deformation of
Ti-6211 at room temperature. Slip bands have been observed
traversing entire prior beta grains in room temperature
tensile tests, however, this was not observed in samples
after room temperature creep.

4.3.2 Creep at 453 K

Creep tests were conducted for several microstructures
at 453K in order to relate temperature effects to resulting
creep rates. 453K was chosen since it is above room tem-
perature but substantially below what is generally
considered to be the high temperature creep regime for
titanium. Figure 23 shows the creep strain at 453K to be
much greater than at 298K although creep saturation still
occurred at this temperature. Creep saturation at this
temperature was also reported by Chakrabarti and Nichols
for Ti-6Al-4V[13]. All three microstructures (W1, W8 and
W9) crept at 453K exhibited greater creep strains than the
as-received structure crept at room temperature. It should
be noted, however, that σ_{ys} is lower at 453K than at 298K,
hence, the load becomes a much larger percentage of yield.
Figure 24 shows the occurrence of cross-slip in the W1, W8
and W9 microstructures. Although a stress level of 608 MPa
is a larger fraction of the yield strength at 453K, the
occurrence of cross slip is not entirely due to stress.

creep rates. Figure 22a shows evidence of slip traces con-
fined to alpha platelets in the W15 structure. Figure 22b
shows lack of compatibility across an α/β/α interfacial
region.

W15 (664 MPa/298K)   W15 (664 MPa/298K)
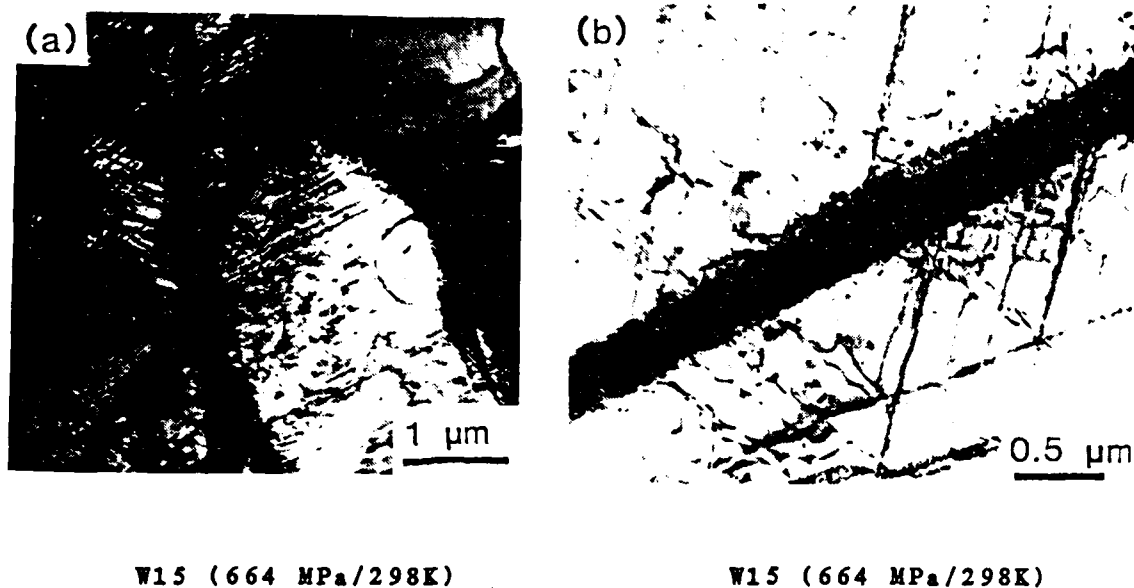
Fig. 22.   Lack of slip compatibility across α/β and
            α/martensite interfaces results in short slip
            lengths and low creep rates at room temperature
            for the W15 microstructure.

The slightly higher creep rate experienced by W12 over
W15 may be a result of the presence of small colonies in
the basket-weave structure, though this has not been stric-
tly proven. These colonies may accommodate slip for short
distances whereas the martensite in the W9 and W15
microstructures prevents any slip compatibility. The
stress level experienced during static creep testing was
usually below the yield strength and is low compared to

low creep strains relative to the as-received structures.

W8 (684 MPa/298K)   W12 (668 MPa/298K)
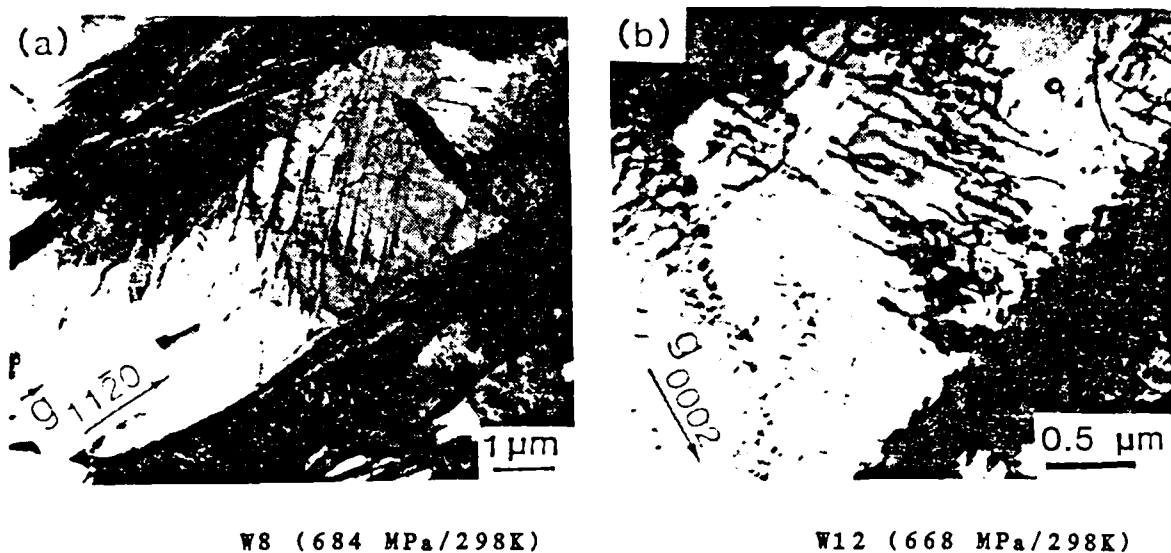
Fig. 21.   Slip confined to the alpha phase of the W8 structure
            (a) and a parallel array of dislocations in a large
            W12 alpha platelet (b).

W3 exhibits a martensitic microstructure in which each platelet displays a different crystallographic orientation. Lin, Starke, et al have shown that interfaces between martensitic plates serve as slip barriers and complex substructures due to quenching hinder dislocation movement[5]. As a result, the W3 microstructure exhibits the lowest creep strains at room temperature. The W9 and W15 structures consist of alpha plates in a retained beta and martensite matrix. As previously mentioned, no Burgers orientation relationship exists between alpha, beta and martensite phases in this structure, therefore, slip lengths are short and these microstructures exhibit low
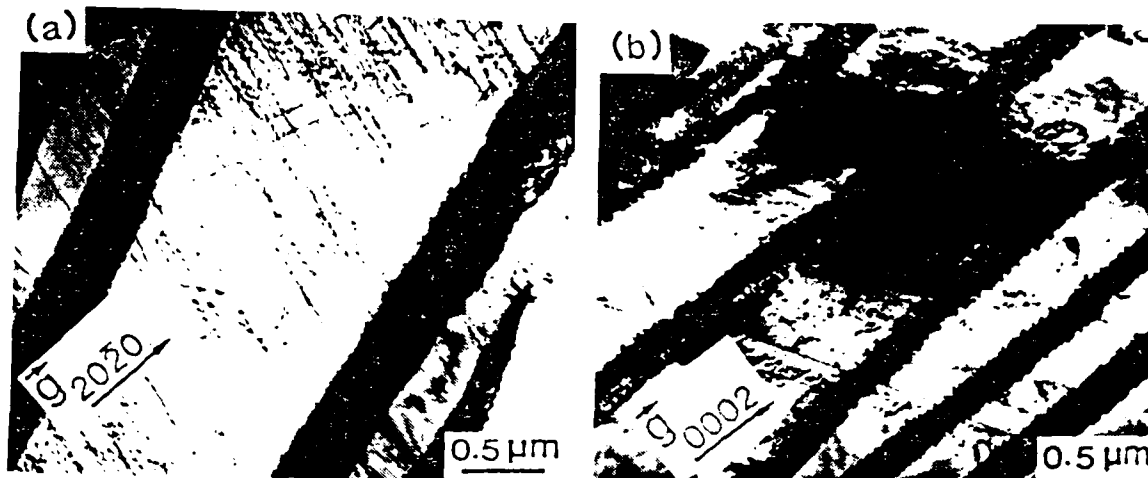
W1 (684 MPa/298K) W11 (632 MPa/298K)

Fig. 20. Parallel arrays of dislocations in the W1 structure
(a) and long slip lengths associated with widely
spaced deformation barriers in W11 (b).

Sliding along colony boundaries and α/β interfaces
also contributes to high creep rates in the W1 and W11
structures. These contributions will be addressed later in
a separate section.

Creep dislocation structures for W8 and W12 are shown
in Figure 21. Small colonies interspersed among large
alpha platelets result in short slip lengths and many α/β
interfaces without a Burgers orientation relationship.
Figure 21a shows slip confined to within the alpha phase in
the W8 structure. Figure 21b similarly shows parallel
arrays of dislocations confined to the alpha phase in the
W12 structure. The overall lack of slip compatibility in
the basket-weave Widmanstättten microstructures results in

predominance of planar slip. Straight dislocations and the operation of a single slip system at room temperature were the typical features in the alpha phase where cross slip was only rarely observed. Lin, Starke, et al observed similar deformation substructures in a previous Ti-6211 tensile study[5]. Dislocation features for the W1 and W11 microstructures are shown in Fig. 20. Figure 20a shows an array of straight dislocations in parallel alignment and passing through beta plates. Due to the Burgers orientation relationship existing between the alpha and beta phases in the colony structure, planar slip was able to pass through the beta platelets and extend the length of an entire colony. Continuous slip within a colony is illustrated by Fig. 20b where the slip traces offset dark bcc beta platelets. Long slip lengths due to widely spaced deformation barriers are responsible for the highest creep rates and greatest deformation occurring in the W1 and W11 microstructures at room temperature.
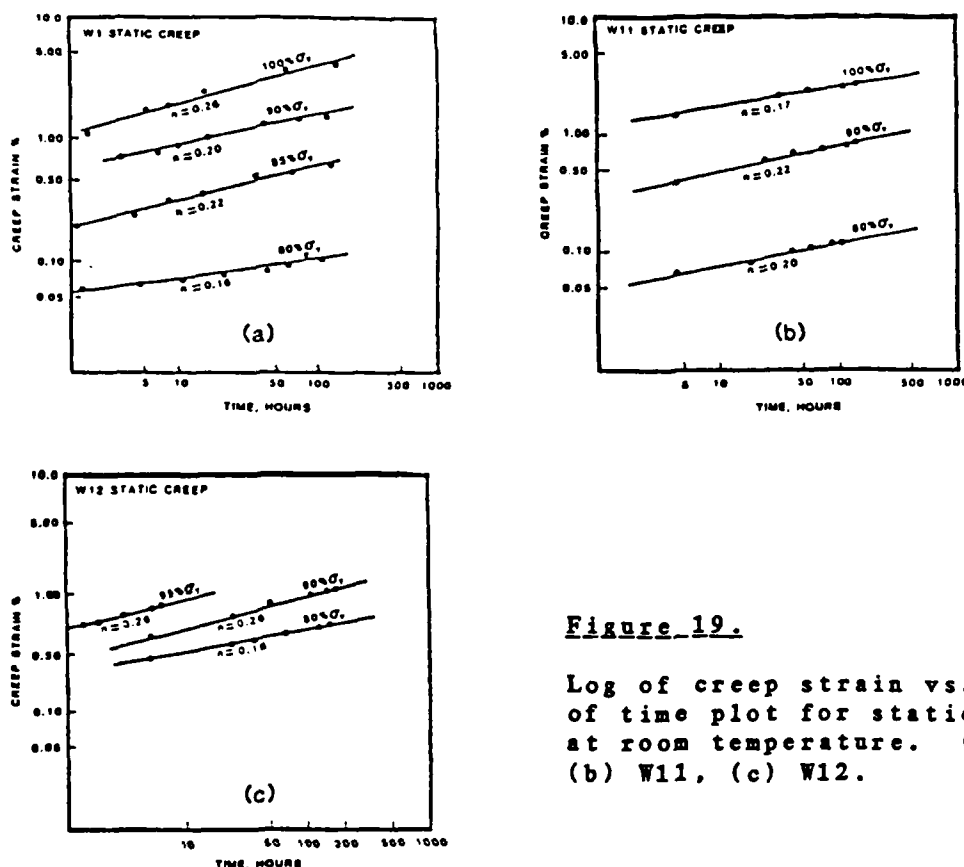
Figure 19.

Log of creep strain vs. log of time plot for static creep at room temperature. (a) W1, (b) W11, (c) W12.

The onset of creep (proportional limit) was experimentally determined for both the W11 and W12 microstructures and is shown in Appendix III. Creep strain is evident in the W11 structure between 55 % σ_{ys} and 65 % σ_{ys} while plastic deformation occurs in the W12 structure between 50 % and 60 % of yield.

As previously stated, no strong texture was observed for any of the microstructures of interest. The differences in creep response are most likely due to variations in phase morphology or slip length which is determined by the spacing of potential slip barriers. Creep-deformed specimens examined under TEM show a
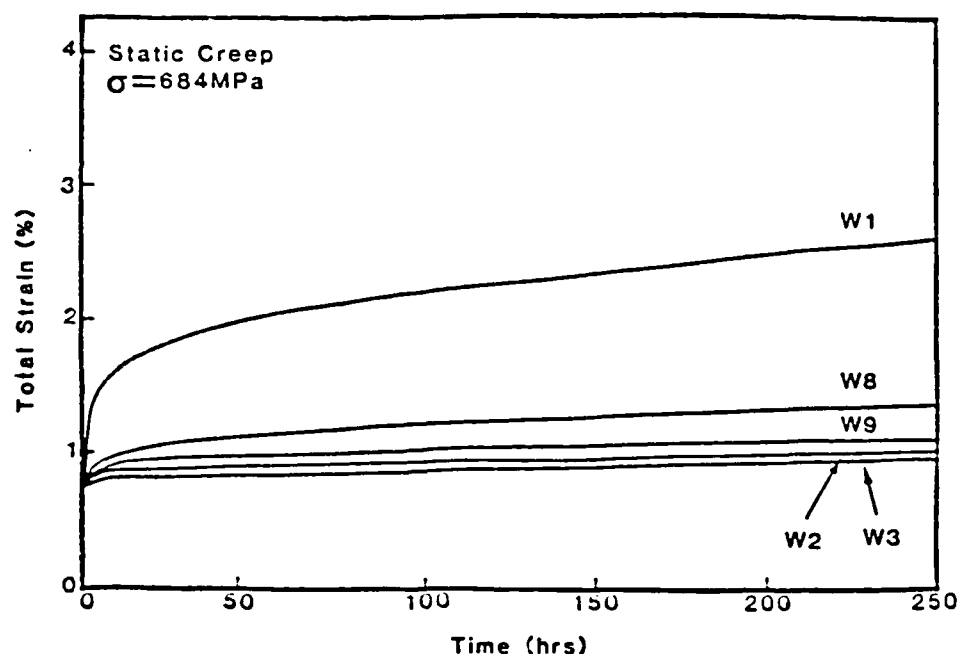
creep stress and n is the time exponent.

Fig. 18.   Room temperature creep curves for various micro-
structures at a stress level of 684 MPa.

A least   squares fit method was used to determine the
time exponent n for the W1, W11 and W12 microstructures and
these results are shown in Figure 19.   Ti-6211 n values
vary with microstructure and stress level but generally
fall below 0.3.   The dependence of creep strain on creep
stress is also illustrated by Fig.   19.   The curves in Fig.
19   are normalized to percentages of yield for each
individual microstructure as opposed to Fig. 18 where an
absolute stress value was used to generate all of the cur-
ves.   Increases in creep rates are proportionally much
higher between 90 % and 100 % σ_{ys} than they are between 80
% and 90 % σ_{ys}.

equivalent to 90 % σ_{ys} of W1, are shown in Figure 18. These curves are typical of low temperature titanium creep testing where creep is initially rapid and decreases gradually at high stress levels or quickly at lower stress levels. All of the creep curves generated at room temperature below the yield stress level-off and exhibit creep saturation (creep exhaustion) due to a lack of recovery. This is commensurate with previous findings by other authors[9,13-18]. Heat II structures W11, W12 and W15 exhibit similar trends to the respective Heat I microstructures W1, W8 and W9. Heat II microstructures creep slightly more at an absolute stress value due to their lower yield strengths.

Figure 18 indicates that the simulated HAZ microstructures are more creep resistant at high stress levels (80 % to 100 % σ_{ys}) at room temperature than the microstructures from the as-received rolled plate, W1 and W11. Structural integrity, therefore, is not sacrificed for good weldability in Ti-6211. A summary of room temperature creep data may be found in Appendix II.

Creep of Ti-6Al-2Nb-1Ta-0.8Mo at low temperature is of the transient type where the creep-strain/time relationship agrees with the previous findings of Chu[15-18] and can be fit to the following empirical power function:

$$\varepsilon_c = At^n \qquad \text{(Eq. 17)}$$

where ε_c = creep strain (total strain minus elastic strain), A is a constant dependent upon microstructure and

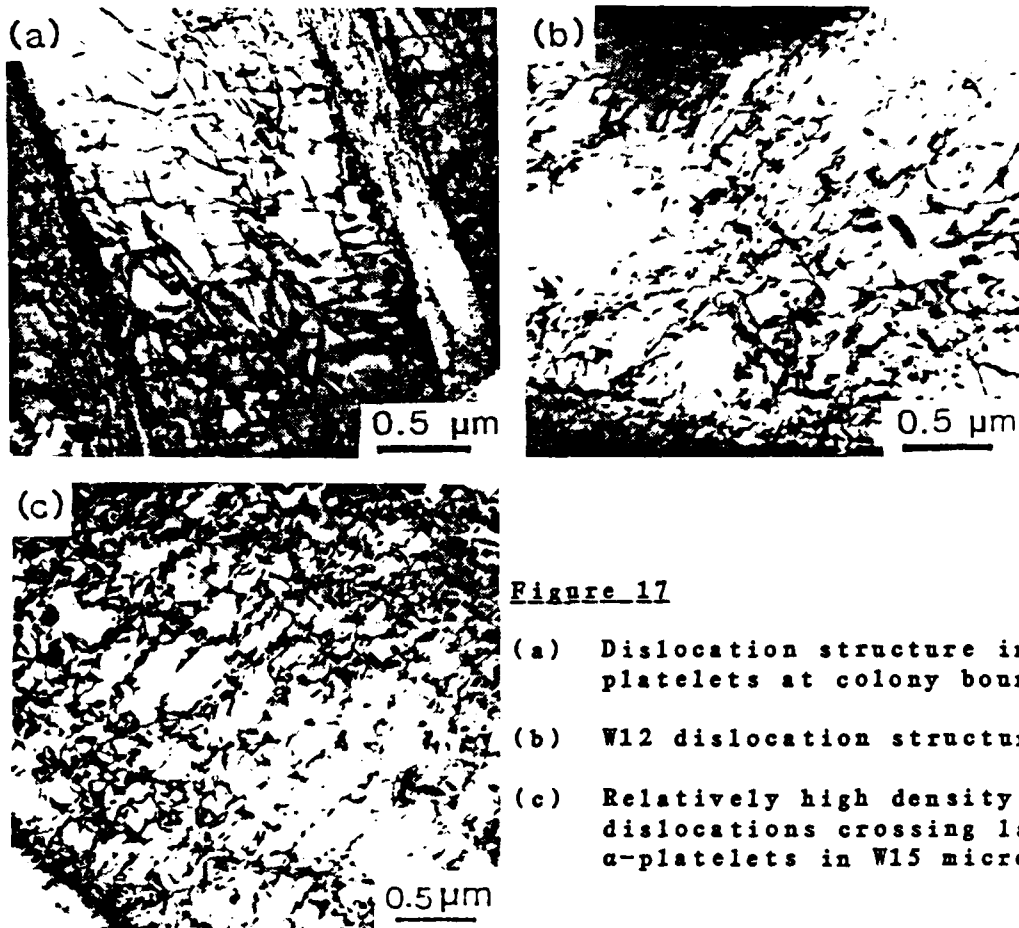# TENSILE DEFORMATION SUBSTRUCTURES AT ROOM TEMPERATURE

Figure 17

(a) Dislocation structure in W11 platelets at colony boundary.

(b) W12 dislocation structure.

(c) Relatively high density of planar dislocations crossing large α-platelets in W15 microstructure.

4.3 Creep at Ambient Temperatures

4.3.1 Room Temperature Creep

Creep curves for the W1, W2, W3, W8 and W9 microstructures tested at a stress level of 684 MPa, which is

Dislocation dipoles and loops were frequently observed in the samples subjected to high temperature creep while no distinct coarse slip bands were observed on the surface of the heavily crept samples. This type of dislocation substructure has also been reported for the Ti-6Al-4V alloy by Hall[48]. These types of configurations may result from the jog or climb of dislocations which are activated by exposure to high temperature during creep. Fig. 26 illustrates the effects of temperature on dislocation substructures in Ti-6211 creep. Fig. 26a shows dislocations at the end of a colony in the W11 structure while Fig. 26b exhibits high dislocation densities in the W11 structure crept at 823K. High dislocation densities are typically found in specimens crept above 773K and this may be due to the influence of diffusion in the high temperature regime as illustrated by Fig. 25. As test temperature increases in the crept samples, the thickness of beta platelets decreases due to phase transformation. This decrease in beta phase may liberate dislocations which migrate to the large alpha platelets as shown in Fig. 26b. Dislocation movement may be stress-assisted and densities may be related to the release of beta stabilizers which had been previously tied into the thicker beta regions. Attempts at determining changes in elemental compositions in and near beta platelets due to elevated creep temperatures were unsuccessful due to the small percentages of beta stabilizing elements present.
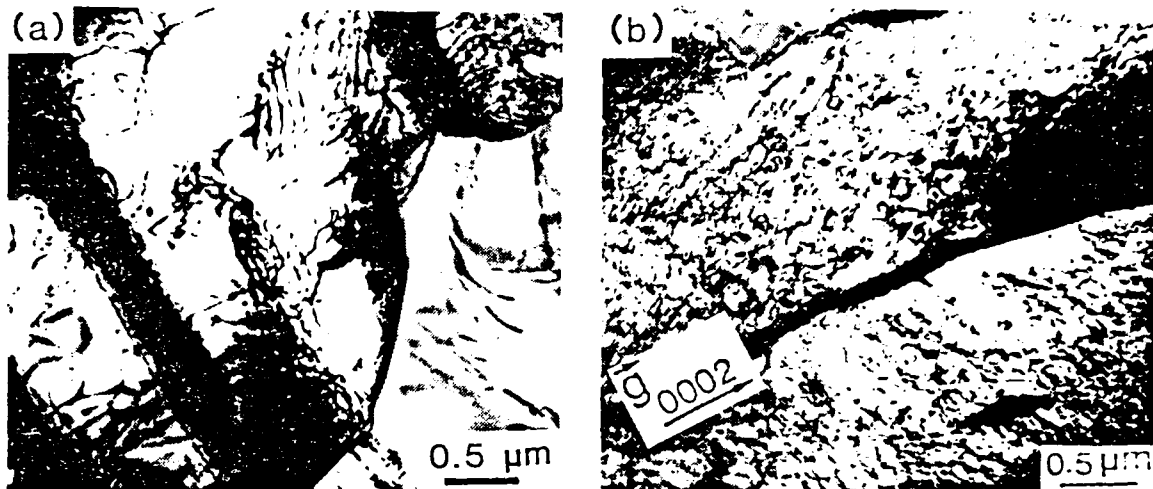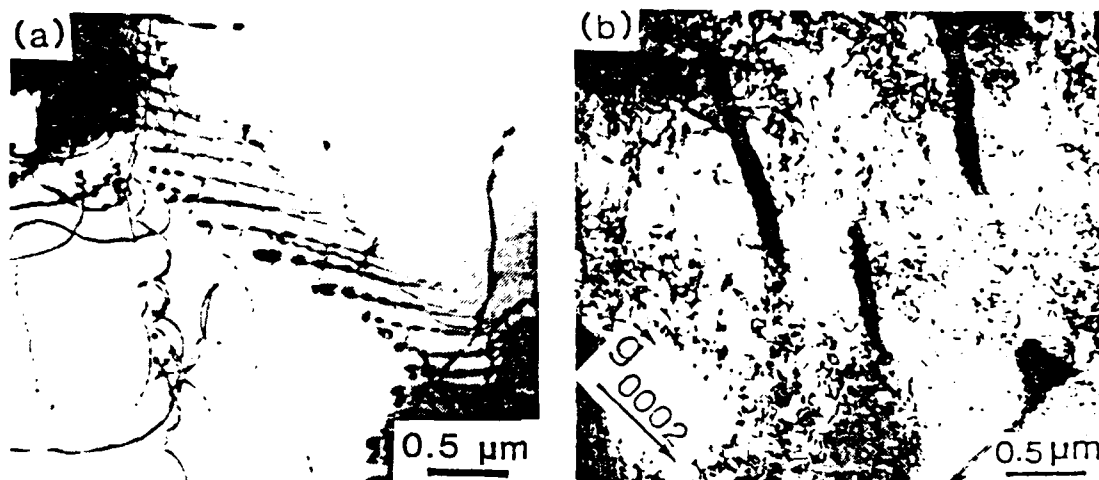
W11 structure (723K/400 MPa)   W11 structure (823K/400 MPa)

Fig. 26   High temperature dislocation structures in the
           W11 microstructure at 723K (a) and 823K (b).

The variation in W12 dislocation structures between 723K and 873K is illustrated by Figure 27. Figure 27a shows the 723K crept specimen with hexagonal networks and a low density of wavy dislocations. The overall lack of dislocations evident in Fig. 27a is most likely a result of annealing and dislocation annihilation. The cell structures, however, are difficult to anneal since they are pinned in low energy configurations. At a temperature of 723K, dislocation densities are less than at room temperature due to annealing but do generate hexagonal cell structures which cannot be easily annealed by exposure to the relatively low temperatures experienced during creep. This would indicate that stress operates and controls the dislocation mechanisms in this temperature range. Tem-

perature activates dislocation generation mechanisms at slightly higher temperatures as shown in Fig. 27b. This is certainly in agreement with the data presented in Fig. 25. Fig. 27b shows a W12 specimen crept at 873K where the high rate of dislocation generation (as discussed for W11) overcomes the annihilation evident at 723K. Thinned beta platelets once again indicate phase transformation at high test temperatures and high stress levels.

W12 structure (723K/400 MPa)   W12 structure (873K/400 MPa)

Fig. 27.   W12 dislocation substructures showing hexagonal
            networks at 723K (a) and a high density of
            dislocation loops at 873K (b).

Figure 28 shows representative micrographs of the W15 microstructure. Fig. 28a shows an overview of the high density of dislocations present in the W15 structure. At 823K and 400 MPa this micrograph would indicate higher densities than found in either the W11 or W12 microstructures, this is probably due to residual effects of the

quench experienced during heat treatment. High dislocation densities may also account for low creep strains compared to other microstructures at high temperature. Fig. 28b shows dislocations associated with a beta platelet.
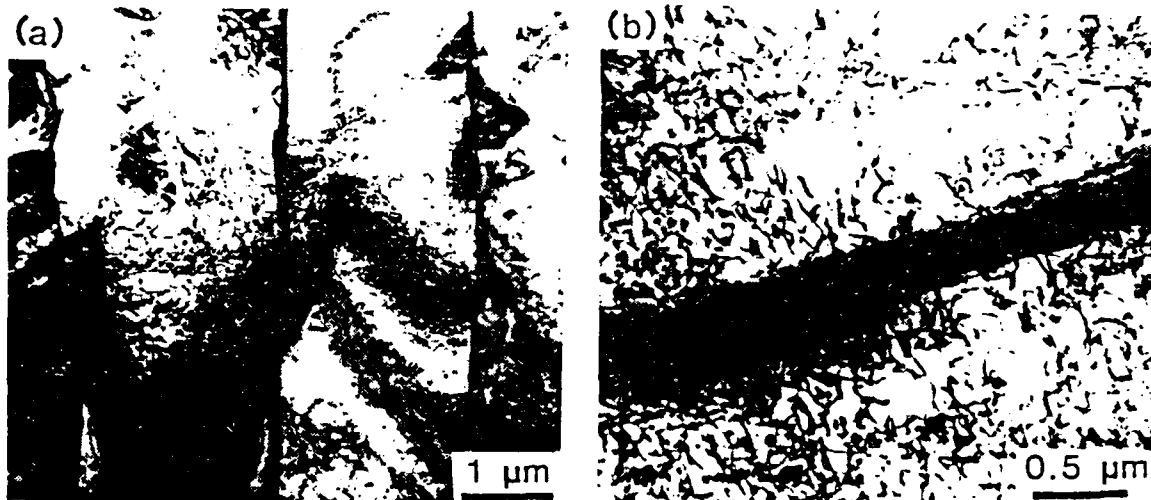
W15 structure (823K/400 MPa)   W15 structure (823K/400 MPa)

Fig. 28 Highest densities of dislocations are present in the W15 structure.

4.4.3 High Temperature Creep Rupture

The W11 structure exhibits a longer life at high temperatures than either the W12 or the W15 beta-annealed microstructures. This is mainly due to differences in microstructure and crack initiation mechanisms. The W11 structure has a much higher ductility than the recrystallized structures and can withstand greater necking prior to fracture. The equiaxed grain shapes of W12 and W15 allow for grain boundary sliding and strain localization in the

grain boundary alpha phase (particularly along the thick G.B.α of W12). Figure 29 shows fracture surfaces of ruptured W11 and W12 structures.
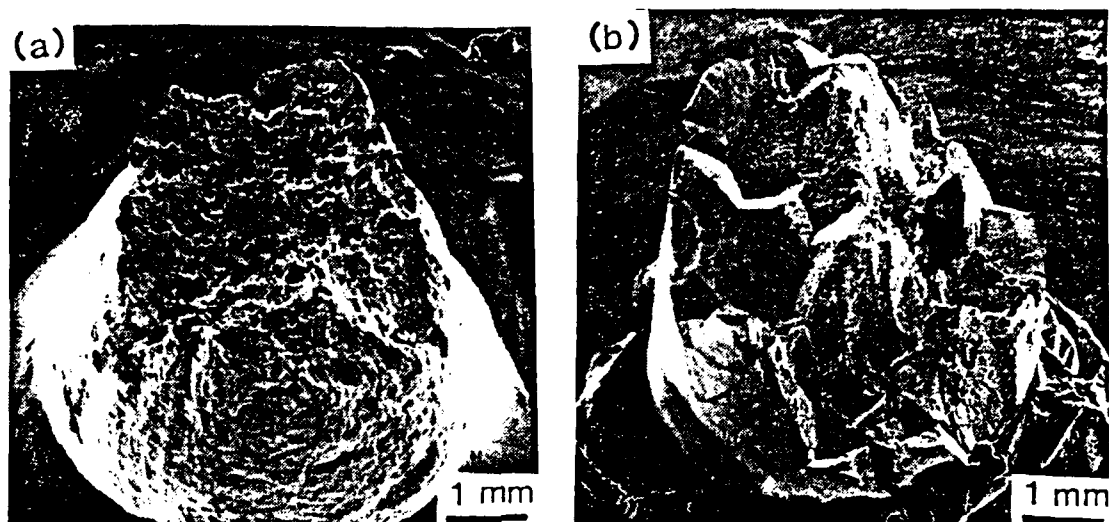
W11 structure (873K/400 MPa)   W12 structure (873K/400 MPa)

Fig. 29.   Creep rupture of the W11 structure (a) and
            intergranular fracture of W12 (b).

The W11 structure has an elongated grain structure in the rolling direction with the longer edge parallel to the loading axis and, consequently, a small percentage of the grain boundaries are subjected to high shear stress.   In fact, creep rupture occurred in the W11 structure by microvoid formation and coalescence at colony boundaries. The fracture mechanisms involved in creep rupture at high temperature are similar to hot tensile tests performed earlier in this study and by other authors[7]. Void growth by diffusion and interfacial sliding, however, plays a more

significant role in creep rupture since they are time-dependent processes. Since the diffusional growth of cavities is driven by tensile stresses across the boundary[55], the voids nucleated at transverse boundaries tend to grow faster and coalesce into cracks. Creep rupture in W12 samples occurred by intergranular fracture through microvoid formation. Fig. 30 shows cross-sections of ruptured W12 and W15 specimens after polishing and etching. Fracture paths were found to follow the G.B.α/matrix interface.

(a) ... 0.1 mm   (b) ... 0.1 mm
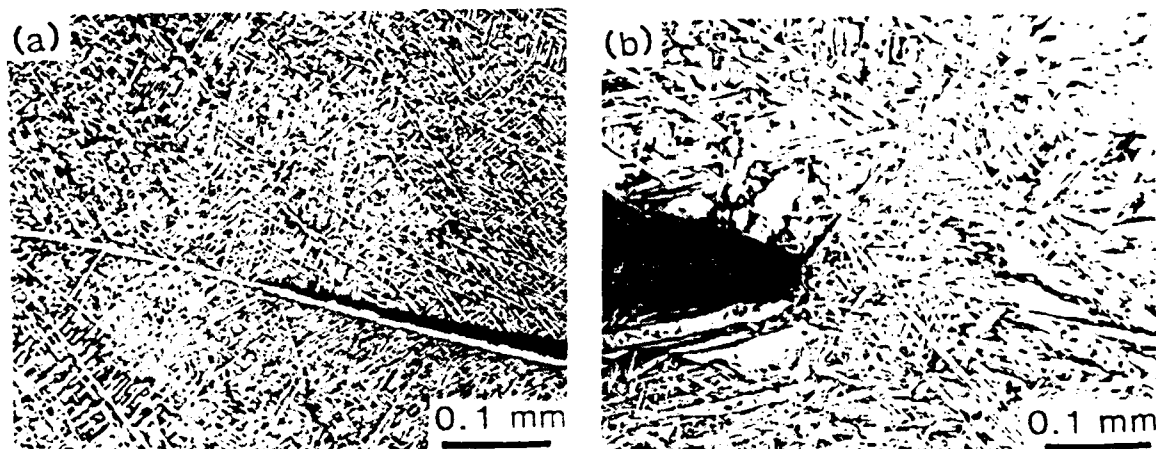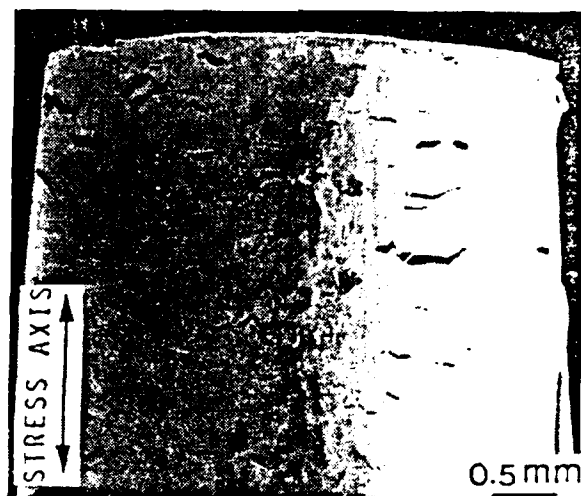
W12 structure (873K/400 MPa)   W15 structure (823K/400 MPa)

Fig. 30.   Cross-section of secondary crack following G.B.α in W12 structure (a) and branching in the W15 structure (b) at a grain boundary triple point.

All three microstructures exhibit large dimples on fracture surfaces due to extensive void growth prior to rupture. Figure 31 shows a W11 creep rupture specimen and

secondary cracks along short colony boundaries perpendicular to the stress axis.

W11 structure (823K/400 MPa)

Fig. 31. SEM micrograph displaying microcracks perpendicular to the stress axis in a W11 creep rupture specimen.

4.5 Cyclic Creep

Cyclic creep tests of the W1, W2, W3, W8 and W9 microstructures were performed under conditions of constant load amplitude (304 MPa), square wave form and at a stress ratio of R=0.11. Fig. 32 shows cyclic creep strains plotted against the actual loading time and superimposed on the plot of static creep curves.

An increase in creep rate and cyclic creep acceleration was observed in all five microstrucutres. Meshii and co-workers[73] explained the cyclic creep acceleration in terms of the reduction of internal stress by recovery dur-

ing the unloading period. Enhanced creep rates induced by cyclic loading may be attributed to dislocation rearrangements during unloading[74] allowing a further strain increment to accumulate upon reloading. This explanation appears to be applicable to the Ti-6211 alloy system.

Most structural components used in engineering applications are subjected to some form of cyclic loading where a small fluctuating load is superimposed on a larger static load. A square wave loading spectrum with an R ratio of 0.9 and a period of two minutes was applied to the W1 condition of the Ti-6211 alloy and the resulting creep response is shown in Fig. 33. The cyclic creep curve is situated above the static creep curve with the same mean stress, i.e., 85 % σ_{ys}. The cyclic creep curve is, however, lower than the static curve with the same peak stress, i.e., 90 % σ_{ys}. Cyclic creep acceleration, therefore, did not occur when compared to static creep with the same peak stress, although this type of cyclic creep acceleration has been observed in many metals[73-75]. The end result is that the static creep curve generated at the same stress level as the peak stress on the cyclic curves can be used as a guideline for the Ti-6211 alloy whenever cyclic creep is of concern in structural design.

TEM examinations did not reveal a noticeable difference in dislocation substructures between static and cyclic crept samples. Odegard and Thompson studied the effect of prestrain on creep in Ti-6Al-4V at room

temperature[14] and found that small degrees of prestrain could enhance subsequent creep. A certain amount of prestraining can lower the internal stress and thereby enhance the creep rate. This prestraining effect can also be used to explain the cyclic creep acceleration occurring in the loading-unloading cyclic creep of Ti-6211. The mechanisms involved in the reduction of internal stress, however, are not clear.
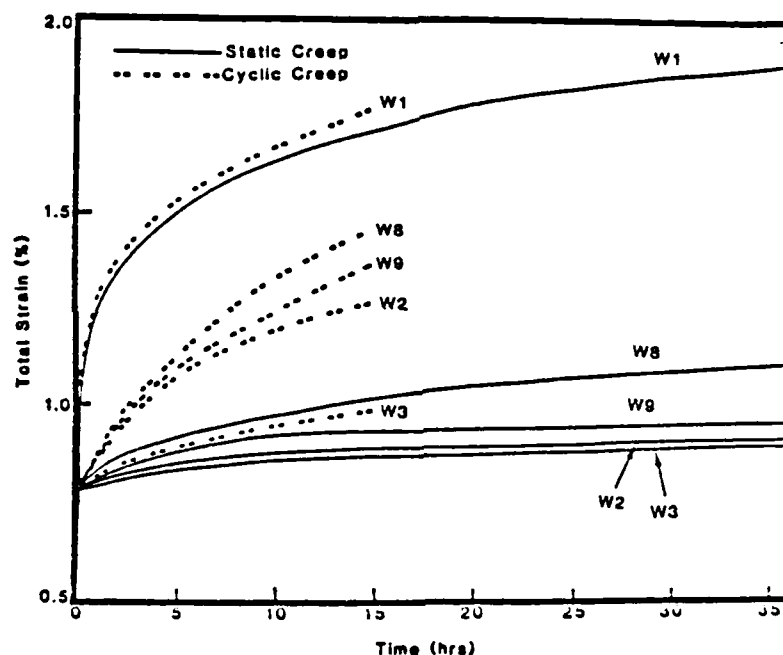
Fig. 32. Comparison of cyclic creep with static creep at room temperature. (σ = 684 MPa for static creep. $\Delta\sigma$ = 304 MPa, R = 0.11 for cyclic creep.)
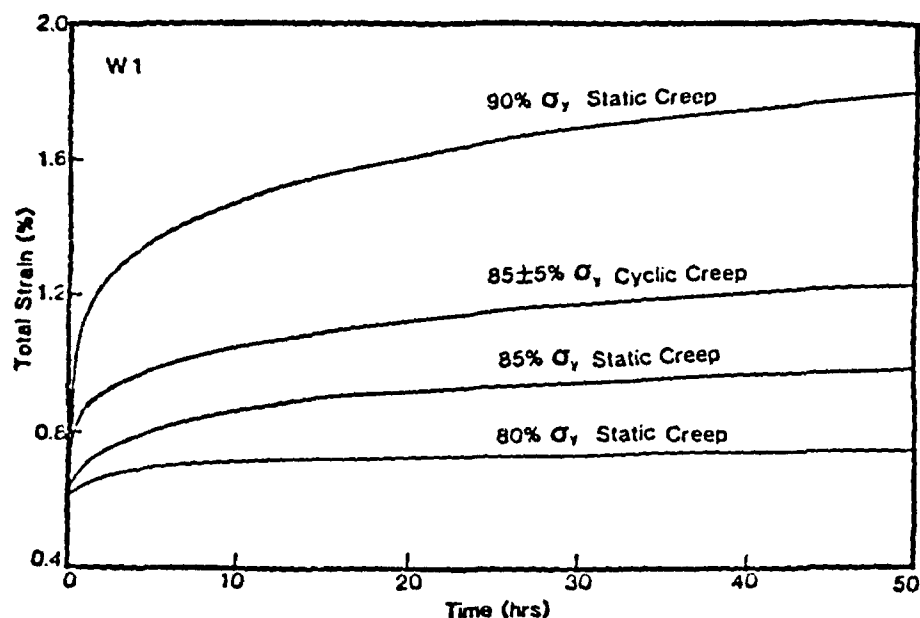
W11 structure at 298K

Fig. 33. Creep curves for static creep and cyclic creep
with a small fluctuating load.

4.6 Interface Sliding and Surface Deformation

4.6.1 Sliding Characteristics

Sliding at grain boundaries and other such interfaces
has been found to contribute to the creep strains
experienced by many alloy systems. Varying degrees of
sliding have been found to occur with differing creep test
parameters and different microstructures in the Ti-6211

alloy along three intrinsic interfaces: grain boundaries, colony boundaries and alpha/beta phase boundaries. Deformation at slip traces as well as large deformation bands which are unassociated with particular boundaries also contribute to creep and tensile deformation and are frequently observed in surface deformation studies.

4.6.2 Interface Sliding at Room Temperature

An investigation concerned with characterizing and quantifying the sliding deformation of the W11, W12 and W15 structures has been conducted for tensile and creep testing. Creep testing was performed at percentages of the yield strengths of the individual microstructures. Surface sliding has been observed by monitoring the offsets of gold grid networks which were electroplated onto specimen sur-faces prior to deformation. The 5μm (or 1μm) wide gold grid lines illustrate the magnitude and origin of sliding contributions to creep strain and tensile ductility. Relating surface deformation characteristics to deformation substructure is difficult due to a lack of internal markers. In some cases, however, a comparison of disloca-tion structures may yield valuable information regarding the nature of interfacial sliding. In several cases the contributions of grain boundary or surface sliding (ε_{gbs}) have been calculated as a percentage of the total strain (ε_T)[61]. The results of room temperature creep and tensile sliding contribution calculations are listed for

all three microstructures in Tables 4A and 4B. These calculations are approximations and should be considered as such. The competition between the contributing factors of sliding deformation coupled with strain localization and necking make $\varepsilon_{gbs}/\varepsilon_T$ calculations possible but not precise. Thermally processed dual phase titanium structures are susceptible to interface sliding due to the complexity of the microstructures and variety of sub-grain boundaries.

4.6.2.1 W11 Microstructure

Creep Deformation

Grid deformation specimens were crept to saturation for the as-received structure at 80 %, 90 % and 95 % σ_{ys}. Below 80 % σ_{ys} evidence of surface deformation during creep was tenuous. At 80 % σ_{ys} with a creep saturation of ε_c=0.47 % (480 hrs) no noticeable grid distortions were seen across either the 5μm gold grid lines or smaller 0.5μm to 1.0μm residual polishing scratches. Very small deformation ridges were occaisionally witnessed along favorably oriented (45° to stress axis) colony boundaries but deformation was not large enough to disturb grid networks. No grain boundary sliding was seen.

As-received specimens crept at 90 % σ_{ys} indicate, by surface observation, no obvious slip traces within individual colonies and no grain boundary deformation. Alpha/beta interface sliding was not seen for specimens

crept at 190 hours and $\varepsilon_c = 1.6$ % but was evident at saturation and 1010 hours (2.6 % ε_c). Although little overall deformation is evident at relatively small creep strains, the predominance of sliding tends to occur along colony boundaries and along deformation ridges oriented at 45° to the stress axis. Offsets generally appear to be less than 0.5μm as can be seen in Fig. 34a. Figure 34b is a TEM micrograph of a colony boundary in the W11 structure crept at 298K and 90 % σ_{ys}. Planar arrays of dislocations are evident, as previously shown in Fig. 20, but heavy non-planar dislocations can be seen in alpha platelet bordering perpendicular platelets of the adjoining colony. While some of these dislocations may be residual dislocations from heat treatment it is likely that the more dense networks are, in part, a result of interfacial sliding during creep.

A significant amount of deformation becomes evident in specimens loaded to 95 % σ_{ys}. Fig. 35a shows a W11 specimen tested at 210 hours (2.8 % ε_c). Slip bands become evident within individual colonies shearing β-platelets due to the Burgers orientation relationship. These slip lines generally initiate at one colony boundary and terminate at the opposite colony. Most deformation occurs along favorably oriented colony boundaries as illustrated by Fig. 35a. Fig. 35b shows large deformation bands, which at initial stages (210 hrs) followed α/β interfaces or colony boundaries, passing through all boundaries at approx. 45° to the stress axis after 700 hours (3.7 % ε_c). Grain boun-
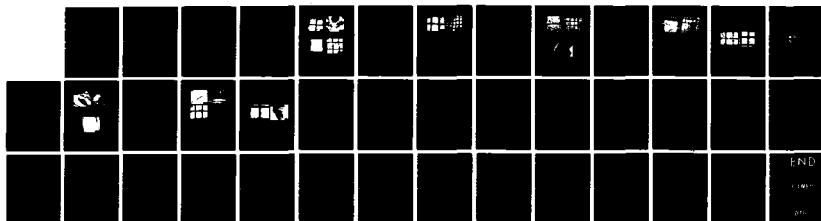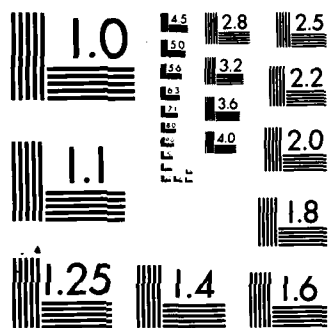
MICROCOPY RESOLUTION TEST CHART

NATIONAL BUREAU OF STANDARDS-1963-A

daries are not thought to play a significant role during creep straining of the as-received structure. Surface deformation contributions were not calculated at 740 hours due to strain gage failure and complexity of contributing factors but calculations are shown in Appendix V for W11 at 95 % σ_{ys} (210 hrs/2.8 % ε_c). Approximately 60 % of the overall plastic deformation was attributed to interfacial sliding.

TABLE 4A. INTERFACIAL SLIDING CONTRIBUTIONS TO CREEP STRAIN

MICROSTRUCTURAL DESIGNATION	TEMPERATURE (K)	$\%\sigma_{YS}$ AND HOURS OF TEST	ACTIVE[*] INTERFACE	$\epsilon_{GBS}/\epsilon_T$ (%)[**]
W11	298	90%/1010 HRS	COLONY BOUNDARIES	10
W11	298	95%/210 HRS	COLONY BOUNDARIES	59
W12	298	90%/750 HRS	GRAIN BOUNDARIES	20
W15	298	100%/940 HRS	ALPHA LATH/ MARTENSITE INTERFACES	25

[*] THIS DOES NOT MEAN THAT OTHER INTERFACES OR MECHANISMS DO NOT CONTRIBUTE TO CREEP STRAIN SIMULTANEOUSLY.

[**] NEGLIGIBLE CONTRIBUTIONS ARE CONSIDERED TO BE BELOW 10%.

TABLE 4B. Interfacial Sliding Contributions to Tensile Strain

Microstructural Designation	Temperature (K)	Total Sample Strain (%)	Active* Interface	$\epsilon_{GBS}/\epsilon_T$ (%)**
W11	298	3.0	Colony Boundaries	77
W11	298	10.0	Colony Boundaries	42
W11	823	6.5	Grain Boundaries	62
W12	298	6.0	Alpha/Beta Interfaces	67
W12	673	4.5	Grain Boundaries	25
W12	673	4.5	Alpha/Beta Interfaces	35
W15	298	5.0	Alpha Lath/Martensite Interfaces	80
W15	298	7.2	Alpha Lath/Martensite Interfaces	72
W15	673	5.0	Alpha Lath/Martensite Interfaces	73

* This does not mean that other interfaces or mechanisms do not contribute to tensile strain simultaneously.

** Negligible contributions are considered to be below 10%.
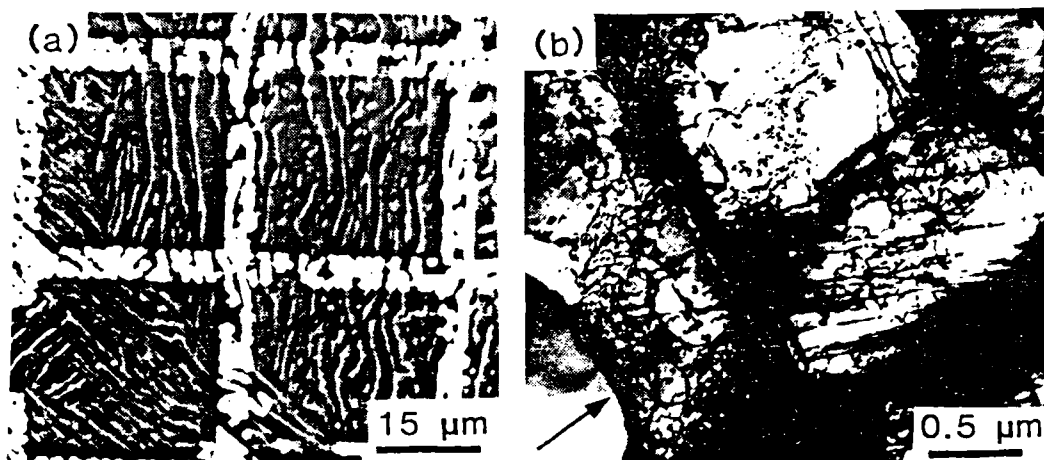
Figure 34. Small deformation ridge at 90 % σ_{ys} and 298K (1010 hrs /2.6 % ε_c) in (a) and TEM dislocation network in same specimen at colony boundary (b).
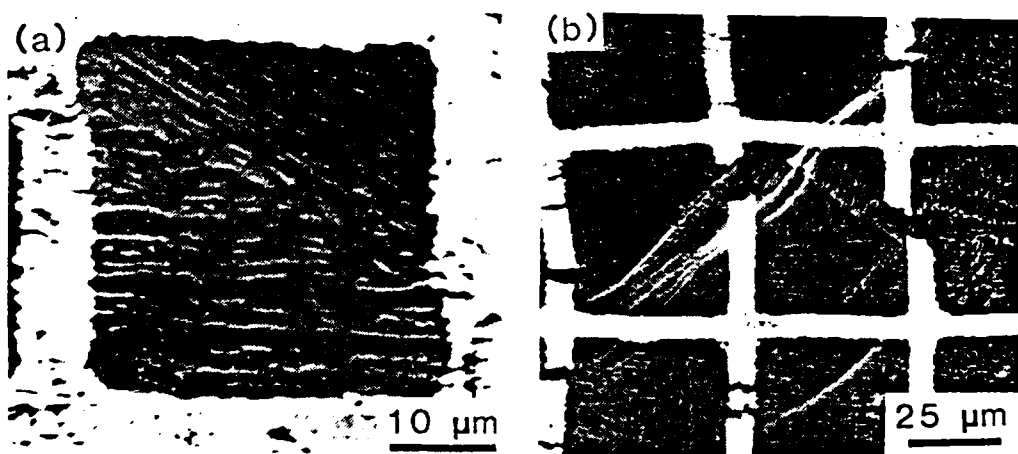

Figure 35. Sliding at colony boundaries and slip traces (298K) within colony structure (a) at 95 % σ_{ys} (210 hrs/2.8 % ε_c) and massive deformation distorting grid network (b) 95 % σ_{ys} (740 hrs/3.7 % ε_c).

Tensile Deformation

Room temperature tensile tests were performed on W11 grid-deposited specimens to plastic strains of 2.0 %, 5.0 %, 9.0 % and 12.3 %. These tests were run to compare results to the low temperature creep investigation. The fundamental differences between surface deformation during tensile and creep testing are based on (1) strain rate dependencies and (2) magnitudes of deformation which might be unobtainable with standard creep procedures. The dependence of deformation on strain rate is addressed for titanium[76] and other systems by many authors[77,78]. Almost all of the boundary sliding occurred along colony boundaries for the low strain specimens (2 % ε_p) with some α/β offsets evident (Fig. 36a). At higher strains, from 5 % ε_p and up, grain boundary sliding becomes evident as well as frequent deformation ridges (Fig. 36b). Sliding along the various interfaces in the W11 structure is not homogeneous throughout the microstructure, especially at higher strains where deformation banding leads to cracking.
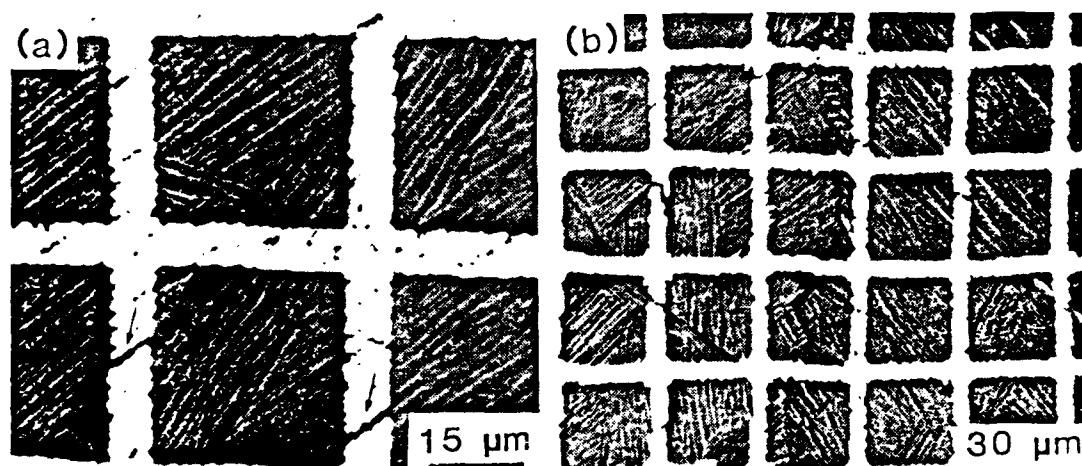
Figure 36a.   Figure 36b.

Sliding occurring almost entirely   Colony and grain boundary
along colony boundaries at low   sliding with some deforma-
plastic strains.   tion bands at higher
                                      strain.

4.6.2.2 W12 Microstructure

Creep Deformation

Grid networks were placed on W12 specimen surfaces

crept at 90 % and 95 % σ_{ys} since below approx. 85 % σ_{ys} no

surface deformation was visible. In general, the grid

distortions and surface deformation due to creep in the

ambient temperature regime and at creep stress levels below

the tensile yield strength were slight. Few surface slid-

ing calculations could be made and it is thought that

interface sliding contributions at low temperature and moderately high stress levels are small. Figure 37a shows a very small sliding component to deformation along a prior beta grain boundary at 90 % σ_{ys} and 750 hours (1.5 % ε_c) of creep. Fig. 37b shows a W12 grid structure after saturation (ε_c=1.7 %) at 1780 hours of creep where the grid network is very slightly offset across a prior-β grain boundary approaching G.B. triple point. Similar effects were seen at 95 % σ_{ys} and in neither case was deformation visible along Widmanstätten basket-weave platelets at such low strains. Fig. 38 illustrates the appearance of dislocation elbows indicating the presence of cross slip in large scattered α-platelets. Planar slip in a single operative slip system, as seen in Fig. 22, is expected at 95 % σ_{ys} and 298K. It is suggested that the second slip system may be activated by limited sliding along large α-platelet/beta interfaces as commonly observed during tensile testing of the same structure. Cross slip, therefore, may indicate the presence of platelet sliding as a result of creep strains.

W12 (750 hrs/1.5 % ε_c)   W12 (1780 hrs/ 1.7 % ε_c)
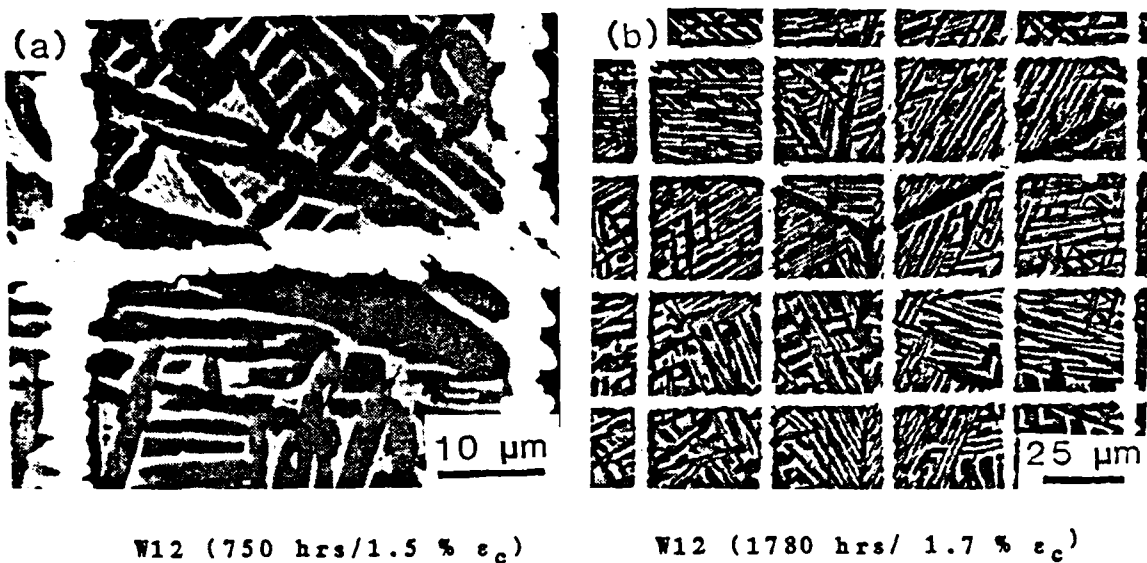
Fig. 37.   Insignificant sliding contributions as illustrated
           by minor grid distortions at room temperature
           in W12 structure at a stress level of 90 % σ_{ys} after
           (a) 750 hrs, (b) 1780 hrs and saturation.
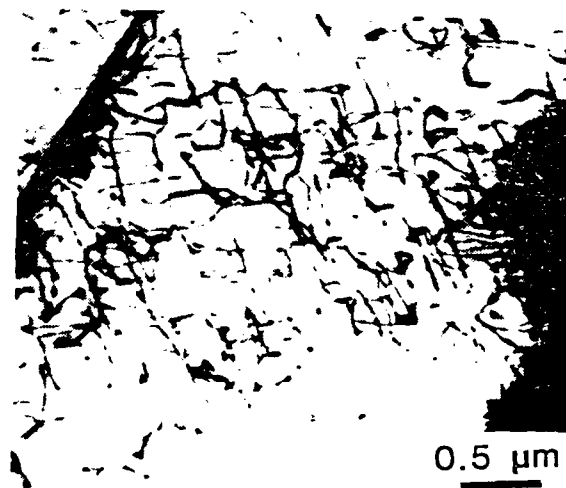
Fig. 38.   TEM micrograph showing presence of cross slip in W12
           specimen crept at 95 % σ_{ys} (298K).   Cross slip may
           indicate alpha lath sliding.

Tensile Deformation

Grid deposited tensile deformation specimens were strained to 1 %, 3.7 % and 5.2 % ε_p. Slip bands were observed in regions of small colony structures and were oriented at 45° to the stress axis. Deformation was fairly localized in the specimen deformed to 1 % ε_p. The 5.2 % ε_p specimen characteristics were identical to those of the 3.7 % ε_p specimen only more pronounced. Fig. 39a shows sliding along a large α-platelet/matrix interface after 3.7 % ε_p. Offsets occurred both parallel to the platelet and out of the plane of the micrograph, vertical to the specimen surface. The majority of surface offsets occur along large, favorably oriented α-lath/matrix interfaces. Fig. 39b also illustrates this point while indicating the severe bending which occurs at thick G.B.α. Surface contours become evident along the faceted boundaries of the equiaxed grains but very little actual sliding was observed.

(a)   (b)

5 µm   30 µm

W12 (298K/3.7 % ε_p)   W12 (298K/3.7 % ε_p)
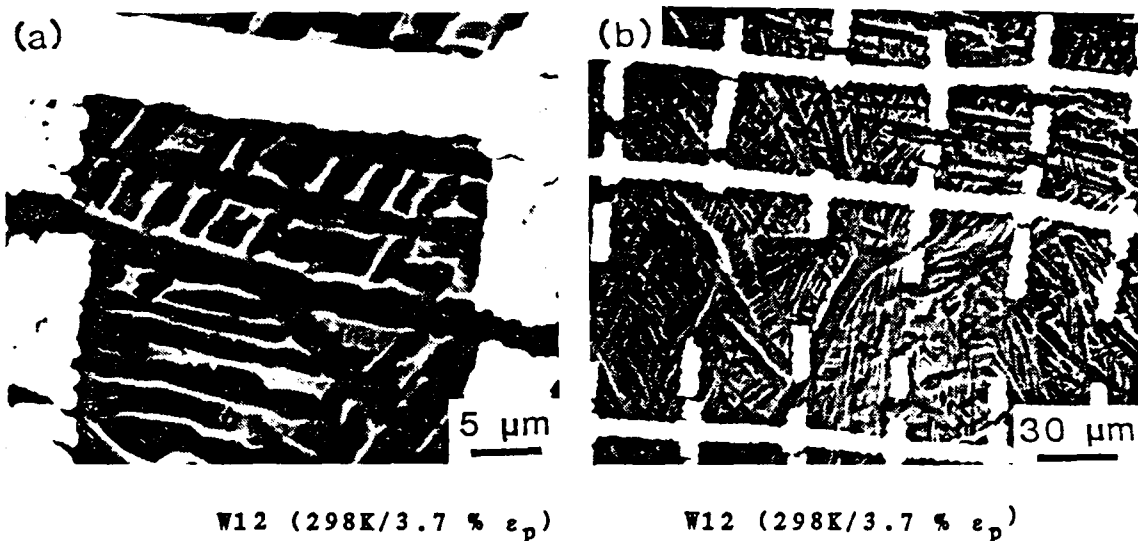
Fig. 39.   Evidence of sliding at alpha lath/matrix interfaces
           in (a) the W12 structure as well as bending along
           grain boundaries (b).

4.6.2.3   W15 Microstructure

Creep Deformation

Deformation of W15 grid deposition specimens crept at

90 % σ_{ys} and 100 % σ_{ys} was, in many respects, similar to

the W12 structure. Fig. 40a shows slight bending of grid

network across α-lath/martensite (or retained beta) inter-

faces. Sliding is barely visible at low strain rates (1.5

% ε_c).   After 950 hours and creep saturation this

microstructure exhibits very small amounts of G.B. sliding

and faceting at straight grain boundaries. As in the W12

structure, sliding occurs preferentially at large α-laths

and prior beta grain boundaries which are oriented favorably to the stress axis. Figure 40b shows more noticeable sliding occurring along α-lath/martensitic interface in a specimen crept for 940 hours to exhaustion (2.2 % ε_c) at a stress level just below the 100 % σ_{ys} level. Deformation along grain boundaries is proportionally less at this stress level than at the 90 % σ_{ys} limit.
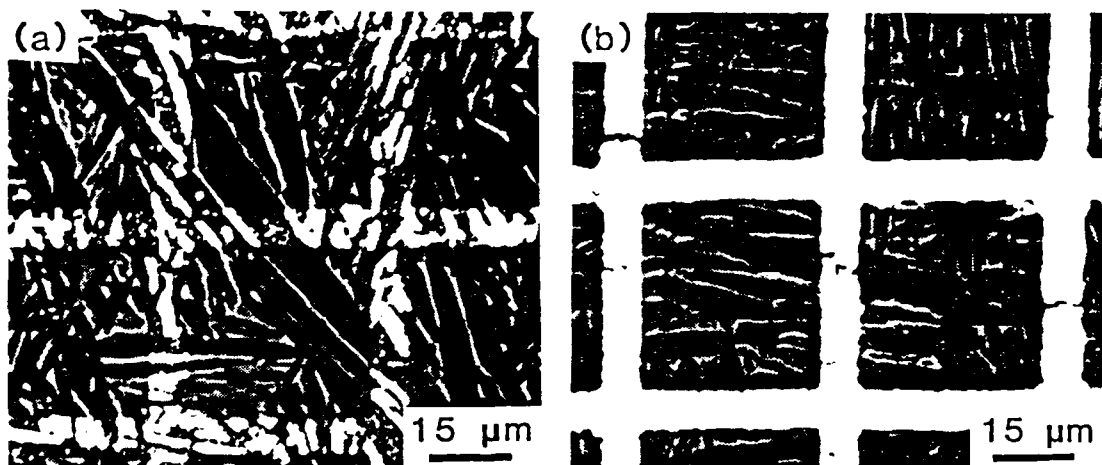
W15 (950 hrs/1.5 % ε_c)   W15 (940 hrs/2.2 % ε_c)

Fig. 40.   Evidence of slight bending of fiducial network at 90 % σ_{ys} along α-lath interfaces (a) and more substantial sliding occurring at higher stresses, 100 % σ_{ys} (b). Both specimens tested at room temperature.

Tensile Deformation

Tensile specimens strained to 4.1 % ε_p in the W15 structure exhibit heavy surface deformation along α-lath

boundaries as shown in Fig. 41. Some grain boundary slid-
ing is evident but is only a small contribution when com-
pared to the frequency of sliding along platelet boun-
daries. It is thought that the sliding at α-lath boun-
daries is primarily resonsible for the creep strain in the
W15 structure while fracture actually occurs inter-
granularly as in the W12 structure due to the continuous
soft alpha along the grain boundaries.
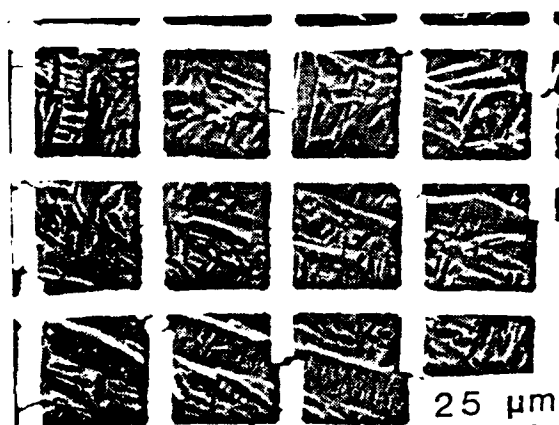
W15 Structure (298K/4.1 % ε_p)

Figure 41.

Heavy sliding occurring along α-lath/
martensitic boundaries during tensile
strains in the W15 microstructure.

4.6.3 Interfacial Sliding at Elevated Temperatures

High temperature tensile specimens for all three
microstructures were strained to prescribed strain per-
centages at temperatures ranging from 453K to 823K with
grid networks in place. Crept specimens experienced a

Determination of Proportional Limit for Creep at Room Temperature

W12 STRUCTURE

75 %σ_{ys}

70 %σ_{ys}

65 %σ_{ys}

60 %σ_{ys}

55 %σ_{ys}

50 %σ_{ys}

Incrementally Loaded Specimens
(From 50 %σ_{ys} to 80 %σ_{ys})

TOTAL HOURS OF TESTING

TOTAL STRAIN (%)

APPENDIX III

Determination of Proportional Limit for
Creep at Room Temperature

W11 STRUCTURE

Total strain (%) versus total hours of testing for W11 structure. Curves labeled 80 %σys, 75 %σys, 70 %σys, 65 %σys, 60 %σys, 55 %σys, and 50 %σys. Incrementally Loaded Specimens (From 50 %σys to 80 %σys).

APPENDIX II

SUMMARY OF ROOM TEMPERATURE CREEP DATA

SPECIMEN DESIGNATION	CREEP STRESS (MPA)	CREEP STRAIN* TO SATURATION (%)	TIME EXPONENT n
W1	608	0.16	0.16
W1	646	0.71	0.23
W1	684	1.84	0.20
W1	760	4.36	0.27
W2	684	0.50	0.09
W3	684	0.39	0.07
W8	684	0.76	0.24
W9	684	0.43	0.15
W11	562	0.15	0.20
W11	632	1.03	0.23
W11	702	3.11	0.17
W12	594	0.66	0.18
W12	668	1.23	0.26
W12	705	1.01	0.26

* SATURATION STRAIN IS ESTIMATED AT APPROX. 500 HRS OF TESTING AFTER WHICH THE CREEP STRAIN IS NEGLIGIBLE.

Tensile Curves Relating Strength to Temperature

Tempered Martensite (W15)

* Yield Strength
o UTS

Tensile Curves Relating Strength to Temperature

Basket-Weave Structure (W12)

* Yield Strength
o UTS

STRESS LEVEL (MPa)

TEMPERATURE (C)

APPENDIX I

Tensile Curves Relating Strength to Temperature

As-Received Structure (W11)

* Yield Strength
o UTS
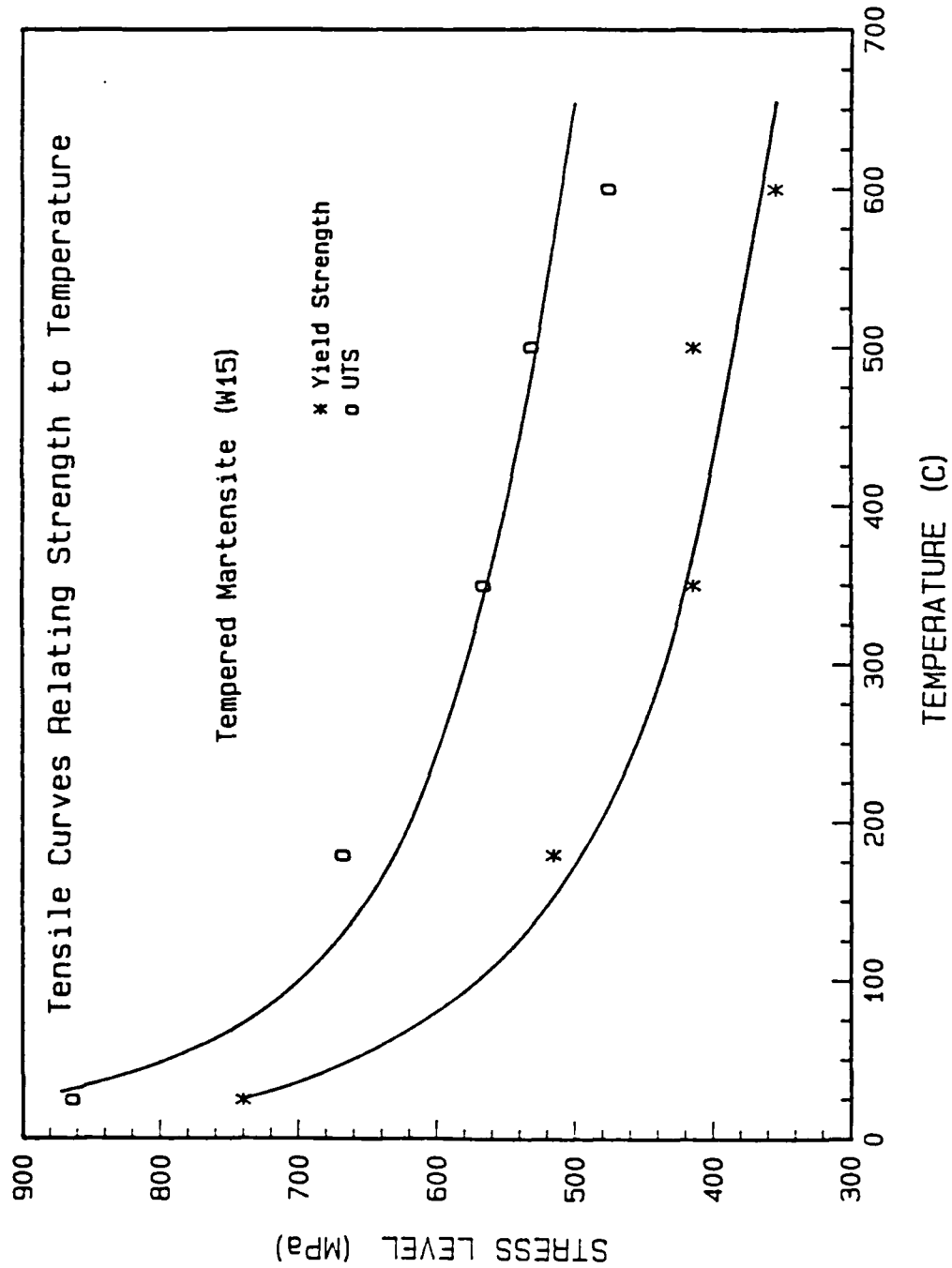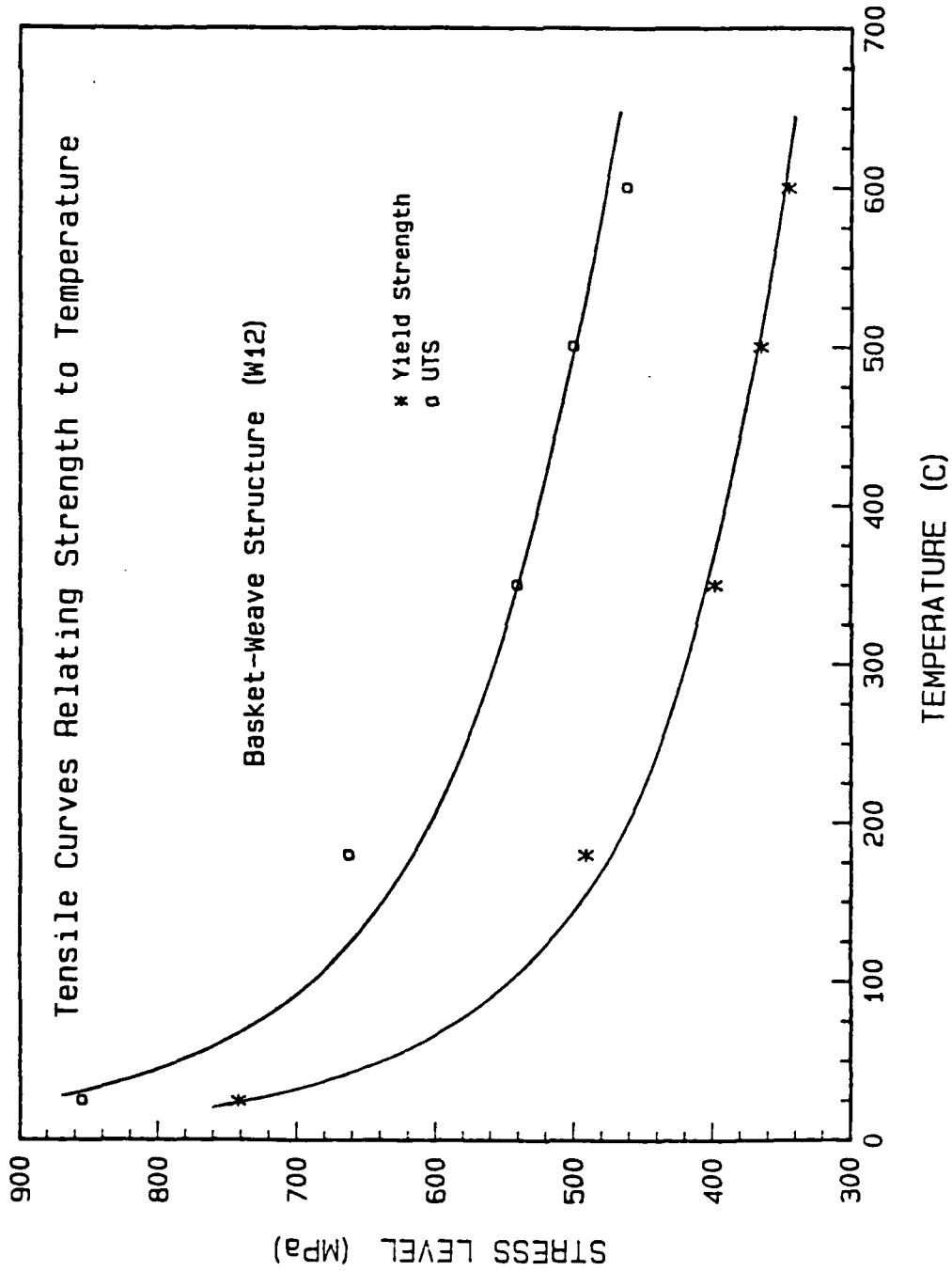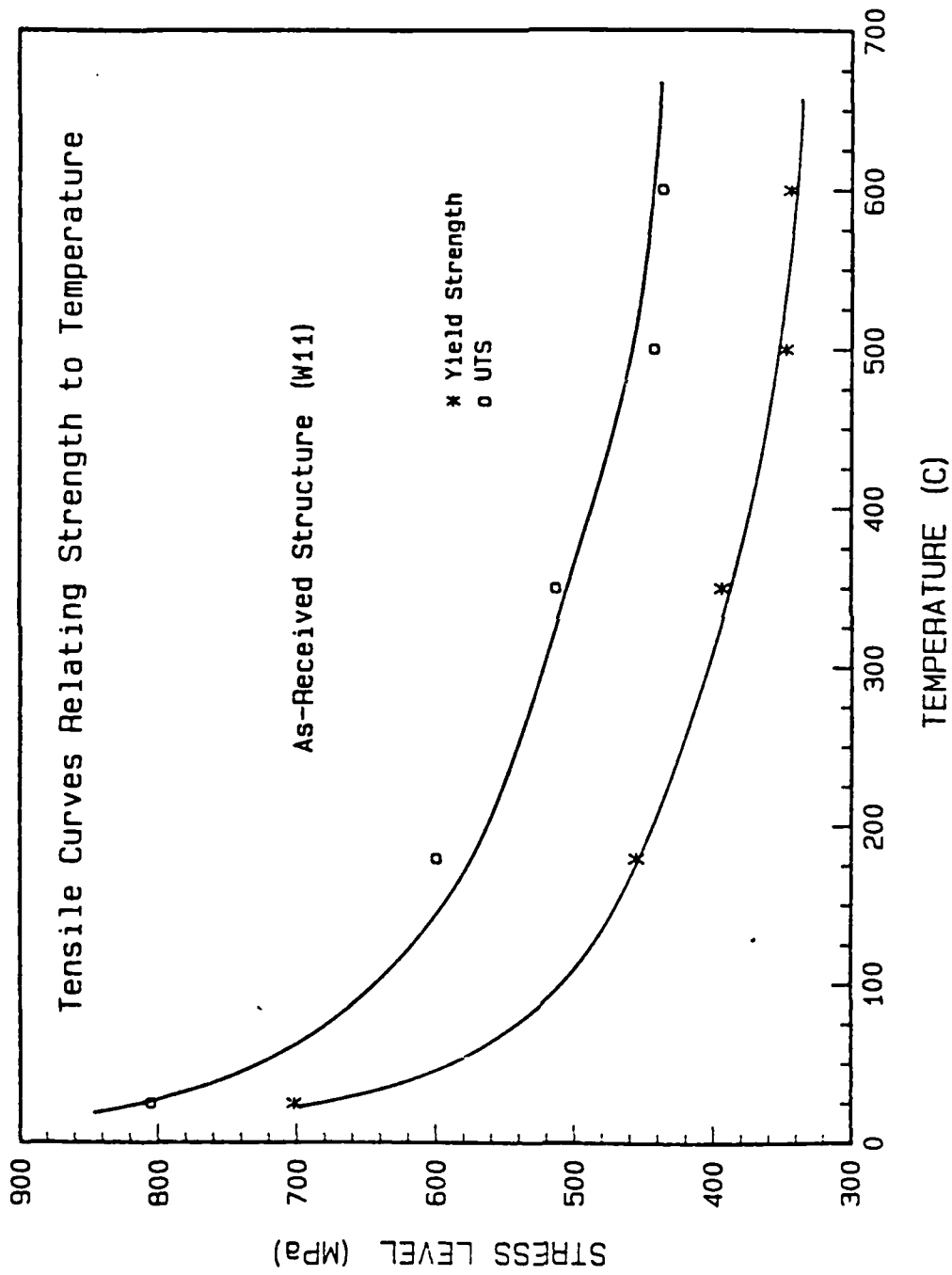
α/β interfaces while the beta-annealed equiaxed structures experience grain boundary sliding and α/β, α/martensite sliding.

4. Cyclic creep with a loading-unloading spectrum exhibits
   cyclic creep acceleration. Reduction of internal stress
   due to the accumulated creep strain accounts for this acceler-
   ation. Cyclic creep acceleration did not occur when compared
   to the static creep response at the same stress level as the
   peak stress on the cyclic curve. Therefore, the static creep
   curve with a stress level equivalent to the peak stress on the
   cyclic curve can be used as a guideline for the Ti-6211 alloy
   whenever cyclic creep is of concern for structural design.

5. For creep at high temperatures, the temperature dependence
   of steady-state creep rate indicates that diffusion
   controlled dislocation movement is the rate-controlling
   process for creep.

6. High temperature creep rupture in the as-received structures
   occurs by microvoid formation and coalescence along colony
   boundaries while the beta-annealed structures experience
   intergranular fracture prompted by microvoid formation and
   coalescence. The colony structures exhibit a longer creep
   life at high temperature while crack paths in the recrystal-
   lized microstructures follow the G.B.α/matrix interface.

7. Sliding along grain boundaries, colony boundaries and phase
   boundaries contributes substantially to the creep and tensile
   strains experienced by the Ti-6211 alloy under certain test
   conditions. The colony type Widmanstätten structures exhibit
   appreciable amounts of sliding along colony boundaries and

CHAPTER V

CONCLUSIONS

1. The Ti-6211 alloy shows transient type low temperature creep with work hardening and a lack of recovery resulting in creep saturation. Planar arrays of straight dislocations and a single operative slip system were observed after creep at room temperature. Dynamic recovery and thermally-activated cross slip enhance the creep processes at 453K.

2. Creep strain at ambient temperatures is strongly dependent upon creep stress and microstructure. Colony type Widmanstätten structures exhibit the highest creep rates due to a Burgers orientation relationship and associated long slip lengths. Sliding at colony boundaries or alpha/beta interfaces also contributes to the enhanced creep rates.

3. Microstructures simulating the HAZ of a weld display good creep resistance characteristics at both high and low temperatures and actually enhance the creep strength of the material. this is largely due to reduced slip lengths resulting from recrystallization and the subsequent loss of phase orientation relationship.

interfaces. Sharp deformation features are no more apparent at high temperature than in the room temperature specimens but more laths appear to become active. It should be noted that much more bending and less actual sliding and cracking occur at elevated temperatures. Fig. 45b shows an α-platelet spaced between two martensitic regions. Heavy dislocation structures exhibiting some degree of planarity may indicate interface sliding.

(a)   (b)

10 µm   1 µm

W15 structure (673K/4.1 % ε_p)   W15 structure (823K/400 MPa)
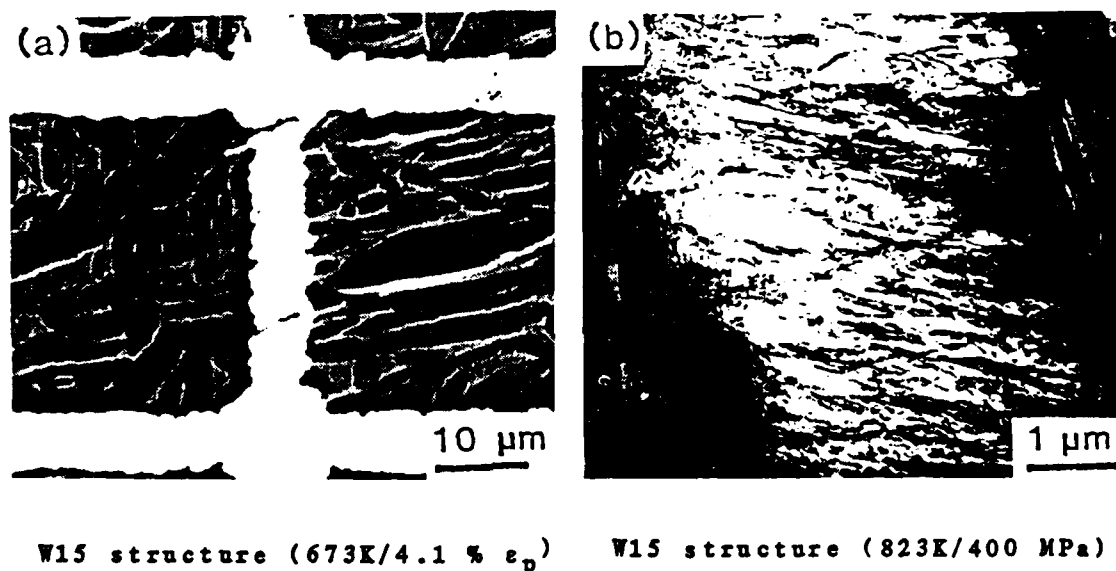
Fig.45.   Many α-lath/martensite interfaces serve as
          sources for sliding at elevated temperature (a). High
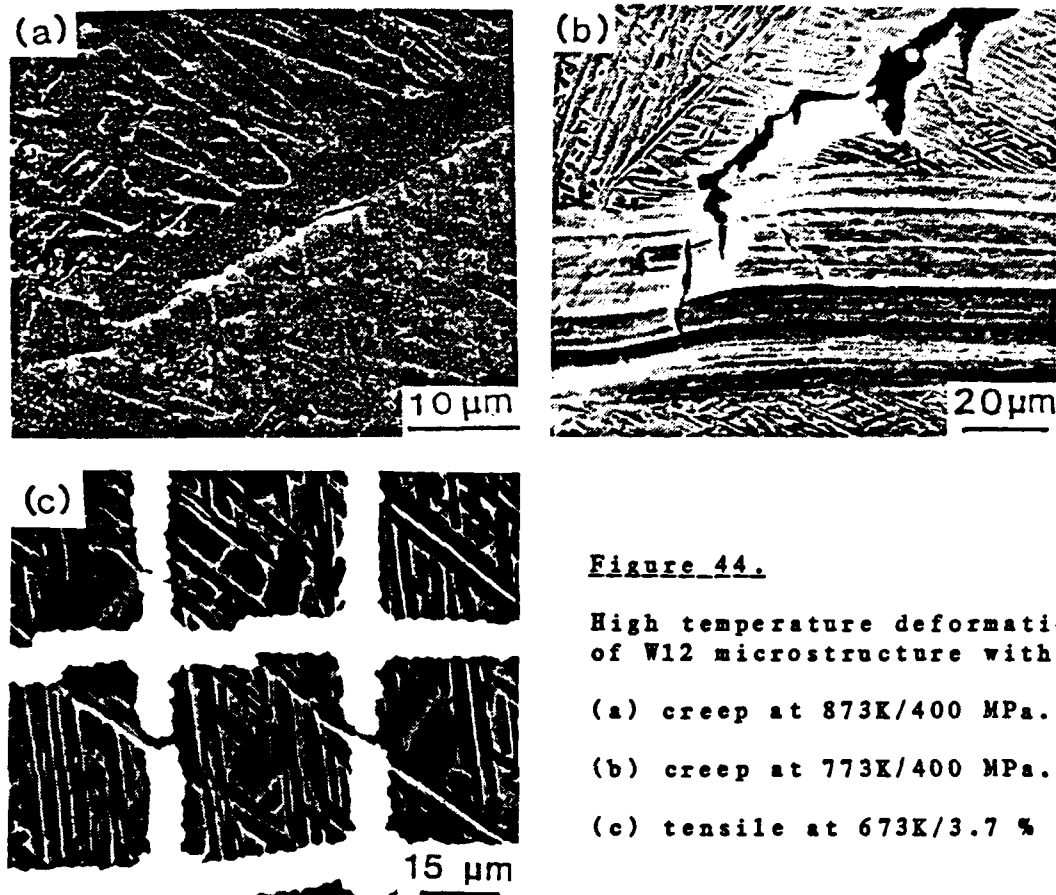   densities of dislocations along α-lath/martensite
          interfaces (b).

Figure 44.

High temperature deformation
of W12 microstructure with:

(a) creep at 873K/400 MPa.

(b) creep at 773K/400 MPa.

(c) tensile at 673K/3.7 % ε_p.

4.6.3.3 W15 Microstructure

High temperature deformation of the W15 structure
closely resembles deformation behavior of the W12 struc-
ture, the primary difference being α-lath/beta (W12) vs
α-lath/martensite (W15) sliding. Creep deformation is
favored along grain boundaries while tensile deformation is
active along grain boundaries, alpha-laths and generates
occaisional large deformation bands. Figure 45a
illustrates sliding occurring along α-lath/martensite

4.6.3.2 W12 Microstructure

Fig. 44 illustrates the effects of temperature on W12 creep. Slight cracking and heavy sliding were observed along the G.B.α/matrix interfaces (Fig. 44a). Little G.B. deformation was experienced at room temperature. Fig. 44b shows crack path following G.B.α/matrix interface and bending the surrounding matrix as shown by the fiducial scratch. Time-dependent diffusional effects tend to enhance grain boundary deformation in the equiaxed structures while short term tensile testing also activates deformation along favorably oriented lath structures (Fig. 44c).
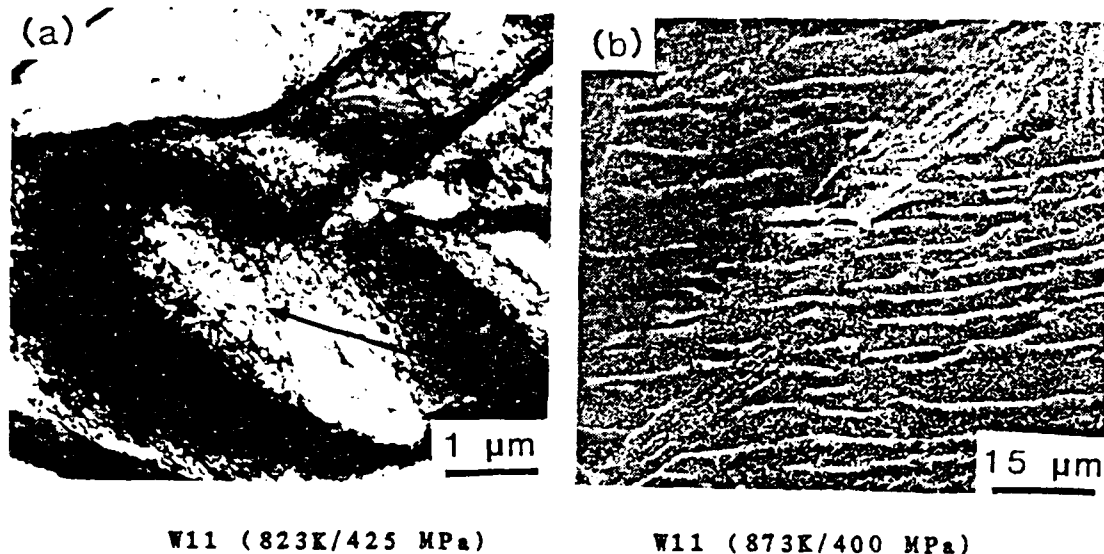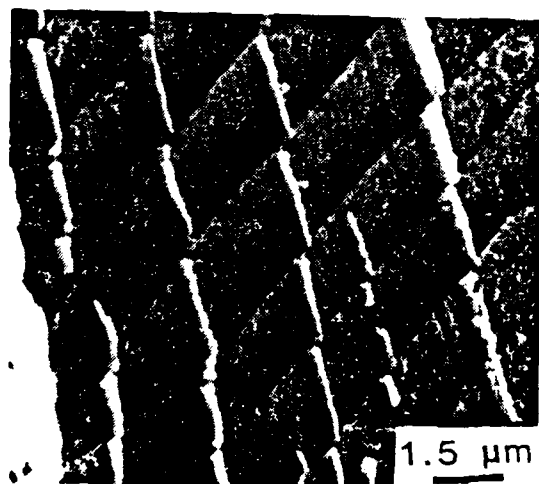
W11 (823K/425 MPa)　　　　　　W11 (873K/400 MPa)

Fig. 42.　Dislocation structures at elevated temperature during creep of W11 (a) and surface deformation showing α/β interface cracking (b).

W11 (673K/5.0 % ε_p)

Fig. 43.　Surface deformation during high temperature tensile testing.

variety of stress levels and temperatures up to 873K without the benefit of surface grid networks.

4.6.3.1 W11 Microstructure

Creep strains experienced at elevated temperatures are enhanced due to time dependent diffusional effects. Heaviest deformation occurs along colony boundaries as in the room temperature testing. TEM micrograph in Fig. 42a shows a large α platelet and adjacent colony. The dislocation density in the platelet is much higher than in the surrounding platelets and may indicate sliding at the platelet/colony interface. Fig. 42b shows the increased role of alpha/beta interface sliding and cracking in the W11 structure at 873K. Deformation during high temperature tensile testing focuses on the colony structures. While the colony boundaries deform heavily at room temperature, the activation of heavy slip (0.25µm) within colonies becomes pronounced at high temperatures (Fig. 43). This finding is interesting since very little slip was found during creep testing at elevated temperatures where interfacial sliding seemed to contribute most heavily to the deformation.

APPENDIX IV

Summary of High Temperature Creep Data

Sample Designation	Temperature ($^{\circ}$K)	Stress (MPa)	Strain Rate (Sec^{-1})	Rupture Time (Sec)
W11	698K	400	2.93×10^{-10}	-
W11	773K	400	2.15×10^{-9}	-
W11	823K	400	2.82×10^{-8}	6.34×10^{5}
W11	823	350	3.57×10^{-9}	-
W11	823	450	3.22×10^{-7}	1.70×10^{5}
W12	773	400	2.38×10^{-9}	
W12	823	400	3.12×10^{-8}	5.94×10^{5}
W12	873	400	9.64×10^{-7}	2.41×10^{4}

APPENDIX V

Sample Calculation for Determination of ε_{gbs} Contribution to Creep Strain

W11 Structure

Expression for grain boundary sliding (Equation No. 16):

$$\varepsilon_{gbs} = k'n_1\overline{w}_1$$

where:

$$k' = 1.5$$

n_1 = Number of grains or deformation barriers per unit length in the undeformed specimen measured parallel to the stress axis.

Approximately every third colony in the W11 structure is favorably oriented for creep deformation or sliding so:

Colony linear intercept length = 45μm, or:

Deformation barrier spacing = 3 x 45μm, so:

$$n_1 = 1/3(45\mu m) = 1/135\mu m$$

$\overline{\omega}_1$ = Average value of measured grid offsets at active deformation barriers in direction perpendicular to the stress axis and in the plane of the surface.

therefore:

$$\overline{\omega}_1 = 1.5\mu m$$

$$\varepsilon_{gbs} = (1.5)(1/135 \times 10^{-6}m)(1.5 \times 10^{-6}m)$$

$$\varepsilon_{gbs} = 0.0167$$

Total creep strain was approximately 2.8 %, therefore:

$$\varepsilon_{gbs}/\varepsilon_T = 0.0167/0.028 \text{ or } 60 \text{ %}$$

The contribution of colony sliding to creep deformation was approximately 60 %.

BIBLIOGRAPHY

1. D. S. Shih, "Investigation of the Effect of Microstructure and Texture on the Fatigue Properties and Deformation Modes of an Alpha + Beta Titanium Alloy, Ti-6211", Thesis, Georgia Tech., 1983.

2. M. J. Donachie, Jr., ed., "Titanium and Titanium Alloys Source Book", ASM, Metals Park, Ohio, 1982.

3. R. T. Chen, Original project proposal for Ti-6211 creep study and background research. Unpublished (1981).

4. S. Shih, F. S. Lin, S. Spooner and E. A. Starke, Jr., "The Effect of Microstructure and Texture on the Mechanical Properties of an Alpha-Beta Titanium Alloy", ASM, Nov. 3-4, 1981.

5. F. S. Lin, E. A. Starke, Jr., S. B. Chakrabortty and A. Gysler, "Investigation of the Effect of Microstructure on the Deformation Modes and Mechanical Properties of Ti-6211", Submitted to Met. Trans.

6. R. T. Chen, W. H. Miller and E. A. Starke, Jr., "Effects of Microstructure on Creep Behavior of Ti-6211", Titanium '84, Proc. Fifth Int. Conf. on Titanium, AIME, Warrendale, PA, in press.

7. D. M. Bowden, "Hot Ductility Loss in Synthetic Weld Heat-Affected Zones in the Alloy Titanium 6211", Thesis, Georgia Tech., 1981.

8. W. P. Roe, H. R. Palmer and W. R. Opie, "Diffusion of Oxygen in Alpha and Beta Titanium", Trans. ASM, Vol. No. 52, 191 (1960).

9. M. A. Imam and C. M. Gilmore, "Room Temperature Creep of Ti-6Al-4V", Met. Trans., Vol. No. 10A, 419 (1979).

10. W. H. Reimann, "Room Temperature Creep in Ti-6Al-4V", J. of Mater., JMLSA, Vol. 6, No. 4, 926 (1971).

11. A. J. Hatch, J. M. Partridge and R. G. Broadwell, "Room Temperature Creep and Fatigue Properties of Titanium Alloys", J. Materials, Vol. No. 2, 111 (1967).

12. A. W. Thompson and B. C. Odegard, "The Influence of Microstructure on Low Temperature Creep of Ti-5Al-2.5Sn", Met. Trans., Vol. No. 4A, 899 (1973).

13. A. K. Chakrabarti and E. S. Nichols, "Creep Behavior of Cast Ti-6Al-4V Alloy", Titanium '80 Proc. Fourth Int. Conf. on Titanium, AIME, Warrendale, PA, 1081 (1981).

14. B. C. Odegard and A. W. Thompson, "Low Temperature Creep of Ti-6Al-4V", Met. Trans., Vol. No. 5A, 1207 (1974).

15. H. P. Chu, "Room Temperature Creep and Stress Relaxation of a Titanium Alloy", J. of Mater., JMLSA, Vol. 5, No. 3, 633 (1970).

16. H. P. Chu, "Room Temperature Creep of a Ti-6211 Alloy Weldment", DTNSRDC Report 28-175 (April 1972).

17. H. P. Chu, "Effect of Yield Strength on Room-Temperature Creep of Ti-6Al-2Cb-1Ta-1Mo Alloy", DTNSRDC Report 28-898 (February 1974).

18. H. P. Chu, "Second Progress Report on the Investigation of Creep-Fatigue of Titanium Alloy Ti-6Al-2Cb-1Ta-0.8Mo", Progress Report, DTNSRDC (December 1981).

19. J. B. Borradaile and R. H. Jeal, "Mechanical Properties of Titanium Alloys", Titanium '80, Proc. Fourth Int. Conf. on Titanium, AIME, Warrendale, PA, 141 (1980).

20. J. D. Whittenberger and T. J. Moore, "Elevated Temperature Flow Strength, Creep Resistance and Diffusion Welding Characteristics of Ti-6Al-2Nb-1Ta-0.8 Mo", Met. Trans., Vol. No. 10A, 1597 (1979).

21. J. A. Wert and N. E. Paton, "Enhanced Superplasticity and Strength in Modified Ti-6Al-4V Alloys", in press.

22. J. C. Chesnutt, C. G. Rhodes and J. C. Williams, "Relationship Between Mechanical Properties, Microstructure and Fracture Topography in $\alpha + \beta$ Titanium Alloys", ASTM, Phila., PA, 99 (1976).

23. W. A. Baeslack III and Y. Mahajan, "Intergranular Fracture of Heat-Treated Weldments in a High-Strength Alpha-Beta Titanium Alloy", Scripta. Met., Vol. No. 13, 959 (1979).

24. K. S. Chan, C. C. Wojcik and D. A. Koss, "Deformation of an Alloy with a Lamellar Microstructure: Experimental Behavior of Individual Widmanstatten Colonies of an $\alpha - \beta$ Titanium Alloy", Met. Trans., Vol. No. 12A, 1899 (1981).

25. W. A. Baeslack III and Y. Mahajan, "Observation of Alpha-Beta Interface Sliding in a Titanium Alloy Weld Metal", Met. Trans., Vol. No. 11A, 1234 (1980).

26. S. Ankem and H. Margolin, "The Role of Elastic Interaction Stresses on the Onset of Plastic Flow for Oriented Two Ductile Phase Structures", Met. Trans., Vol. No. 11A,

963 (1980).

27. I. P. Jones and W. B. Hutchinson, "Stress-State Dependence
     of Slip in Titanium-6Al-4V and Other H.C.P. Metals",
     Acta. Met., Vol. No. 29, 951 (1981).

28. S. P. Agrawal, G. A. Sargent and H. Conrad, "Hexagonal
     Dislocation Networks in Titanium", Met. Trans., Vol. No. 5,
     2415 (1974).

29. M. A. Greenfield and H. Margolin, "The Mechanism of Void
     Formation, Void Growth, and Tensile Fracture in an Alloy
     Consisting of Two Ductile Phases", Met. Trans., Vol. No. 3,
     2649 (1972).

30. G. E. Dieter, "Mechanical Metallurgy", 2´nd ed., McGraw-Hill
     Book Company, New York, N.Y., 1976.

31. R. E. Reed-Hill, "Physical Metallurgical Principles", D. Van
     Nostrand Co., New York, N.Y., 1973.

32. P. G. McVetty, "Interpretation of Creep Test Data", ASTM
     Proceedings, Vol. No. 43, 707 (1943).

33. Oding, "Stress Relaxation in Metals", Oliver and Boyd, ed.,
     London, England, 1965.

34. R. T. Chen, "Creep of Metals", Unpublished lecture notes on
     creep, University of Virginia, 1983.

35. J. Gittus, "Creep, Viscoelasticity and Creep Fracture in
     Solids", Applied Science Publishers LTD, London, England,
     1975.

36. S. M. L. Sastry, P. S. Pao and K. K. Sankaran, "High Temper-
     ature Deformation of Ti-6Al-4V", Titanium `80, Proc. Fourth
     Int. Conf. on Titanium. AIME, Warrendale, PA, 873 (1981).

37. G. Malakondaiah and P. Rama Rao, "Creep of Alpha-Titanium
     at Low Stresses", Acta. Met., Vol. No. 29, 1263 (1981).

38. Rune Lagneborg, Int. Metall. Rev., Vol. No. 17, 130 (1972).

39. S. N. G. Chu and J. C. M. Li, "Impression Creep; a New
     Creep Test", J. of Mat. Sci., Vol. No. 12, 2200 (1977).

40. H. Yu and J. C. M. Li, "Computer Simulation of Impression
     Creep by the Finite Element Method", J. of Mat. Sci.,
     Vol. No. 12, 2214 (1977).

41. S. N. G. Chu and J. C. M. Li, "Impression Creep of β-Tin
     Single Crystals", Mat. Sci. and Engr., Vol. No. 39, 1 (1979).

42. S. N. G. Chu and J. C. M. Li, "Pencil Slip in β-Tin
     Single Crystals", J. of Mat. Sci., Vol. No. 15, 2733
     (1980).

43.   E. C. Yu and J. C. M. Li, "Impression Creep of LiF Single Crystals", Philo. Mag., Vol. 36, No. 4, 811 (1977).

44.   S. N. G. Chu and J. C. M. Li, "Photoelastic Studies of Three-Dimensional Stress Field Caused by a Cylindrical Punch", J. of App. Phys., Vol. 51. No. 6, 3338 (1980).

45.   N. E. Paton and M. W. Mahoney, "Creep of Titanium-Silicon Alloys", Met. Trans., Vol. No. 7A, 1685 (1976).

46.   M. R. Winstone, R. D. Rawlings and D. R. F. West, "The Creep Behavior of Some Silicon-Containing Titanium Alloys", J. of Less Common Metals, Vol. No. 39, 205 (1975).

47.   A. Rosen and A. Rottem, "The Effect of High Temperature Exposure on the Creep Resistance of Ti-6Al-4V", Mat. Sci. and Engr., Vol. No. 22, 23 (1976).

48.   I. W. Hall, "The Effect of Oxygen on the Creep Properties and Dislocation Configurations in Ti-6Al-4V", Scand. J. Metallurgy, Vol. No. 6, 45 (1976).

49.   J. Blackburn and J. C. Williams, "The Preparation of Thin Foils of Titanium Alloys", Trans. AIME, Vol. No. 239, 287 (1967).

50.   R. Zeyfang, R. Martin and H. Conrad, "Low Temperature Creep of Titanium", Mat. Sci. and Engr., Vol. No. 8, 134 (1971).

51.   D. G. Attwood and P. M. Hazzledine, "A Fiducial Grid for High-Resolution Metallography", Metallography 9, 483 (1976).

52.   S. Ankem and H. Margolin, "Alpha-Beta Interface Sliding in Ti-Mn Alloys", Met. Trans., Vol. No. 14A, 500 (1983).

53.   G. H. Edward and M. F. Ashby, "Intergranular Fracture During Power-Law Creep", Acta. Met., Vol. No. 27, 1505 (1979).

54.   A. J. Perry, "Review: Cavitation in Creep", J. of Mat. Sci., Vol. No. 9, 1016 (1974).

55.   R. Raj and M. F. Ashby, "Grain Boundary Sliding and Diffusional Creep", Met. Trans., Vol. No. 2A, 1113 (1971).

56.   T. J. Chuang and J. R. Rice, Acta. Met., Vol. No. 21, 1625 (1973).

57.   J. R. Hancock, Met. Sci. J., Vol. No. 10, 319.

58.   S. Baik and R. Raj, "Mechanisms of Creep-Fatigue Inter-action", Met. Trans., Vol. No. 13A, 1215 (1982).

59. E. H. Aigeltinger, "A Technique for the Measurement of Diffusion Creep from Marker Line Displacements", J. of Mat. Sci., Vol. No. 9, 644 (1974).

60. W. A. Rachinger, "Relative Grain Translations in the Plastic Flow of Aluminum", J. Inst. of Metals, Vol. No. 81, 33 (1952).

61. T. G. Langdon, "The Effect of Surface Configuration on Grain Boundary Sliding", Met. Trans., Vol. No. 3A, 797 (1972).

62. R. L. Bell, C. Graeme-Barber and T. G. Langdon, "The Contribution of Grain Boundary Sliding to the Overall Strain of a Polycrystal", Trans. AIME, Vol. No. 239, 1821 (1967).

63. R. N. Stevens, "Calculation of the Deformation Caused by Grain Boundary Sliding During the Creep of Polycrystalline Solids", Trans. AIME, Vol. No. 236, 1762 (1966).

64. R. N. Stevens "Grain Boundary Sliding in Metals", Met. Rev., Vol. No. 11, 129 (1966).

65. R. N. Stevens, "Discussion of `The Contribution of Grain Boundary Sliding to the Overall Strain of a Polycrystal´", Trans. AIME, Vol. No. 242, 2238 (1968).

66. T. G. Langdon, "Grain Boundary Sliding as a Deformation Mechanism During Creep", Phil. Mag., Vol. No. 22, 689 (1970).

67. A. Gittins, "Discussion of `Calculation of the Deformation Caused by Grain Boundary Sliding During the Creep of Polycrystalline Solids´", Trans. AIME, Vol. No. 239, 922 (1967).

68. H. E. Davis, G. E. Troxell and C. E. Wiskocil, "The Testing and Inspection of Engineering Materials", McGraw-Hill Book Company, Inc., New York, N.Y., 1941.

69. F. Dyment and C. M. Libarrati, J. of Mat. Sci., Vol. No. 5, 434 (1970).

70. P. J. Bania and J. A. Hall, "Creep Studies of Ti-6242-Si Alloy", Titanium `84, Proc. Fifth Int. Conf. on Titanium, AIME, Warrendale, PA, in press.

71. R. P. Elliot, "Diffusion in Titanium and Titanium Alloys", ASD-TDR, Vol. No. 62, 561 (October 1962).

72. E. A. Gulbransen and K. F. Andrew, "Kinetics of the Reactions of Titanium with O_2, N_2 and H_2", Trans. AIME, Vol. No. 185, 741 (1949).

73. D. K. Shetty and M. Meshii, "Plastic Deformation of

Aluminum Under Repeated Loading", Met. Trans., Vol. No. 6A, 349 (1975).

74. J. T. Evans and R. N. Parkins, "Creep Induced by Load Cycling in a C-Mn Steel", Acta. Met., Vol. No. 24, 511 (1976).

75. C. E. Feltner, Trans. AIME, Vol. No. 227, 798 (1963).

76. E. W. Lee, E. A. Starke, Jr., and C. J. Beevers, "The Effect of Strain Rate on the Monotonic and Cyclic Properties of Beta Ti-V Alloys", in press.

77. J. E. Dorn, J. Mitchell and F. Hauser, "Dislocation Dynamics", Experimental Mechanics, Vol. No. 5, 353 (1965).

78. H. Mughrabi, K. Herz and X. Stark, "The Effect of Strain-Rate on the Cyclic Deformation Properties of α-Iron Single Crystals", Acta. Met., Vol. No. 24, 659 (1976).

79. H. G. Paris, B. G. LeFevre and E. A. Starke, Jr., "Deformation Behavior in Quenched and Aged Beta Ti-V Alloys", Met. Trans., Vol. No. 7A, 273 (1976).

PROFESSIONAL PERSONNEL

Dr. Edgar A. Starke, Jr., Principal Investigator
Dr. Fu-Shiong Lin
Dr. Wolfgang Ruch
Dr. R.T. Chen

GRADUATE STUDENTS

William H. Miller, M.S., University of Virginia, January, 1985
Donald Shengduen Shih, Ph.D., Georgia Institute of Technology, June, 1983.
David M. Bowden, M.S., Georgia Institute of Technology, September, 1982.

PRESENTATIONS

1.   R.T. Chen and E.A. Starke, Jr., "Low Temperature Creep of Ti-6Al-2Nb-1Ta-0.8Mo," paper presented at TMS-AIME Annual Meeting, Atlanta, Georgia, March, 1983.

2.   E.A. Starke, Jr., "Deformation and Creep Behavior," presentation at ONR-DTNSRCC Ti-100 Workshop Review, Annapolis, June, 1983.

3.   W.H. Miller, Jr., R.T. Chen and E.A. Starke, Jr., "The Effect of Microstructure on Creep Behavior of Ti-6211, presented at the Fall AIME Meeting, Detroit, Michigan, September, 1984.

4.   D.S. Shih, F.S. Lin and E.A. Starke, Jr., "Effect of Texture on the Fatigue Properties of a Near-Alpha Ti Alloy," presented at the AIME Meeting, Detroit, Michigan, September, 1984.

5.   Donald S. Shih, Fu-Shiong Lin, and E.A. Starke, Jr., "The Effect of Microstructure and Texture on the Low Cycle Fatigue Properties of Ti-6Al-2Nb-1Ta-0.8Mo," presented at the Fifth International Conference on Titanium, Munich, West Germany, September, 1984.

6.   R.T. Chen and E.A. Starke, Jr., "Effects of Microstructure on Creep Behavior of Ti-6211," presented at the Fifth International Conference on Titanium, Munich, West Germany, September, 1984.

7.   Donald S. Shih, F.S. Lin and E.A. Starke, Jr., "The Effect of Microstructure and Texture on the Fatigue Crack Propagation of an Alpha + Beta Titanium Alloy," presented at the Fifth International Conference on Titanium, Munich, West Germany, September, 1984.

8.   D.M. Bowden and E.A. Starke, Jr., "Hot Crack Susceptibility in Titanium 6211," presented at the Fifth International Conference on Titanium, Munich, West Germany, September, 1984.

PUBLICATIONS

1. David M. Bowden and E.A. Starke, Jr., "The Effect of Microstructure and Deformation Behavior on the Hot Ductility of Ti-6Al-2Nb-1Ta-0.8Mo," Met. Trans. A 15A, 1984, p. 1687.

2. F.S. Lin, E.A. Starke, Jr., S.B. Chakrabortty and A. Gysler, "the Effect of Microstructure on the Deformation Modes and Mechanical Properties of Ti-6Al-2Nb-1Ta-0.8Mo: Part I. Widmanstätten Structures," Met. Trans. A 15A, 1984, p. 1229.

3. Fu-Shiong Lin, E.A. Starke, Jr., and A. Gysler, "The Effect of Microstructure on the Deformation Modes and Mechanical Properties of Ti-6Al-1Ta-0.8Mo: Part II. Equiaxed Structures," Met. Trans. A 15A, 1984, p. 1873.

4. D.M. Bowden and E.A. Starke, Jr., "Hot Cracking Susceptibility in Titanium 6211," Proceedings of the Fifth International Conference on Titanium, Munich, West Germany, September, 1984 (in press).

5. Donald S. Shih, F.S. Lin and E.A. Starke, Jr., "The Effect of Microstructure and Texture on the Fatigue Crack Propagation of an Alpha + Beta Titanium Alloy," Proceedings of the Fifth International Conference on Titanium, Munich, West Germany, September, 1984 (in press).

6. Donald S. Shih, Fu-Shiong Lin and E.A. Starke, Jr., "The Effect of Microstructure and Texture on the Low Cycle Fatigue Properties of Ti-6Al-2Nb-0.8Mo," Proceedings of the Fifth International Conference on Titanium, Munich, West Germany, September, 1984 (in press).

7. R.T. Chen, W.H. Miller, Jr., and E.A. Starke, Jr., "Effects of Microstructure on Creep Behavior of Ti-6211," Proceedings of the Fifth International Conference on Titanium, Munich, West Germany, September, 1984 (in press).

8. E.W. Lee, S.B. Chakrabortty and E.A. Starke, Jr., "The Effect of Overload on the Fatigue Crack Propagation in Metastable Beta Ti-V Alloys," Met. Trans. A 15A, 1984, p. 511.

9. R.T. Chen and E.A. Starke, Jr., "TEM Studies of Microstructures in IM, PM, Mechanically Alloyed and Rapidly Solidified Al-Li Base Alloys," Proceedings of the 1984 Metallography Symposium/Metals Congress, Detroit, Michigan, September, 1984 (in press).

10. E.W. Lee, E.A. Starke, Jr., and C.J. Beevers, "The Effect of Strain Rate on the Monotonic and Cyclic Properties of Beta Ti-V Alloys," Mater. Sci. & Engr. (in press).

THESES

1. David M. Bowden, "Hot Ductility Loss in Synthetic Weld Heat-Affected Zones in the Alloy Titanium 6211," Ph.D. Thesis, Georgia Institute of Technology, September, 1982.

2.   Donald Shengduen Shih, "Investigation of the Effect of Microstructure and Texture on the Fatigue Properties and Deformation Modes of an Alpha + Beta Titanium Alloy, Ti-6Al-2Nb-1Ta-0.8Mo," Ph.D. Thesis, Georgia Institute of Technology, June, 1983.

3.   William H. Miller, Jr., "The Effect of Microstructure on the Creep Behavior of Ti-6Al-2Nb-1Ta-0.8Mo," M.S. Thesis, University of Virginia, January, 1985.

DISTRIBUTION LIST

UNIVERSITY OF VIRGINIA
School of Engineering and Applied Science

The University of Virginia's School of Engineering and Applied Science has an undergraduate enrollment of approximately 1,500 students with a graduate enrollment of approximately 500. There are 125 faculty members, a majority of whom conduct research in addition to teaching.

Research is a vital part of the educational program and interests parallel academic specialties. These range from the classical engineering disciplines of Chemical, Civil, Electrical, and Mechanical and Aerospace to newer, more specialized fields of Biomedical Engineering, Systems Engineering, Materials Science, Nuclear Engineering and Engineering Physics, Applied Mathematics and Computer Science. Within these disciplines there are well equipped laboratories for conducting highly specialized research. All departments offer the doctorate; Biomedical and Materials Science grant only graduate degrees. In addition, courses in the humanities are offered within the School.

The University of Virginia (which includes approximately 1,500 full-time faculty and a total full-time student enrollment of about 16,000), also offers professional degrees under the schools of Architecture, Law, Medicine, Nursing, Commerce, Business Administration, and Education. In addition, the College of Arts and Sciences houses departments of Mathematics, Physics, Chemistry and others relevant to the engineering research program. The School of Engineering and Applied Science is an integral part of this University community which provides opportunities for interdisciplinary work in pursuit of the basic goals of education, research, and public service.

END

FILMED

10-85

DTIC